Chapter 11

Observation of Fungi, Bacteria, and Parasites in Clinical Skin Samples Using Scanning Electron Microscopy

Ran Yuping, Zhuang Kaiwen, Hu Wenying, Huang Jinghong, Feng Xiaowei, Chen Shuang, Tang Jiaoqing, Xu Xiaoxi, Kang Daoxian, Lu Yao, Zhang Ruifeng, Ran Xin, Wan Huiying, Lama Jebina, Dai Yalin and Zhang Chaoliang

Additional information is available at the end of the chapter

http://dx.doi.org/10.5772/61850

Abstract

This chapter highlights the description of the clinical manifestation and its pathogen and the host tissue damage observed under the Scanning Electron Microscope, which helps the clinician to understand the pathogen's superstructure, the change of host subcell structure, and the laboratory workers to understand the clinical characteristics of pathogen-induced human skin lesions, to establish a two-way learning exchange database with vivid images

Keywords: Fungi, Bacteria, Parasite, Clinical Skin Samples, SEM

1. Introduction

In dermatovereology department, skin infections by fungi, bacteria, and, parasites are very common in routine clinical practice. Differentiation and identification of these pathogens are a huge challenge and very important for the patient's diseases diagnosis and treatment. Scanning electron microscope (SEM) is a very strong tool for detection and observation of pathogens from the clinical samples that helps us obtain a direct proof of the pathogen on the surface of the skin samples of the lesion. Based on the detailed morphologic image, we can recognize the ultrastructural of the pathogen and understand the pathogenesis of the skin-infected diseases. During recent years, we collected a lot of pathogenic microorganisms' photographs taken by SEM. These pathogens include fungi (*Trichophyton violaceum*, *Microsporum canis*, *Mucor irregularis*, *Lichtheimia* (*Absidia*) *corymbifera*, *Alternaria arboresce*, *Fon-*

secaea pedrosoi, *Aspergillus fumigatus* and *Malassezia*), bacteria (*Propionibacterium acnes*), and parasites (*Pediculosis pubis* and *Demodicid mites*) *in vivo* or *in vitro*. The diagnosis and clinical manifestation, the kinds of sample and the image of the pathogens are summarized in the Table 1.

Diagnosis	Clinical manifestation	Sample	Image of pathogen by SEM
Tinea capitis	Erythema, scales on the scalp; hair broken and hair loss	Infected hair	Fungus (*Trichophyton violaceum*)
Tinea capitis	Excessive scales and hair loss on the scalp	Infected hair	Fungus (*Microsporum canis*)
Malassezia folliculitis	Slightly pruritic, monomorphic follicular papules and pustules	Keratotic plug of pustule of hair follicle	Fungus (*Malassezia*)
Pityriasis versicolor	Erythema and scaly, hyperpigmentation or hypopigmentation of skin	Scales	Fungus (*Malassezia*)
Mucormycosis	Progressive red plaque around the inner canthus	Cultured colony	Fungus (*Mucor irregularis*)
Mucormycosis	Purulent granuloma of left forearm	Cultured colony	Fungus (*Lichtheimia corymbifera*)
Cutaneous alternariosis	An ulcer covered with crust on left anterior tibia	Cultured colony	Fungus (*Alternaria arboresce*)
Chromoblastomycosis	Red plaque in the left knee	Cultured colony	Fungus (*Fonsecaea pedrosoi*)
Primary laryngeal aspergillosis	Hoarseness, severe paroxysmal coughing and tachypnea	Biopsy tissue	Fungus (*Aspergillus fumigatus*)
Acne	Recurrent papule and pustule acne	Pustule	Bacteria (*Propionibacterium acnes*)
Pediculosis pubis	Intense itching of the scalp	Parasite	Parasite (*Pubic lice*)
Demodicid mites	Itching, multiple erythema, papules, pustules	Hair follicle plug	Parasite (*Demodex folliculorum*)

Table 1. Summary of diagnosis and clinical manifestation, kinds of sample, and the image of the pathogens observed by SEM

2. Methods

All samples for SEM were taken from clinical patients. These samples included infected hair, scales, colony of culture, and tissue of skin biopsy. The samples for SEM were fixed in 2% glutar-aldehyde for 4 h at 4 ˚C, dehydrated through four gradations of alcohol solutions (50%, 70%, 95%, 100%, progressively) for 15 min each, then soaked in isoamyl acetate for 30 min. The specimens were prepared after critical-point drying method, under which condi-

http://dx.doi.org/10.5772/61850

tion they were gilded in a vacuum chamber and observed under the SEM, FEI Inspect F50, equipped with an FEG gun operated at 30 kV at high vacuum.

3. Results

3.1. Tinea capitis

Tinea capitis is a common superficial fungal infection of scalp hair follicles and surrounding skin. It often affects children rather than adults. Its pathogens are dermatophytes, usually species in the genera *Microsporum* and *Trichophyton*, such as *Microsporum canis*, *Trichophyton tonsurans*, and *Trichophyton violaceum* [1]. The clinical manifestation of tinea capitis is highly variable, depending on the causative organism, type of hair invasion and degree of host inflammatory response. Common features are patchy hair loss with varying degrees of scaling and erythema. However, the clinical signs may be subtle and diagnosis can be challenging. A number of clinical patterns exist [2]. The accurate diagnosis of tinea capitis usually depends on the laboratory investigation, mainly including direct microscopy with 10%–30% potassium hydroxide and fungal culture. It can confirm the diagnosis by detecting or isolating the causal organism by either of these two methods. Tinea capitis always requires systemic antifungal treatment. Topical treatment is only used as adjuvant therapy to systemic antifungals as topical antifungal agents do not penetrate the hair follicle. Recommended drug in systemic treatment include itraconazole, terbinafine, or griseofulvin.

Figure 1. a. A 9-year-old boy, weighing 25kg, presented to our clinic with slightly itching, multiple patchy areas of gray scaling lesions on the scalp and obvious hair loss.

We describe two cases of tinea capitis due to *T. violaceum* [3] and *M. canis* [4]. The first patient is a 9-year-old boy, weighing 25 kg, presented to our clinic because of multiple, slightly itching and patchy areas of gray scales on the scalp associated with hair loss (Fig. 1). The diagnosis of tinea capitis caused by *T. violaceum* was established by direct microscopic examination, culture, and slide-culture. The scanning electron microscope revealed that the infected hairs were destroyed by abundant fungus (Fig. 2). The boy was cured after receiving 4 weeks of systemic treatment with itraconazole 125 mg per day and topical treatment with 1% naftifine–0.25% ketaconazole cream, after wash with 2% ketaconazole shampoo once a day.

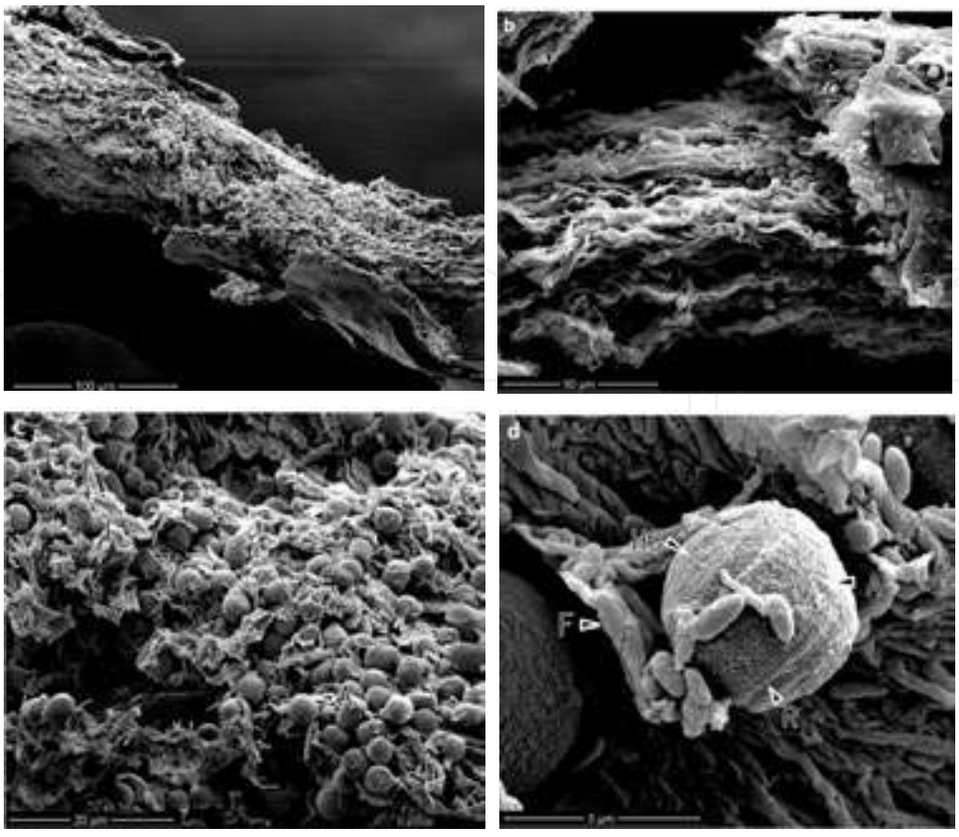

Figure 2. a-b. Cuticle layers of hair shaft were seriously destroyed and a large part had been lost, exposing the fibril cortex inside which many arthrospores were noted. c. High magnification of "a" showing the cuticle layers completely destroyed with the residual cortex fully filled with arthroconidia (A) and distorted fibril bundles (F). d. An arthrospore (A) at high magnification showing irregular convex granules on the chitinous surfaces and the poles bordered by a protruding ring structure (R), bulged by a hemispherical convex (HC). Numerous residual fibril fragments (F) noted around the spore as well as on its surface.

Figure 2. a-b. Cuticle layers of hair shaft were seriously destroyed and a large part had been lost, exposing the fibril cortex inside which many arthrospores were noted. c. High magnification of "a" showing the cuticle layers completely destroyed with the residual cortex fully filled with arthroconidia (A) and distorted fibril bundles (F). d. An arthrospore (A) at high magnification showing irregular convex granules on the chitinous surfaces and the poles bordered by a protruding ring structure (R), bulged by a hemispherical convex (HC). Numerous residual fibril fragments (F) noted around the spore as well as on its surface.

The second patient is a 5-year-old boy in good health, weighing 19 kg and presented at our clinic with a 1-month history of excessive scales and hair loss on the scalp (Fig. 3a). He had been previously diagnosed with tinea capitis in a local hospital, and received oral itraconazole 100 mg per day for 14 days administered with water. However, the area of hair loss enlarged slightly. Additionally, he had a history of direct contact with a pet dog. Direct microscopic examination (with 10% KOH) of broken hair strands showed numerous spores inside as well as outside of the hair strand. Simultaneously, strands were observed under SEM, and there were many round spores in and around the hair strand (Fig. 4a, b). Fungal culture revealed yellow filamentous colonies, which were identified as *Microsporum canis* with ITS1/4-PCR, sequence-based molecular validation (Accession Number: KT003284). A diagnosis of tinea capitis caused by *Microsporum canis* was confirmed. According to his weight, the boy was treated with itraconazole using the same dose as before, but in this course each dose was administered with whole milk instead with water before. After the 14-day course, clinic assessments showed the hair loss area was smaller and without scales (Fig. 3b). With the same examinations as before, only a few spores were detectable by direct microscopic examination. The number of spores was markedly reduced in hair strands, and

The second patient is a 5-year-old boy in good health, weighing 19 kg and presented at our clinic with a 1-month history of excessive scales and hair loss on the scalp (Fig. 3a). He had been previously diagnosed with tinea capitis in a local hospital, and received oral itraconazole 100 mg per day for 14 days administered with water. However, the area of hair loss enlarged slightly. Additionally, he had a history of direct contact with a pet dog. Direct microscopic examination (with 10% KOH) of broken hair strands showed numerous spores inside as well as outside of the hair strand. Simultaneously, strands were observed under SEM, and there were many round spores in and around the hair strand (Fig. 4a, b). Fungal culture revealed yellow

http://dx.doi.org/10.5772/61850

round spores were now very irregular under SEM (Fig. 4c, d). The boy continued therapy for a total of 40 days. Clinical assessment of the treatment showed that there was no apparent hair loss and all of the same examinations now appeared to be normal (Fig. 3c). Upon clinical examination during the follow-up after 3 months, there was no recurrence following the end of the treatment [4].

Figure 3. a. A 5-year-old boy presented with 1-month history of scalp scales and hair loss, who had received oral itraconazole 100 mg per day with water for 14 days; b. The patch with hair loss was smaller and without scale after oral itraconazole 100 mg per day with whole milk for 14 days; c. There was no apparent hair loss on scale after 40 days at end of treatment.

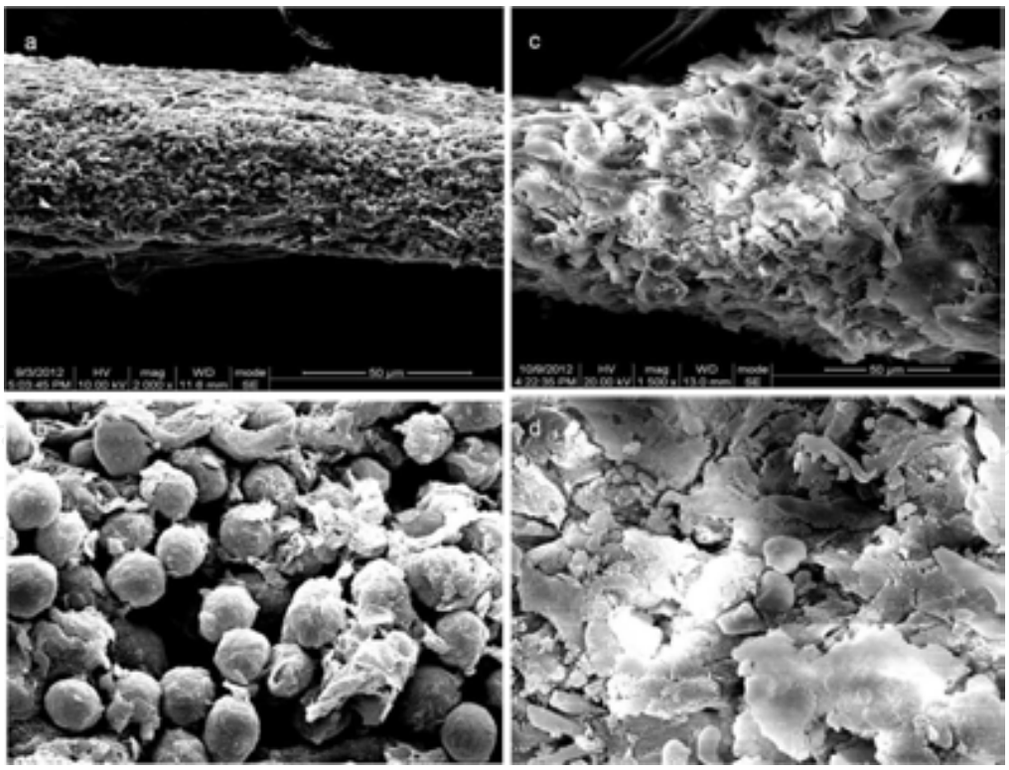

Figure 4. a-b. After oral itraconazole 100 mg per day with water for 2 weeks, broken hair strands with many round spores in and around the hair strands were evident under scanning electron microscopy (SEM); c-d. Oral itraconazole 100 mg per day with whole milk for 14 days, the number of spores were markedly reduced in broken hair strands, and spores appeared very irregular under SEM.

3.2. *Malassezia* folliculitis (*Pityrosporum* folliculitis)

Malassezia folliculitis is most commonly seen in teenagers and adults, which is characterized by pruritic, monomorphic follicular papules and pustules on the upper trunk, arms, neck and occasionally on the face. It is due to excessive growth of *Malassezia* spp. within the hair follicle, with resulting inflammation (from yeast products and free fatty acids produced by fungal lipase). Only yeast forms are observed, no hyphal forms as in pityriasis versicolor [5]. Diagnostic studies include microscopic evaluation of the presence of yeast, cultures, and biopsies. Additionally, Woods lamp can be used to illuminate the lesions, which portray a yellow-green fluorescence. Both topical and oral antifungal agents are effective agents in the treatment of *Malassezia* folliculitis and are commonly combined to hasten resolution and maintain clearance. Topical regimens include daily wash with ketoconazole shampoo 2%, then 1% naftifine-0.25% ketaconazole cream. For severe cases, it needs systemic administration of antifungal agents. Commonly used regimens include oral fluconazole 150 mg weekly for 2–4 weeks, and itraconazole 200 mg daily for 2–4 weeks [6].

The following is a case of *Malassezia* folliculitis due to *Malassezia* spp. The patient is a 25-year-old man, who was presented to our clinic because of slightly pruritic, monomorphic follicular papules and pustules on the upper trunk and neck (Fig. 5a). The diagnosis of *Malassezia* folliculitis was established by direct microscopic examination, culture, and scanning electron microscopy. The scanning electron microscope of the hair follicle from the upper trunk revealed a large number of yeast of two kinds, orbicular-ovate and globular (Fig. 5 b-c). The man was cured after receiving 4 weeks of systemic treatment with itraconazole 200 mg per day and topical treatment with 1% naftifine–0.25% ketaconazole cream after wash with 2% ketaconazole shampoo once a day.

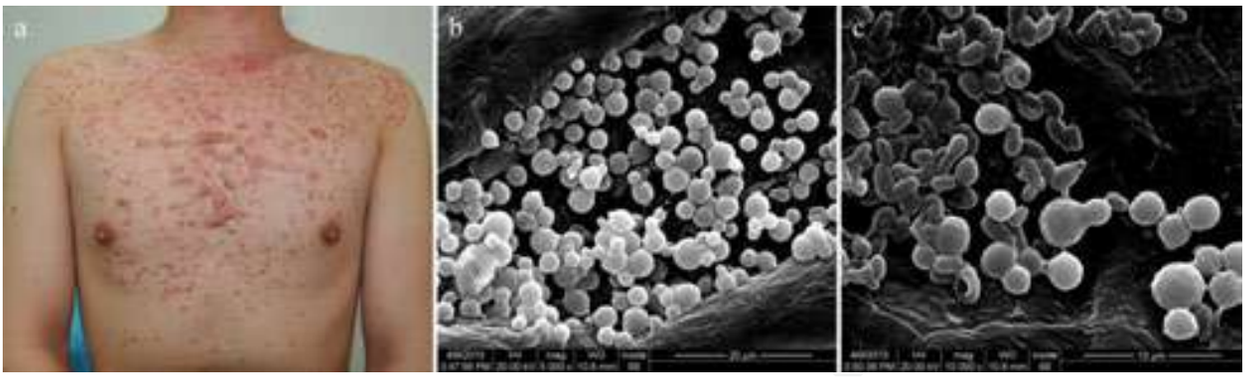

Figure 5. a. A 25-year-old man with complains of slightly pruritic, monomorphic follicular papules, pustules, and secondary keloid on the upper trunk and neck. b-c. SEM of the hair follicle from the upper trunk. These demonstrated a large number of globular or orbicular-ovate yeasts of budding daughter cell, with collar structure around the budding. b. Globular yeast. c. Orbicular-ovate and globular yeast in the same sample.

3.3. Pityriasis versicolor

Pityriasis versicolor is a superficial fungal infection of the skin and caused by *Malassezia*, a lipophilic yeast, which is part of the normal skin flora. Certain environmental, genetic, and

http://dx.doi.org/10.5772/65256

a more lipid-rich environment for *Malassezia* to grow. Adolescents and young adults who are physically active are also susceptible populations [9].

immunological factors can lead to the development of disease [7]. The prevalence is as high as 50% in tropical areas [8]. Prevalence increases significantly in childhood and adolescence, probably because of increased sebum production, which allows for a more lipid-rich environment for *Malassezia* to grow. Adolescents and young adults who are physically active are also susceptible populations [9].

This is a case of pityriasis versicolor due to *Malassezia* spp. A 27-year-old man was presented to our clinic with extensive erythema and scaly for 6 months (Fig. 6a). The scaly was scraped and observed through SEM. Under SEM, numerous hyphae and spores that resemble "banana and grapes" (Fig. 6b and c). Treatment with oral itraconazole 200 mg bid and topical use of 1% naftifine–0.25% ketoconazole cream after wash with ketoconazole shampoo was effective.

This is a case of pityriasis versicolor due to *Malassezia* spp. A 27-year-old man was presented to our clinic with extensive erythema and scaly for 6 months (Fig. 6a). The scaly was scraped and observed through SEM. Under SEM, numerous hyphae and spores that resemble "banana and grapes" (Fig. 6b and c). Treatment with oral itraconazole 200 mg bid and topical use of 1% naftifine–0.25% ketoconazole cream after wash with ketoconazole shampoo was effective.

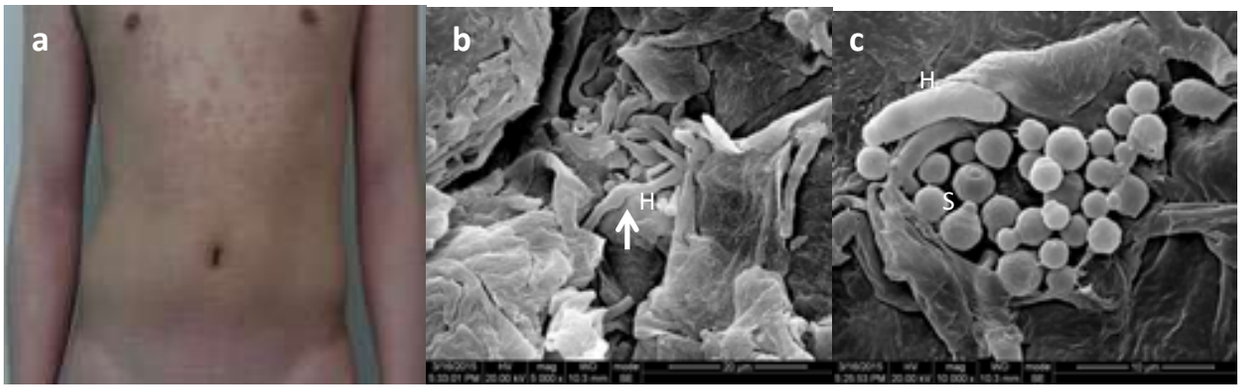

Figure 6. a. A 27-year-old man presented in our clinic with extensive erythema and scaly for 6 months. b. Under SEM, numerous hyphae (H) went through the scaly, length of which is about 10–20 μm. c. Under SEM, abundant of 3–5 μm in diameter grapes-like spherical *Malassezia* spores (S) with budding daughter cell, with collar structure around the budding, and banana-like haphae (H).

Figure 6. a. A 27-year-old man presented in our clinic with extensive erythema and scaly for 6 months. b. Under SEM, numerous hyphae (H) went through the scaly, length of which is about 10–20 μm. c. Under SEM, abundant of 3–5 μm in diameter grapes-like spherical *Malassezia* spores (S) with budding daughter cell, with collar structure around the budding, and banana-like haphae (H).

3.4. Mucormycosis

Mucormycosis is a clinically rare and fatal opportunistic fungal infection, which invades nasal, brain, lung, gastrointestinal tract, skin, and other parts with acute, subacute, or chronic process. The routes of invasion contain respiratory tract, digestive tract, skin, and neonatal umbilical region [10]. Its pathogens are fungi in the order *Mucorales*, usually species in the genera *Mucor*, *Rhizopus*, and *Lichtheimia* (*Absidia*), such as *Mucor irregularis*, *Rhizopus stolonifer*, and *Lichtheimia corymbifera*. *M. irregularis* is a newly recognized fungal pathogen described in China [10]. Amphotericin B and its lipid derivatives are considered as the effective drugs to treat mucormycosis.

3.4. Mucormycosis

Mucormycosis is a clinically rare and fatal opportunistic fungal infection, which invades nasal, brain, lung, gastrointestinal tract, skin, and other parts with acute, subacute, or chronic process. The routes of invasion contain respiratory tract, digestive tract, skin, and neonatal umbilical region [10]. Its pathogens are fungi in the order *Mucorales*, usually species in the genera *Mucor*, *Rhizopus*, and *Lichtheimia* (*Absidia*), such as *Mucor irregularis*, *Rhizopus stolonifer*, and *Lichtheimia corymbifera*. *M. irregularis* is a newly recognized fungal pathogen described in China [10]. Amphotericin B and its lipid derivatives are considered as the effective drugs to treat mucormycosis.

The following is a description of two cases of primary cutaneous mucormycosis caused by *Mucor irregularis* [10] and *Lichtheimia corymbifera* [11], respectively. One of the cases is of a 47-year-old farmer, who presented to our clinic with a history of progressive red plaque around the inner canthus (Fig. 7a), following dacryocystectomy about a year earlier. Linear, aseptate hyphae were seen by direct KOH examination and in biopsy. Fungal culture re-

presented to our clinic with a history of progressive red plaque around the inner canthus (Fig. 7a), following

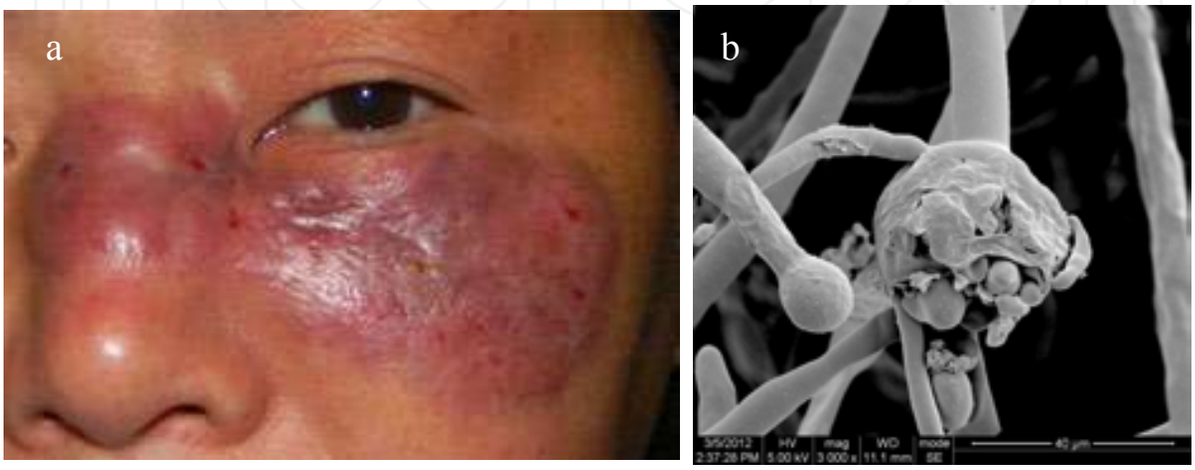

Figure 7. a. A 47-year-old farmer was presented to our clinic with 1-year history of progressive red plaque around the inner canthus. Faint yellow exudation was oozing from the ulceration at the center of plaque. Some scales were also observed on the plaque. b. SEM observations revealed non-apophysate sporangia with pronounced columellae and conspicuous collarette at the base of the columella following sporangiospore dispersal.

The other case is of a 69-year-old female farmer, who presented to our clinic with the history of a progressive purulent granuloma of her left forearm (Fig. 8a) following a fracture of left forearm about 11 months earlier. Broad, nonseparate hyphae were seen in pathologic study with methenamine silver stain (Fig. 8b). Fungal culture revealed white filamentous colonies that were identified as *Lichtheimia corymbifera* by nucleotide sequencing of rRNA gene. The scanning electron microscope showed that the sporangia are slightly pear-shaped instead of spherical. The sporangiophores of *Lichtheimia corymbifera* formed a conical apophysis and

Figure 7. A 47-year-old farmer was presented to our clinic with 1-year history of progressive red plaque around the inner canthus. Faint yellow exudation was oozing from the ulceration at the center of plaque. Some scales were also observed on the plaque. b. SEM observations revealed non-apophysate sporangia with pronounced columellae and conspicuous collarette at the base of the columella following sporangiospore dispersal.

Antimicrobial susceptibility test indicated that *Lichtheimia corymbifera* is most sensitive to terbinafine and itraconazole. The patient was discharged after 6 weeks of treatment of oral intraconazole with surgery [11].

3.5. Cutaneous alternariosis

Alternaria, an opportunistic fungus, is pigmented (also known as dematiaceous or phaeoid) filamentous fungi, which are well-known soil saprophytes and plant pathogens that infrequently cause infection in humans. Although *Alternaria* usually infects immunocompromised patients [12], in rare cases it infects healthy or immunocompetent individuals as well.

The other case is of a 69-year-old female farmer, who presented to our clinic with the history of a progressive purulent granuloma of her left forearm (Fig. 8a) following a fracture of left forearm about 11 months earlier.

http://dx.doi.org/10.5772/61850

susceptibility test indicated that *Lichtheimia corymbifera* is most sensitive to terbinafine and itraconazole. The patient was cured after 6 weeks of therapeufil alliance of oral intraconazole with surgery [11].

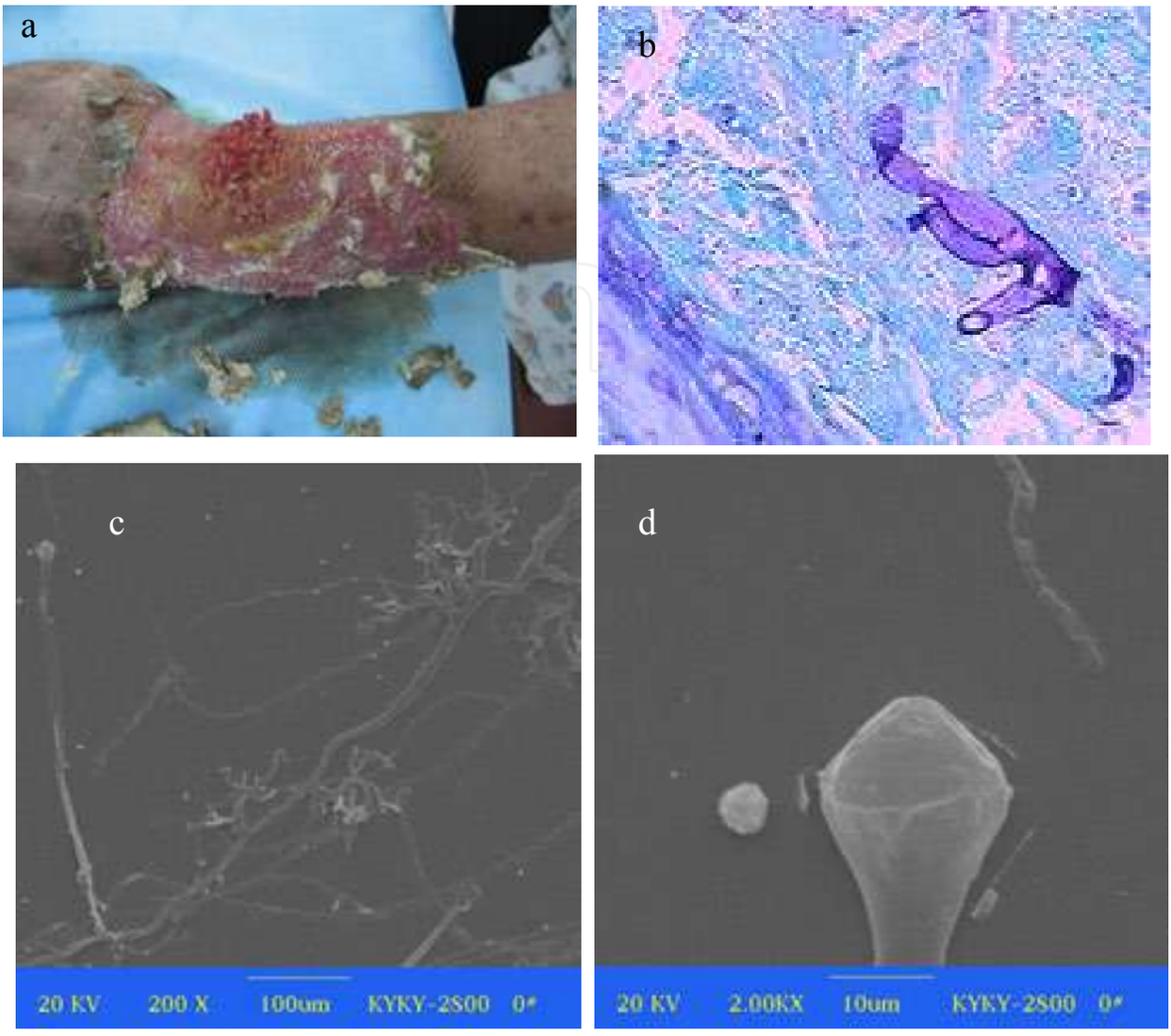

Figure 8. a. A 69-year-old female was presented to our clinic with a progressive purulent granuloma of her left forearm. b. Broad nonseparate hyphae were seen in pathologic study (methenamine silver stain, ×200). c-d. The sporangiophores of *Lichtheimia corymbifera* forming a conical apophysis and arising at points on the stolon that was between the rhizoid and not opposite them. SEM showed the sporangia were slightly pear-shaped instead of spherical (20kv, ×2000).

Figure 8. a. A 69-year-old female was presented to our clinic with a progressive purulent granuloma of her left forearm. b. Broad nonseparate hyphae were seen in pathologic study (methenamine silver stain, ×200). c-d. The sporangiophores of *Lichtheimia corymbifera* forming a conical apophysis and arising at points on the stolon that was between the rhizoid and not opposite them. SEM showed the sporangia were slightly pear-shaped instead of spherical (20kv, ×2000).

There is no standard therapy for cutaneous alternariosis and the patients are usually treated with surgical resection and/or antifungal therapy.

We described the case of a healthy individual with cutaneous alternariosis due to infection with *Alternaria arborescens* [13]. A 28-year-old man presented at our clinical with a one-month history of ulcers covered with crust on his left anterior tibial (Fig. 9a). Fungal culture of the tissue revealed dark grey-white colonies with a dark-brown underside (Fig. 9b) and the SEM observation of the slide culture revealed beaked conidia (Fig. 9c). Based on the morphological features and molecular identification, the patient was diagnosed as cutaneous alternariosis. He was successfully treated with oral itraconazole and topical wet dressing of amphotericin B.

3.5. Cutaneous alternariosis

Alternaria, an opportunistic fungus, is pigmented (also known as dematiaceous or phaeoid) filamentous fungi, which are well-known soil saprophytes and plant pathogens that infrequently cause infection in humans.

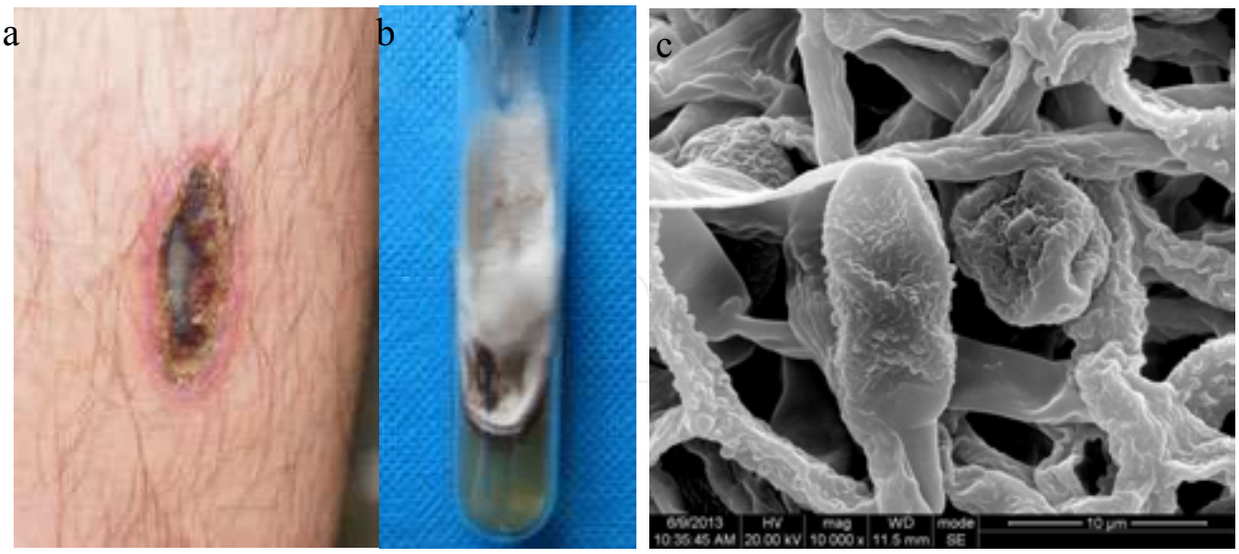

Figure 9. a. Ulcer with an overlying crust on the patient's skin of left anterior tibia. b. Fungal culture of the tissue revealed dark grey-white colonies with a dark-brown underside. c. SEM observation of slide culture revealed beaked conidia.

Figure 9. a. Ulcer with an overlying crust on the patient's skin of left anterior tibia. b. Fungal culture of the tissue revealed dark grey-white colonies with a dark-brown underside. c. SEM observation of slide culture revealed beaked conidia.

3.6. Chromoblastomycosis

3.6. Chromoblastomycosis

Chromoblastomycosis is a chronic fungal infection of the skin and subcutaneous tissue caused by dematiaceous fungi. Common pathogenic fungi are *Fonsecaea pedrosoi*, *Phialophora verrucosa*, *Cladophialophora carrionii*, among others. These fungi exist in the natural environment in soil, water, vegetation, or wood splinters, and usually are inoculated in the skin tissue of human body by a traumatic injury. A higher incidence is reported in tropical and subtropical countries. Cutaneous lesions can be nodules, papules, and/or ulcerations and mostly affect the lower limbs. The diagnosis of chromoblastomycosis is based on direct examination, culture, and histopathology. On treatment, long courses of antifungal agents such as itraconazole, terbinafine can be used alone or in combination with surgical excision and physical treatments (cryotherapy or, mostly, thermotherapy). However, long duration of treatment is needed and cure rate of the disease is low [14].

In this part we describe a case of chromoblastomycosis due to *Fonsecaea pedrosoi*. A 34-year-old male presented at our clinic with a 12-year history of red plaque in the left knee (Fig. 10a). The patient's left knee was punctured by a fragment of a brick 12 years ago. The pathogenic fungus was isolated and identified as *Fonsecaea pedrosoi*. SEM observation: dematiaceous hyphae with many well-defined septa, conidiophores and oval brown spores arranged in a clump could be seen. The surfaces of conidiogenous cells were smooth. Oval spores were arranged around conidiophores (Fig. 10b). The patient was diagnosed as chromoblastomycosis and was treated with oral terbinafine 250 mg twice a day and thermotherapy with a small electronic heating pad (42°C, more than one hour per day) after applying topical cream containing 1% naftifine hydrochloride and 0.25% ketoconazole. The total course was 61 weeks. The crust and pruritus had disappeared and the erythema and plaque had turned smooth and soft.

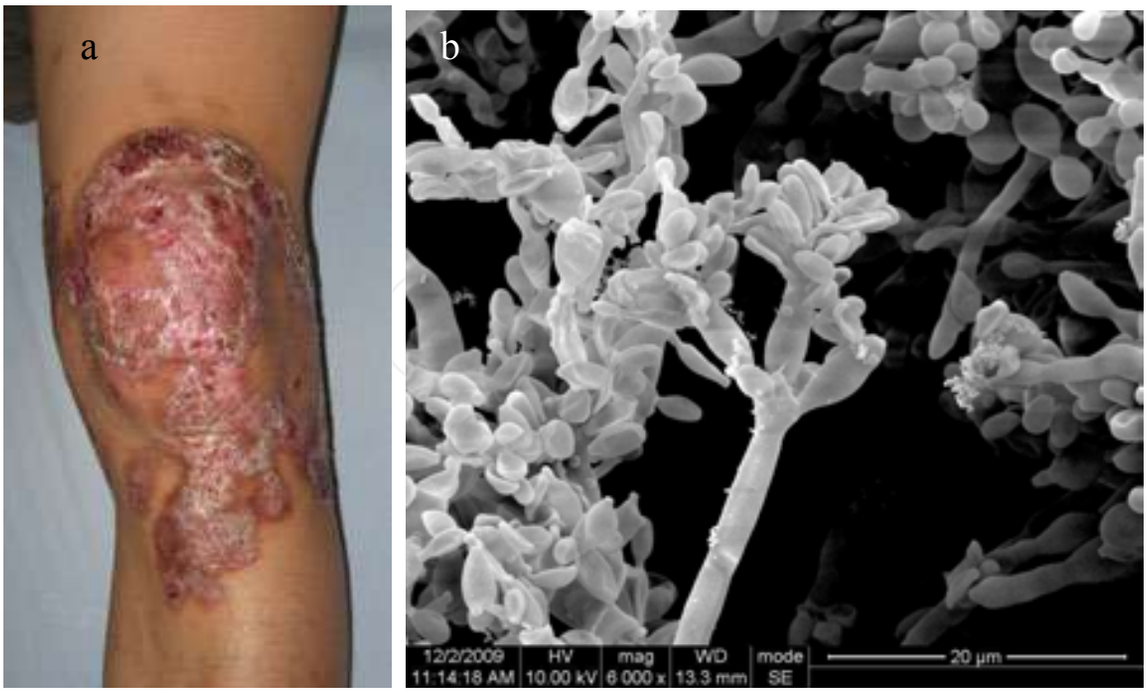

Figure 10. a. A 34-year-old male with a 12-year history of a red plaque in the left knee. b. Under SEM observation: dematiaceous hyphae with many well-defined septa, conidiophores, and oval brown spores arranged in a clump could be seen. The surfaces of conidiogenous cells were smooth. Oval spores were arranged around conidiophores.

observation: dematiaceous hyphae with many well-defined septa, conidiophores, and oval brown spores arranged in a clump could be seen. The surfaces of conidiogenous cells were smooth. Oval spores were arranged around conidiophores.

3.7. Primary laryngeal aspergillosis

Primary laryngeal aspergillosis is a rare opportunistic infection caused by *Aspergillus*. All causes leading to immunocompromisation are generally due to etiological factors [15]. For immunocompetent patients, oral sex (fellatio) may be the primary cause [16]. Airborne spore colonizes in the larynx through inhalation, then white colony grows on vocal cords or/and laryngeal ventricle. It is characterized by chronic hoarseness, with or without systemic or respiratory symptoms involving fever, cough, and tachypnea. It is usually diagnosed by laryngoscopy and biopsy. Systemic antifungal treatment is often effective.

3.7. Primary laryngeal aspergillosis

Primary laryngeal aspergillosis is a rare opportunistic infection caused by *Aspergillus*. All causes leading to immunocompromisation are generally due to etiological factors [15]. For immunocompetent patients, oral sex (fellatio) may be the primary cause [16]. Airborne spore colonizes in the larynx through inhalation, then white colony grows on vocal cords or/and laryngeal ventricle. It is characterized by chronic hoarseness, with or without systemic or respiratory symptoms involving fever, cough, and tachypnea. It is usually diagnosed by laryngoscopy and biopsy. Systemic antifungal treatment is often effective.

We describe in the following a case of primary laryngeal aspergillosis due to *Aspergillus fumigatus*. The patient was a 23-year-old female undergraduate student, who presented with hoarseness, severe paroxysmal coughing, and tachypnea. Laryngoscopy revealed obvious white plaques on the swollen vocal cords and laryngeal ventricle (Fig. 11a). The diagnosis of laryngeal aspergillosis was established by the clinical manifestations and the hyphae branching at 45° angles under microscopy, SEM (Fig. 11b), and pathology. She was cured with oral itraconazole at 200 mg twice a day for 28 days.

3.8. Acne

Acne is a chronic inflammatory disease of the sebaceous–pilosebaceous system. It is estimated to affect 9.4% of the global population [17]. Acne is closely related to the combination of genetic and environmental factors, among which *Propionibacterium acnes* (*P. acnes*) plays a

Figure 11. a. A 32-year-old female undergraduate student presented with hoarseness, severe paroxysmal coughing, and tachypnea. Laryngoscopy revealed obvious white plaques on the swollen vocal cords and laryngeal ventricle. b. SEM of the biopsy tissue revealed hyphae branching at 45° angles destroyed the vocal cords tissue.

device and surgery infections caused by *P. acnes* have also been reported. Strains of *P. acnes* have been classified into several different types [19].

3.8. Acne

Acne is a chronic inflammatory disease of the sebaceous–pilosebaceous system. It is estimated to affect 9.4% of the global population [17]. Acne is closely related to the combination of genetic and environmental factors, among which *Propionibacterium acnes* (*P. acnes)* plays a prominent role [18]. Gram-positive anaerobic bacterium *P. acne* is a major commensal of the follicular plug in human skin. Other diseases such as medical device and surgery infections caused by *P. acnes* have also been reported. Strains of *P. acnes* have been classified into several different types [19].

The following is a description of a case of acne in a 24-year-old girl. She suffered recurrent papule and pustuleacne for 6 months (Fig. 12a-b). We removed the follicular plug with sterile hemostatic forceps and observed it through SEM. Under SEM, abundant rod-shaped bacteria were closely spaced in follicular plug tissue (Fig. 12c). Treatment with oral minocycline 50 mg twice a day and topical use of adapalene gel was effective.

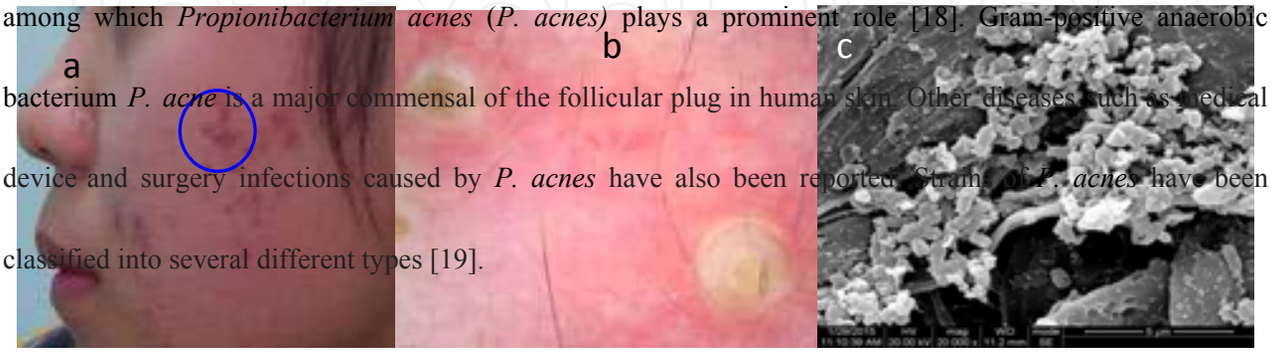

Figure 12. a. A 24-year-old girl who suffered recurrent papule and pustule acne for 6 mouths. b. Under the dermoscopy, the papule was semisphere with tawny follicular plug inside. c. Under SEM, rod-shaped bacteria were closely spaced in follicular plug tissue.

Figure 12. a. A 24-year-old girl who suffered recurrent papule and pustule acne for 6 mouths. b. Under the dermoscopy, the papule was semisphere with tawny follicular plug inside. c. Under SEM, rod-shaped bacteria were closely spaced in follicular plug tissue.

The following is a description of a case of acne in a 24-year-old girl. She suffered recurrent papule and pustuleacne for 6 months (Fig. 12a-b). We removed the follicular plug with sterile hemostatic forceps and observed it through SEM. Under SEM, abundant rod-shaped bacteria were closely spaced in follicular plug tissue (Fig. 12c). Treatment with oral minocycline 50 mg twice a day and topical use of adapalene gel was effective.

3.9. Pediculosis

Pediculosis is a skin disease caused by arthropods. Its pathogens are three lice species including head louse,

http://dx.doi.org/10.5772/61850

3.9. Pediculosis

Pediculosis is a skin disease caused by arthropods. Its pathogens are three lice species including head louse, crab or pubic louse, and body louse, which cause the *Pediculus humanus capitis, Phthirus pubis*, and *Pediculus humanus corpus,* respectively. These three insects are obligate human parasites. They are transmitted by person-to-person contact [20]. Itching in various levels of severity is the primary symptom of pediculosis. Crab louse is about 0.8–1.2 mm in length. Its legs are clawed, except for the first pair, which is shortened and vestigial. In contrast to the oval shape of head and body lice, the crab louse is almost as wide as its length, allowing it to grasp widely spaced pubic hairs [21]. Its crab appearance accounts for its name. Patients with pubic lice may be instructed to launder clothing and bedding and to avoid sexual or other intimate contact until their infestations are cured [22]. In case of infestation of head with pubic lice, the head can be shaved totally and then treated with an occlusive agent such as Vaseline petroleum jelly.

We describe a case of pediculosis on the scalp of a 6-year-old boy caused by the crab louse [23]. The boy was presented to our clinic with the complaint of intense itching of the scalp. There were some small pieces of erythema (in the circle) and a brown dot-like substance on his scalp (Fig. 13a). The dermoscopy revealed a brown parasite (0.9 mm in horizontal axes and 1.2 mm in vertical axes) with two crab-like feet adhered to the scalp (Fig. 13b). Microscopic examination and scanning electron microscope showed the detail of this insect (Fig. 13c-d). Based on these morphological findings, the diagnosis of *Pediculus humanus capitis* caused by crab louse is confirmed. Generally, pediculus humanus capitis is caused by head louse, rarely by crab louse. Where could this pathogen, crab louse, be from? After a detailed inquiry, his father was found to have pediculosis pubis that had been cured. Therefore, the boy was instructed to shave the head totally and then treated with an insecticidal tincture, which was administered to his parents as well. The boy was cured after 15 day of treatment.

3.10. Demodiciosis

Demodiciosis is a kind dermatitis caused by *Demodex*. It often presents some rosacea-1ike lesions. *Demodex* is a genus of tiny parasitic mites that live in or near hair follicles of mammals. Currently, about 65 species of *Demodex* are known [24]. Two species living on humans have been identified: *Demodex folliculorum* and *Demodex brevis*, both frequently referred to as eyelash mites [25]. The adult mites are 0.3–0.4 mm long, and 0.012–0.016 mm in diameter, with *D. brevis* slightly shorter than *D. folliculorum* [26]. Each has a semitransparent, elongated body that consists of two fused segments. Eight short, segmented legs are attached to the first body segment. The body is covered with scales for anchoring itself in the hair follicle, and the mite has pin-like mouth for eating skin cells and sebum, which accumulate in the hair follicles. The mites can leave the hair follicles and slowly walk around on the skin, at a speed of 8–16 mm per hour, especially at night, as they try to avoid light [26]. In most of the cases, the mites go unobserved, without any symptoms, but in certain cases (usually related to a disordered immune system) mite populations can dramatically increase, resulting in a condition known as *demodicosis* or *demodex mite* bite, characterized by itching, inflammation, and other skin disorders.

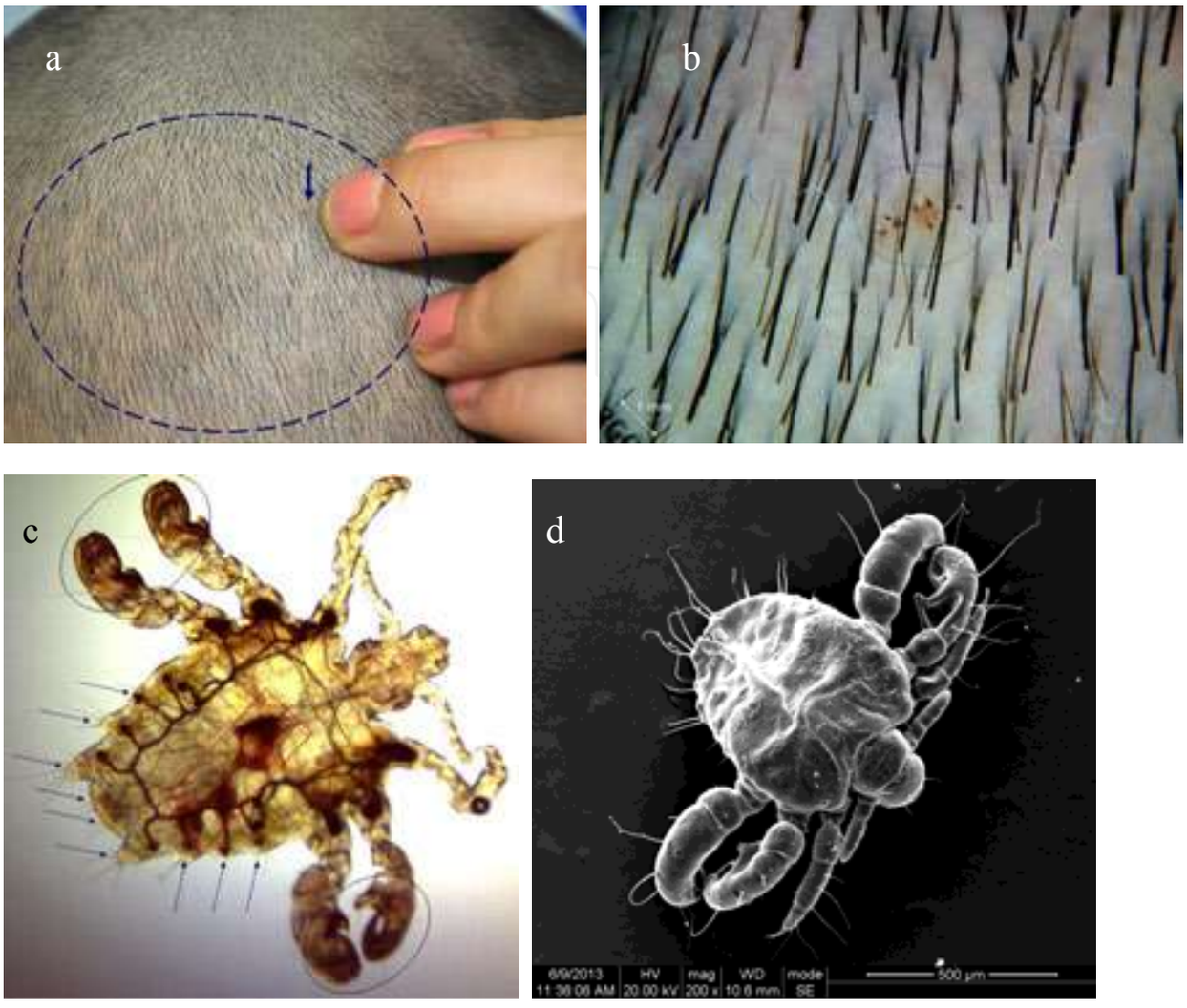

Figure 13. a. There were some small pieces of erythema (in the circle) and a brown dot-like substance on the scalp (arrow). b. The dermoscopy revealed a brown parasite (0.9 mm in horizontal axes and 1.2 mm in vertical axes) with two crab-like feet adhered to the scalp. c. Under the microscope, the parasite was characterized by a flat body like a crab and three pairs of feet in different sizes. There was an area (red box) full of blood in the middle part of the parasite. A large number of short setae (arrow) were noted at the edge of the parasite abdomen. d. The SEM showed a vivid three-dimensional ultrastructure of the parasite; the whole body was composed of three parts including spherical head, chest, and elliptical abdomen; a pair of feelers was noted on the head; the three pairs of feet were in shaped section and curved serrated claws were noted at the end of foot; short setae in different length were not only at the edge of the abdomen but also on the feet.

The following is a description of a case of demodicosis due to *Demodex mites*. The patient is a 28-year-old man, who came to our clinic because of itching, multiple erythema, papules, pustules lesions on the nose and cheek (Fig. 14a). The diagnosis of demodicosis caused by *Demodex mites* was established by direct microscopic examination. The observation of SEM revealed that the parasite consists of two segments. There were four pairs of feet on the side of the head of the parasite and its abdomen was characterized by annular striae on the surface (Fig. 14b). The man was cured after receiving 6 months of topical treatment with 7% albendazole cream once a day.

3.10. Demodiciosis

Demodiciosis is a kind dermatitis caused by *Demodex*. It often presents some rosacea-1ike lesions. *Demodex*

http://dx.doi.org/10.5772/61850

Figure 14. a. A 28-year-old man came to our clinic because of itching, multiple erythema, papules, pustules lesions on the nose and cheek. b. SEM revealed a *Demodex folliculorum*, approximately 0.33 mm in length, in the infected skin. Its elongated body consisted of two segments. There were four pairs of feet on the side of the head of the parasite, and its abdomen was characterized by annular striae on the surface.

Figure 14. a. A 28-year-old man came to our clinic because of itching, multiple erythema, papules, pustules lesions on the nose and cheek. b. SEM revealed a *Demodex folliculorum*, approximately 0.33 mm in length, in the infected skin. Its elongated body consisted of two segments. There were four pairs of feet on the side of the head of the parasite, and its abdomen was characterized by annular striae on the surface.

Author details

Ran Yuping[1*], Zhuang Kaiwen[1], Hu Wenying[1], Huang Jinghong[1], Feng Xiaowei[1], Chen Shuang[1], Tang Jiaoqing[1], Xu Xiaoxi[1], Kang Daoxian[1], Lu Yao[1], Zhang Ruifeng[1], Ran Xin[1], Wan Huiying[1], Lama Jebina[1], Dai Yalin[2] and Zhang Chaoliang[3]

*Address all correspondence to: ranyuping@vip.sina.com

1 Department of Dermatovereology, West China Hospital, Sichuan University, Chengdu, China

2 Department of Medical laboratory, West China Hospital, Sichuan University, Chengdu, China

3 State Key Laboratory of Oral Diseases, West China Hospital of Stomatology, Sichuan University, Chengdu, China

References

[1] Ellabib MS, Agaj M, Khalifa Z, Kavanagh K. *Trichophyton violaceum* is the dominant cause of tinea capitis in children in Tripoli, Libya: Results of a two year survey. *Mycopathologia*. 2001; 153: 145-147.

[2] Yu J, Li R, Bulmer G. Current topics of tinea capitis in China. *Jpn J Med Mycol*. 2005; 46: 61-66.

[3] Zhuang K, Ran X, Lei S, Zhang C, Lama J, Ran Y. Scanning and transmission electron microscopic observation of the parasitic form of *Trichophyton violaceum* in the infected hair from tinea capitis. *Scanning*. 2014; 36: 465-470.

[4] Chen S, Ran Y, Dai Y, Lama J, Hu W, Zhang C. Administration of oral itraconazole capsule with whole milk shows enhanced efficacy as supported by scanning electron microscopy in a child with tinea capitis due to *Microsporum canis*. *Pediatric Dermatology*. 2015; 32:e312–e313

[5] Rubenstein RM, Malerich SA. *Malassezia* (*Pityrosporum*) folliculitis. *J Clin Aesthet Dermatol*. 2014; 7: 37-41.

[6] Hald M, Arendrup MC, Svejgaard EL, Lindskov R, Foged EK, Saunte DM. Evidence-based Danish guidelines for the treatment of *Malassezia*-related skin diseases. *Acta Derm Venereol*. 2015; 95: 12-19.

[7] Renati S, Cukras A, Bigby M. Pityriasis versicolor. *BMJ*. 2015; 350: 1394-1400.

[8] Kaushik A, Pinto HP, Bhat RM, Sukumar D, Srinath MK. A study of the prevalence and precipitating factors of pruritus in pityriasis versicolor. *Ind Dermatol Online J*. 2014; 5: 223-224.

[9] Kyriakis KP, Terzoudi S, Palamaras I, Pagana G, Michailides C, Emmanuelides S. Pityriasis versicolor prevalence by age and gender. *Mycoses*. 2006; 49: 517-518.

[10] Kang D, Jiang X, Wan H, Ran Y, Hao D, Zhang C. *Mucor irregularis* Infection around the inner canthus cured by amphotericin B: A case report and review of published literatures. *Mycopathologia*. 2014; 178: 129-133.

[11] Lu W, Lu J, Ran Y, Lin Z, Wan H, Cui F, Cao L, Pan N, Song X, Chen J, Wanf Y, Yu M. Cutaneous and subcutaneous coinfection by *Lichtheimia corymbifera* and *Candida parapsilosis*: a case report. *Chin J Dermatol*. 2012; 45(10):727-730. (in Chinese)

[12] Anaissie EJ, Bodey GP, Rinaldi MG. Emerging fungal pathogens. *Eur J Clin Microbiol Infect Dis*. 1989; 8: 323-330.

[13] Hu W, Ran Y, Zhuang K, Lama J, Zhang C. *Alternaria arborescens* infection in a healthy individual and literature review of cutaneous alternariosis. *Mycopathologia*. 2015; 179: 147-152.

[14] Krzyściak PM, Pindycka-Piaszczyńska M, Piaszczyński M. Chromoblastomycosis. *Adv Dermatol Allergol/Postepy Dermatologii i Alergologii*. 2014;31(5):310-321. doi: 10.5114/pdia.2014.40949.

[15] Ran Y, Yang B, Liu S, Dai Y, Pang Z, Fan J, Bai H, Liu S. Primary vocal cord aspergillosis caused by *Aspergillus fumigatus* and molecular identification of the isolate. *Med Mycol*. 2008; 46: 475-479.

[16] Ran Y, Li L, Cao L, Dai Y, Wei B, Zhao Y, Liu Y, Bai H, Zhang C. Primary vocal cord aspergillosisand scanning electron microscopical observation of the focus of infection. Mycoses 2011;54:e634-637.

[17] Ran Y, Lu Y, Cao L. Primary laryngeal aspergillosis related to oral sex? A case report and review of the literature. *Med Mycol Case Rep*. 2013; 2: 1-3.

[18] Tan JK, B Ran Y, Lu Y, Cao L.hate K. A global perspective on the epidemiology of acne. *Br J Dermatol*. 2015; 172; Suppl 1: 3-12.

[19] Antiga E, Verdelli A, Bonciani D, Bonciolini V, Caproni M, Fabbri P. Acne: a new model of immune-mediated chronic inflammatory skin disease. *G Ital Dermatol Venereol*. 2015; 150: 247-254.

[20] Yu Y, Champer J, Garbán H, Kim J. Typing of *Propionibacterium acnes*: a review of methods and comparative analysis. *Br J Dermatol*. 2015; 172: 1204-1209.

[21] David C, Flinders, Peter DS. Pediculosis and scabies. *Am Fam Physician*. 2004;69: 341-348.

[22] Ko CJ, Elston DM. Pediculosis. *J Am Acad Dermatol*. 2004, 50: 1-12.

[23] Gunning K, Pippitt K, Kiraly B, Sayler M. Pediculosis and scabies: treatment update. Am Fam Physician. 2012; 15: 535-541.

[24] Ran Y, Feng X, Zhuang K, Zhang C. Dermatoscopy, microscopy and scanning electron microscopy diagnosed scalp pediculosis pubis in a child. *J Clin Dermatol*. 2014;43(12):725-726. (in Chinese)

[25] Rusiecka-Ziółkowska J, Nokiel M, Fleischer M. Demodex – an old pathogen or a new one? *Adv Clin Exp Med*. 2014; 23: 295-298.

[26] Elston CA, Elston DM. Demodex mites. *Clin Dermatol*. 2014; 32: 739-743.

[27] Rufli T, Mumcuoglu Y. The hair follicle mites *Demodex folliculorum* and *Demodex brevis* – biology and medical importance: a review. *Dermatologica*. 1981;162:1-11.

IntechOpen

Chapter 13

Development of Myeloid Dendritic Cells under the Influence of Sexual Hormones Visualized using Scanning and Transmission Electron Microscopy

Josef Neumüller, Sylvia Emanuela Neumüller-Guber, Johannes Huber, Adolf Ellinger and Thomas Wagner

Additional information is available at the end of the chapter

http://dx.doi.org/10.5772/62310

Abstract

Dendritic cells (DCs) are antigen-presenting cells, which are mediated by MHC-class II molecules reacting with T-helper cells, eliciting a broad spectrum of immune reactions at cellular and humoral levels depending on their subtypes. DCs are also able to cross-present peptides from intracellular proteins as well as from intracellular pathogens via MHC-class I molecules by inducing MHC-class I–restricted cytotoxic T cells, which are also able to destroy cells undergoing malignant transformation. DCs originate from $CD34^+$ hematopoietic stem cells but can also develop from monocytes. The local or systemic milieu of cytokines and steroid hormones significantly influences the generation of particular DC subtypes such as the classical myeloid DCs such as cDC1 and cDC2 as well as the plasmacytoid DCs. These subtypes are able to induce specific Th1- and Th17-dependent, Th2-dependent, or regulatory immune responses, respectively. Immature DCs take up extracellular pathogens that are presented by MHC molecules that are upregulated during maturation. Immature and mature DCs can be characterized by morphological and biochemical features that are outlined in this article. In addition, DCs are under control of sexual hormones. Estrogen receptor ligands are potent modulators of hemopoiesis and immune function in health and disease, influencing key cytokines promoting the maturation of DCs. DC differentiation is mainly regulated by binding of estradiol to ERα. Estrogen promotes the differentiation of immature DC subsets derived from bone marrow precursors or from myeloid progenitors. In contrast to estrogen, progesterone inhibits DC maturation, causing a decreased immunity in pregnancy or in postmenopausal women, where elevated levels of progesterone result in the production of Th2 cytokines. The influence of estrogen and progesterone on DC maturation has been demonstrated in own *in vitro* experiments using fluorescence microscopy and cell sorting and, above all, by visualization using SEM and TEM. At the end of

this article, pits and falls concerning the treatment of malignancies with living DC vaccines are discussed.

Keywords: Dendritic cells, MHC antigens, antigen presentation, cross-presentation, cytokines, transcription factors, steroid hormones, anti-tumor vaccine

1. Introduction

Dendritic cells (DCs) are antigen-presenting cells (APCs) interacting with CD4-positive T-Helper (Th) cells via peptide-presenting MHC (HLA) class II molecules and the α/β or γ/δ T-cell receptor and via costimulatory molecules. These interactions provide initiation or modulation of specific kinds of immune reactions triggering effector cells via direct cell contacts as well as by intercellular communications involving a complex cytokine network.

In the first part, the differentiation of myeloid DCs, lymphoid DCs as well as of Langerhans cells (LCs) are explained, including their morphological and immunological characteristics based on their local or systemic sites of activity. Local areas mainly concern the secondary lymphoid organs such as lymph nodes and spleen as well as the mucosa-associated lymphoid tissues (MALT), including the Waldeyer's tonsillar ring and the mucosa lining the respiratory and the gastrointestinal tract. Although the objective of this article is rather morphological, we think that an immunological overview is helpful for understanding the functional interrelations of DCs not only with responding immune cells but also with other cells in the vicinity of locally acting DCs. This will be concisely discussed in the light of our present scientific knowledge.

In the second part, we show own results concerning ultrastructural details from the maturation of myeloid DCs under *in vitro* conditions using TEM and SEM. We started the differentiation of myeloid DCs outgoing from $CD34^+$ hematopoietic stem cells (HSCs) of human umbilical cord blood. In the course of differentiation in a conditioned cell culture medium, the HSCs differentiated into immature DCs and finally into mature myeloid DCs.

In the third part, the maturation of myeloid DCs under the influence of sexual hormones is demonstrated using scanning electron microscopy (SEM), showing images taken from our own investigations. We visualized the mDC maturation under the influence of β-estrogen and progesterone by SEM after flow cytometry and cell sorting.

In the fourth part, the impact of mDCs for anti-tumor therapies is discussed. In this respect, different DC isolation protocols (from HSCs or from monocytes) as well as DC anti-tumor targeting methods are presented. Several efforts to produce an efficacious anti-tumor vaccine using primed autologous DCs were undertaken and clinical trials were carried out with varying success. Some clinical trials were promising, but other clinical applications were disappointing since recurrence of the respective tumor could not be prevented.

http://dx.doi.org/10.5772/62310

2. Functional aspects of DCs in the immune system

During the past years, the view about the differentiation lines of DCs has been changed significantly [1]. In this respect, different efforts were made to find an appropriate nomenclature. Some researchers use a development-orientated nomenclature concerning the development dependency from flt-3L or from macrophage colony–stimulating factor (M-CSF). Another feature of DCs concerns their maturation either from HSCs or from monocytes. Above all, specialized DCs are located in the intestine and other MALTs or in the integument. The DCs of the skin can be divided into epidermal Langerhans cells (LCs) characterized by cytoplasmic Birbeck granules containing Langerin and dermal Langerin-positive as well as Langerin-negative DCs [2]. Langerin (CD207) is a transmembrane protein belonging to the family of C-type II Ca^{2+}-dependent lectins with an extracellular carbohydrate-binding domain specific for mannosyl residues and an intracellular domain with a proline-rich motif. It is taken up from the cell surface by clathrin-dependent receptor-mediated endocytosis and traffics via early endosomes (EEA1) to the endosomal recycling compartment (ERC) but does not reach lysosomes for degradation. Langerin is also localized at the inner band of Birbeck granules [3]. These organelles have a unique ultrastructural morphology and consist of superimposed and zippered membrane components [3]. A second type of nomenclature distinguishes classical or conventional DCs (myeloid DCs) from plasmacytoid DCs based on the distinct morphology, markers, and gene expression profiles. Furthermore, one can distinguish between resident DCs moving directly to lymphatic compartments and migratory DCs entering to a respective tissue and traveling via lymphatic vessels to lymph nodes. Both cell types originate from blood cell precursors. More recently, newer criteria including not only developmental but also functional characteristics refer to regulatory mechanisms such as the initiation of immune tolerance, the role of hematopoietins such as G-CSF, M-CSF, flt-3L, GM-CSF and their receptors responsible for the generation of monocyte-dependent or independent DCs, as well as the significance of various transcription factors, for example, PU.1, mafs, ID2, IRFs, E2-2, and NF-κB, that are responsible for DC development according transcriptional programs [1, 4].

2.1. Antigen presentation

The most important DC function is the uptake of antigenic material via phagocytosis or pinocytosis by immature DCs and its processing into peptides and presentation via the peptide binding groove of MHC (in human HLA) molecules by mature DCs. Uptake of antigenic material is mediated by four alternative pathways: endocytosis, pinocytosis, phagocytosis and macropinocytosis. How the antigenic material is taken up by DCs depends on its features such as the form of the antigen, its solubility, or whether it is part of an immune complex or still associated with a pathogen [5]. During maturation, DCs not only change their dendritic morphology and their ability to take up antigenic material but also upregulate the expression of MHC-class I and MHC-class II molecules. In addition, the mature phenotype is characterized by specific differentiation markers [6]. Antigen presentation is initiated by direct contact with respective subtypes of T-Helper cells via binding to the T-cell receptor (TCR) complex, the CD4 molecule, as well as to additionally required costimulatory molecules expressed at the cell surface of both involved cells [7]. Antigen processing involves an interaction of the endocytic

and lysosomal pathway in the MHC-class II compartment (MIIC) and the presentation by MHC-class II molecules. This process requires an activation of the lysosomal machinery [8] and a stepwise association of the degradation products with the MHC-class II binding groove. This complex process has been summarized in an excellent review by Seliger et al. [9]. Exogenous antigens are internalized via the endocytic pathway. HLA class II heterodimers assemble in the endoplasmic reticulum (ER) with the invariant chains (Ii) to form nonameric a/b–Ii complexes [(ab)3Ii3], targeted to MIIC. The invariant chain Ii protects the binding groove against association with intracellular degradation products shredded by proteasomes. The HLA-class II–associated Ii is degraded in distinct steps, leaving class II–associated Ii peptide (CLIP) within the HLA-class II binding groove. CLIP can then be exchanged for antigenic peptides, a process catalyzed by HLA-DM molecules. The HLA-DM–dependent peptide loading is regulated by HLA-DO molecules. Peptide-loaded HLA-class II molecules are then transported to the cell surface for presentation to $CD4^+$ T cells.

At the EM level, multivesicular and multilamellar bodies are characteristic organelles related to the MCII compartment [10–15]. Although MHC-class II molecules are abundantly expressed at the plasma membrane of DCs, they are also present in immature DCs where they have only a short half-life since they are directed in a recycling pathway. They are actively sorted to luminal vesicles of multivesicular bodies after ubiquitination and subsequently transferred to lysosomes. An increase of MHC-class II molecules at the plasma membrane could be explained by a recruitment of antigen-loaded MHC-class II molecules to the cell surface during maturation by allowing intraluminal vesicles to fuse back with the delimiting membrane of multivesicular bodies. However, there is strong evidence that the enhanced cell surface expression of antigen-presenting MHC-class II molecules is due to their increased synthesis but to a reduced lysosomal degradation [16]. Nevertheless, the stable expression of peptide-loaded MHC-class II molecules requires the intersection of the endocytic and the lysosomal pathway as explained above.

2.2. Cross-presentation

As most of nucleated cells, DCs also express classical MHC-class I molecules presenting intracellular peptides prepared by proteasomes and cytosolic proteases. The peptides are transported by the TAP transporters (heterodimeric multimembrane-spanning polypeptides belonging to the ABC transporter family) from the cytosol into the ER, where their assembly with MHC-class I molecules takes place, assisted by various chaperones, such as calnexin, calreticulin, ER60, and tapasin [9].

In DCs, two alternative pathways for cross-presentation have been reported: the “cytosolic” and the “vacuolar” pathway. In the cytosolic pathway, phagocytosed proteins are transported to proteasomes, where they are degraded and bound to MHC-class I molecules in the ER and directed to the plasma membrane for antigen presentation. This retrotranslocation machinery involves the ER membrane proteins sec61 and p97 ATPase [17]. Alternatively, after degradation by proteasomes, ingested proteins can be re-transported to phagosomes, where they are associated with MHC-class I molecules. In the vacuolar pathway, exogenous proteins are transported to phagosomes, where degradation, alternative to the proteasomes, takes place.

Consecutively, appropriate peptides are bound to the antigen-binding groove of MHC-class I molecules [18, 19].

Bacterial and cellular antigens are also efficiently cross-presented in association with heat-shock proteins such as hsp 70, hsc 70, and hsp 90 and the ER chaperones grp94 /gp96 and their bacterial homologues. Peptide complexes are ingested after binding to specific receptors such as CD91 (the α_2-macroglobulin receptor) and the scavenger receptors LOX-1 and SR-A [5, 20–23].

Only the MHC-class I–restricted $CD8^+$ cytotoxic T-cell (CTL) response can destroy intracellular pathogens such as viruses and intracellular parasitic bacteria as well as cells undergoing malignant transformation. Only professional APCs such as DCs and some macrophages express an efficient combination of co-receptors and MHC-class I molecules to stimulate naive $CD8^+$ T cells [24]. However, cross-presentation of intracellular antigens after degradation of intracellular peptides belonging to internal cell structures and compartments is important for the maintenance of peripheral tolerance to self-antigens (cross-tolerance) [5, 25]. Cross-presentation is also important for vaccination against tumors, which is discussed at the end of this article.

2.3. Types of DCs and their characteristics

The enormous progress in DC research has been achieved mainly in the mouse system. Although many homologies exist between the human and murine immune system, there are also significant differences in the expression of differentiation markers, transcription signatures, and cytokine release. In the mouse system, DCs can be subdivided into classical (cDCs) and plasmacytoid (pDCs) DCs. However, under inflammatory conditions, a new subtype of so-called inflammatory DCs appears. DCs acting in the murine immune system, cDCs, can be further subdivided into "CD8-like" DCs with a $Clec9A^+$/$CD141^+$ phenotype and CD11b-like" DCs with a $CD1c^+$ phenotype. Both of these subsets include resident DCs that are located in secondary lymphoid organs such as lymph nodes, tonsils, and spleen as well as migratory DCs, which are present in peripheral tissues as well as in non-lymphoid organs (skin, liver, lung, kidney, intestine, and other organs). After antigen contact, cells of this subtype migrate via lymphatic vessels into local lymph nodes [19]. In addition, special DC types are present in the skin: the epidermal LCs and dermal DCs, as mentioned above.

In vitro, human DCs can be either derived from $CD34^+$ HSCs, or isolated from bone marrow, umbilical cord blood, or purified monocytes (Fig. 1a and b). In this respect, monocytes represent an immature cell type with a potential to differentiate either into macrophages or into DCs. *In vivo*, similar differentiation lines can be demonstrated, whereas the decision to follow a distinct differentiation line is made in the bone marrow. Surface markers, transcription signatures, as well as growth factors driving differentiation have been summarized in several reviews [6, 26–30].

Depending on their stimulation, DCs are able to promote different T-cell responses. In contrast to the murine immune system, in human system, pDCs (bearing MHC-class II antigens, CD4, CD123, CD80, and CD86) can provoke a Th2 and Th0/Tr1 response, whereas mDCs (bearing

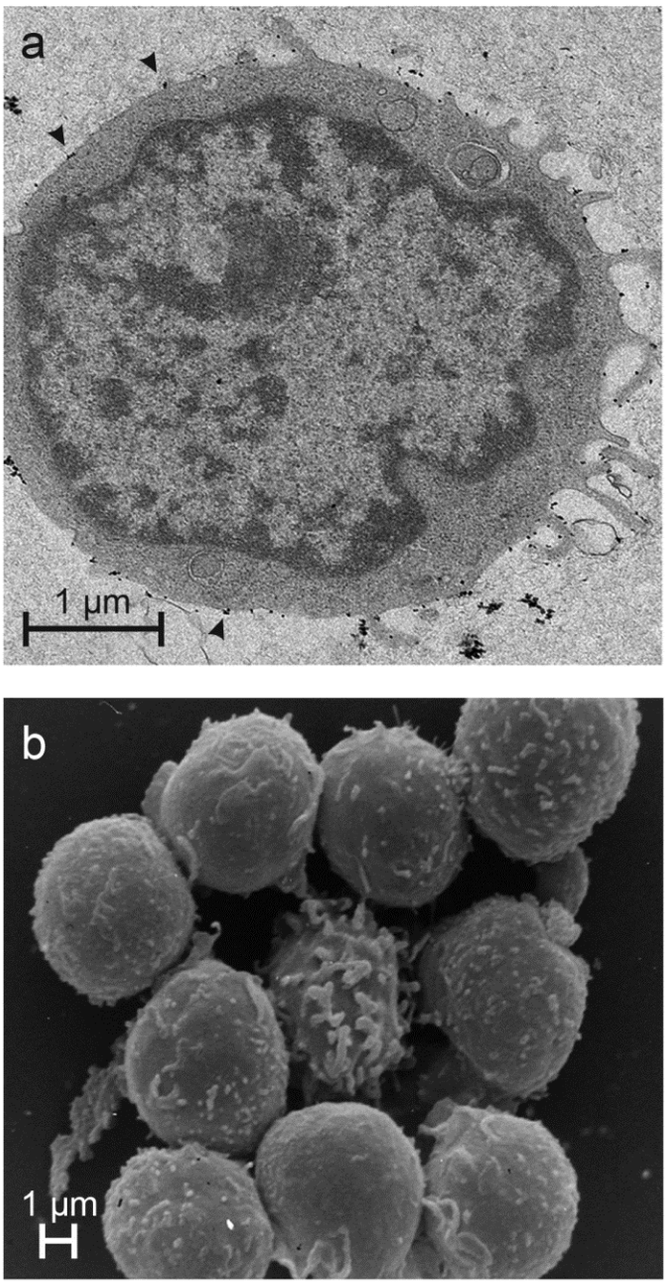

Figure 1. $CD34^+$ HSCs, isolated with paramagnetic particles, coated with an anti-CD34 monoclonal antibody shown by TEM (a) and SEM (b). In Figure 1a, arrowheads mark binding of anti-CD34 antibody-coated amorphous paramagnetic particles (average size: 50 nm).

MHC-class II antigens CD11c, CD80, and CD86) can provoke a Th1 response [6]. Naive $CD4^+$ T cells can differentiate into Th1, Th2, Th17, and regulatory T cells (Tregs). While Th1 cells secrete mainly IFN-γ to eliminate intracellular antigens, Th2 cells produce IL-4, IL-5, and IL-13 to eliminate helminthes and extracellular pathogens [31]. The IL-17-synthesizing Th17 cells are functional in the clearance of extracellular bacteria and fungi [32]. Tregs secrete anti-inflammatory cytokines such as IFN-β and IL-10 and are essential for the maintenance of self-

tolerance and for the prevention of autoimmunity [4, 33]. After activation of the TCR, the signals for $CD4^+$ T-cell differentiation are mediated by binding of specific cytokines to their cognitive receptors that are associated with Janus kinases (Jaks). After phosphorylation of the intracellular domains of the cytokine receptor and activation of Jaks, STATs are also phosphorylated, inducing the expression of genes responsible for the initiation of differentiation by the action of master regulators responsible for the synthesis of Th subtype–specific cytokines [4, 34]. STATs are signal transducers and activators of transcription pathways initiating the expression of master regulator transcription factors belonging to a complex network of other transcription factors. Different STATs are required for Th-specific differentiation lines: STAT4 and 1 for Th1 cells, STAT6 and 5 for Th2 cells, STAT3 for Th17 cells, and STAT5 for Tregs [4].

According to a recent excellent and comprehensive review [35], we can summarize that DCs belong to the entire phagocytic system including monocytes/macrophages in different compartments such as lymphoid and non-lymphoid tissue and blood. In this nomenclature, DCs are subdivided into classical $CD141^+$ myeloid DCs (cDC1), $CD1^+$ myeloid DCs (cDC2), and plasmacytoide DCs (pDCs). DCs can also differentiate from monocytes (moDCs). In the murine system, different development pathways for moDCs and DCs derived from HSCs have been demonstrated. However, because of the research at the transcriptional level, it became evident that these restrictions are not so strong in both humans and mice as previously suggested.

Human DCs can be classified according to Haniffa et al. [35].

2.3.1. $CD141^+$ myeloid DCs (cDC1)

CD141+ myeloid DCs (cDC1)secrete TNFα, CXCL10, and IFNγ, but little IL-12p70. They cross-present necrotic cell–derived and soluble antigens via CLEC9A, but cross-presentation is not totally restricted to this cell type. CD141 (BDCA-3, thrombomodulin), an integral membrane protein, is expressed not only at the cell surface on DCs but also on endothelial and mesothelial cells as well as on monocytes. By binding to thrombin, it serves as its cofactor and reduces blood coagulation by converting thrombin to an anticoagulant enzyme and participates in inhibition of fibrinolysis. In addition, it regulates C3b inactivation by coagulation factor 1 [36].

2.3.2. $CD1c^+$ myeloid DCs (cDC2)

CD1c+ myeloid DCs (cDC2) are characterized by a high expression of the toll-like receptors (TLRs) 1, 2, 4, 5, and 8. They are able to present glycolipid antigens and react with mycobacteria via CD1a and c. They also exhibit reactivity against fungi by involving the receptors Dectin-1 (CLEC7A) and Dectin-2 (CLEC6A), the receptors DEC205 (CD205; CLEC13B), and the macrophage mannose receptor (CD206; CLEC13D). Upon stimulation, these cells secrete IL-1β, TNFα, IL-8, and IL-10. In blood, cDC2 cells can abundantly secrete the enzyme retinaldehyde dehydrogenase (RALDH)2 dependent on the level of vitamin D3. They are able to initiate Th2, Th1, and also Th17 response dependent on stimulation by respective antigens.

CD1c (BDCA-1) acts as antigen-presenting protein binding self- and non-self–lipid and glycolipid antigens and presenting them to T-cell receptors on natural killer T cells [37].

2.3.3. Plasmacytoid DCs (pDCs)

Plasmacytoid DCs (pDCs) strongly express TLR7 and TLR9, enabling the recognition of autologous nucleic acids and viral antigens. Challenging pDCs with viral antigens results in a potent secretion of class-I interferons, mainly IFNα. In response to inflammation, pDCs are recruited to tissues and lymph nodes. They display two main functions: they can polarize Th1 and Th2 response and play an important role in immune tolerance but also in autoimmune disease by initiation of a Treg response. The functional capacity of pDCs increases gradually during fetal life. In this respect, it could be demonstrated that preterm neonates possess an impaired BDCA4 expression and produce lower levels of IFNα. Ultrastructurally, they show an immature morphology [38]. In addition, the *in vitro* maturation of blood DC depends on the upregulation of BDCA3 on pDCs [39].

3. Maturation of myeloid DCs (mDCs)

When challenged by immune stimulatory and pathogenic antigens, mDCs mature into regulatory or stimulatory DCs. The development of regulatory DCs requires tolerogenic stimuli via anti-inflammatory cytokines and mediators such as TGF-β, IL-10, and PGE_2. Regulatory DCs provide induction of Tregs, inhibiting the proliferation of $CD4^+$ $CD8^+$ T-cells and producing anti-inflammatory cytokines such as IL-10 and TGF-β, as well as immune-regulatory molecules such as indoleamine 2,3-dioxygenase (IDO) and programmed cell death protein 1 (PD-1), which suppress activation and proliferation of effector T cells and efficiently induce Tregs [36]. In contrast, stimulatory DCs develop under the influence of proinflammatory signals: inflammatory cytokines, chemokines, pathogen-associated molecular patterns (PAMPs) such as lipopolysaccharide (LPS), flagellin, lipoteichoic acid, peptidoglycan, and viral double-stranded RNA (dsRNA) [40–42]. Additional stimulators are damage-associated molecular patterns (DAMPs) representing host molecules that can initiate and perpetuate inflammatory response that are not caused by infectious agents. DAMPs can be proteins like heat shock proteins or breakdown products of the extracellular matrix such as hyaluronan fragments or other molecules such as ATP, uric acid, heparin, sulfate, or DNA [43–46].

3.1. Immature mDCs

Immature mDCs circulate either in the peripheral blood or migrate into infected tissues where they take up pathogens or cell debris. This uptake is mediated by type C lectin receptors such as CD206, DEC205, or CLEC4A or in the case of PAMPs by toll-like receptors. Antigenic material is ingested by phagocytosis or pinocytosis and directed to the intracellular degradation machinery [36].

In our own experiments, we differentiated mDCs from $CD34^+$ HSCs of human cord blood: Fig. 1a and b. We followed a cultivation protocol established by Strunk et al. [47]. Shortly, mono-

http://dx.doi.org/10.5772/62310

nuclear cells were obtained by centrifugation over the flotation medium Ficoll®-Paque Premium (Sigma-Aldrich, Vienna, Austria). DCs were incubated with paramagnetic particles coated with a monoclonal antibody against CD34, isolated using a magnetic cell separator (MACS®, Miltenyi Biotech, Bergisch Gladbach, Germany), and cultivated in a conditioned RPMI-1640-medium containing 20% FCS, 100 ng/ml GM-CSF, 20 ng/ml SCF, 20 ng/ml TNF-α, and 0,5ng/ml TGF-β1. $CD34^+$ stem cells differentiated into immature mDCs showed an LC-like phenotype ($HLA\text{-}DR^{dim}$, $CD1a^+$, and $Langerin^+$) and grew in clusters. Cultures containing clusters were layered over 7.5% bovine serum albumin solution in phosphate-buffered saline (BSA/PBS, Sigma, St. Louis, MO), where they could be collected and transferred to fibronectin-coated chambered coverslips. Further differentiation to mature DCs has been achieved by addition of 10 μg/ml LPS + 50 ng/ml TNF-α to the culture medium or by supplementing the medium with steroid hormones as outlined later on.

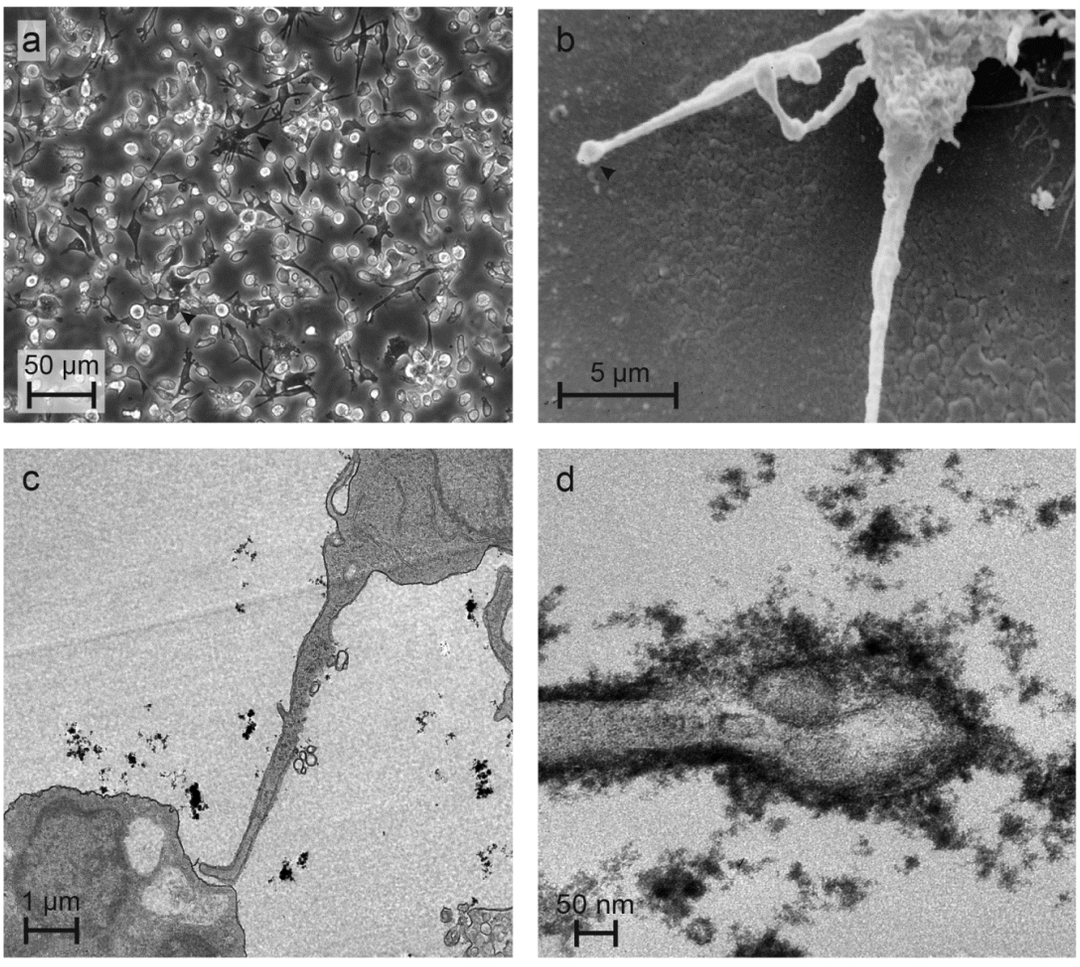

Figure 2. Immature dendritic cells growing in conditioned cell culture medium on the surface of fibronectin-coated chambered coverslips. Fig. 2a shows the appearance of the DC morphology in phase contrast. Fig. 2b and c show extended cell projections with knob-like structure in SEM (Fig. 2b) and TEM (Fig. 2c and at higher magnification in Fig. 2d). Note the prominent coat of the glycocalyx in Fig. 2d. In Fig. 2c paramagnetic particles are visible, which are still present after cell separation but partially detached from the cell surface.

Immature mDCs preferentially extended large dendritic cell processes (Fig. 2 ac) which a knob-like structure as shown in Fig. 2d where we suppose a concentration of the mentioned receptors. In this respect, DCs, located in the lamina propria of the small intestine, extending long cell processes that survey antigens in the lumen of the gut have been demonstrated [48–50].

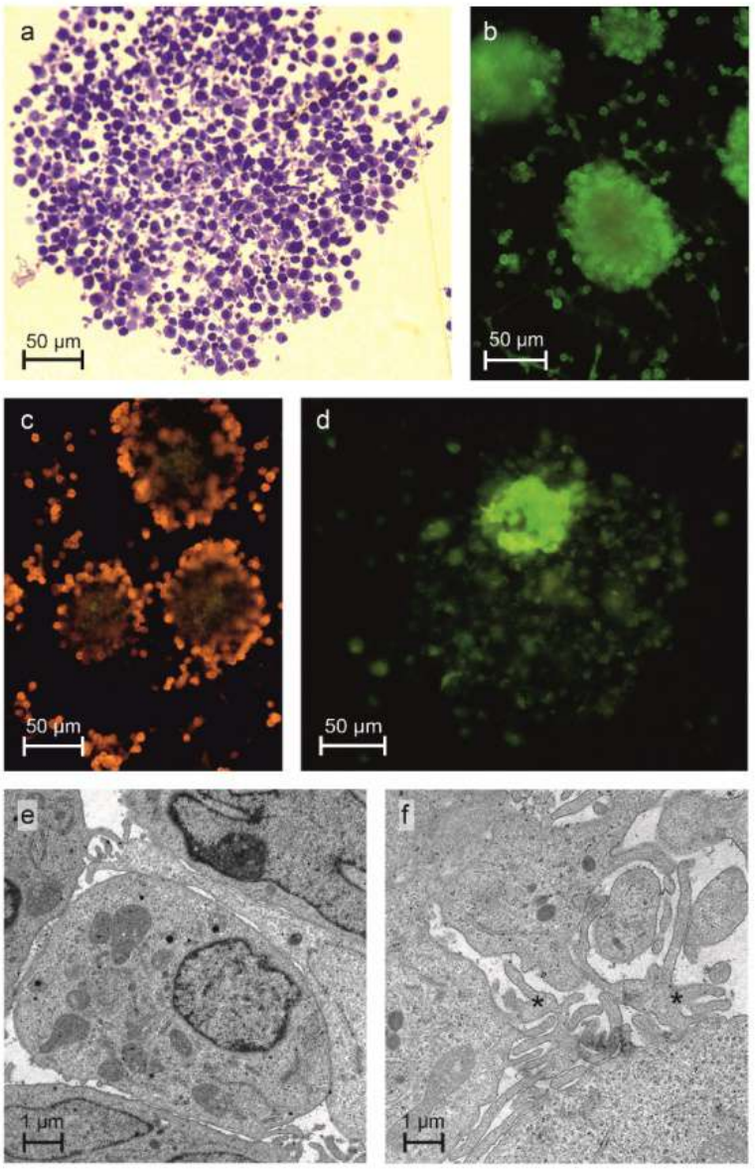

Figure 3. Cultivation and characterization of immature mDC clusters using light microscopy (Fig. 3a), fluorescence microscopy (Fig. 3b, c, and d), and TEM (Fig. 3e and f). Fig. 3a shows a low-magnification image of an adhered cell cluster taken from a 1 µm semithin section stained with toluidine blue. Fig. 3b shows staining with an FITC-conjugated monoclonal antibody against CD1a, and Fig. 3c, a cell surface staining with a PE-conjugated monoclonal anti-HLA DR antibody. In Fig. 3d, only the center of the cluster is positive for E-cadherin cell surface expression using an FITC-conjugated monoclonal antibody against E-cadherin. TEM images show cells with relatively smooth surface in the center of a cluster (Fig. 3e) as well as cells at the periphery of clusters forming interdigitating cell projections, which are marked by stars (Fig. 3f).

After collection of clusters and transfer to fibronectin-coated polystyrol dishes, they adhered again to the growing surface (Fig. 3a). At this stage, they displayed still an immature phenotype till day 7 of cultivation. Under the influence of maturation signals, they differentiated starting from the margins of clusters (Fig. 3). Using fluorescence microscopy, it could be shown that CD1a staining was present at the surface of all mDCs (Fig. 3b), while HLA-DR expression could be found only at the periphery of clusters (Fig. 3c). E-cadherin could also be demonstrated but only in the center of the clusters (Fig. 3d). TEM imaging of the clusters revealed that in their center the surface of cells remained relatively smooth (Fig. 3e), while at the periphery, many interdigitating cell projections were formed (Fig. 3f).

In TEM, immature mDCs display characteristics of high activity as they develop an abundant rough ER and a prominent Golgi apparatus as well as an extended trans-Golgi network (TGN) (Fig. 4a and b). The MIIC compartment is characterized by the presence of abundant lysosomes and multilamellar bodies (Fig. 4c and d). Also autophagosomes engulfing several multilamellar bodies could be demonstrated (Fig. 4e). Interestingly particular endosomes aligned in a pearl-like structure could be shown (Fig. 4f). We regard these structures as special organelles of the endosomal pathway. In a previous publication we could identify similar structures in endothelial progenitor cells also derived from $CD34^+$ HSCs of human cord blood [51, 52]. In this respect, immature mDCs are highly active in antigen uptake and processing.

Regarding *in vitro* conditions, above all under the influence of TGF-β1, mDCs develop a characteristic LC-like ultrastructural morphology by displaying Birbeck granules and Birbeck-like organelles already described in early publications [47, 53, 54], which we could also verify in our experiments (Fig. 5). Birbeck granules store langerin, a mannose-binding lectin.

3.2. Mature mDCs

The maturation of mDCs is accompanied by morphological and functional changes: Mature mDCs lose their capacity to adhere to plastic surfaces. The few long cell processes of immature DCs are replaced by numerous short filopodia (Figs. 6a and b) and veil-like membrane projections while the uptake of antigenic materials is downregulated in favor of antigen presentation as well as of cross-presentation [55]. In this respect, only mature DCs are entirely able to cooperate with lymphocytes (Fig. 6b) by presenting antigens via MHC-class I and II molecules [56]. Maturation of mDCs requires the expression of costimulatory molecules such as CD80, and CD86 and the integrin receptor LFA-1 (CD11a). In addition, the cytokine tumor necrosis factor alpha (TNF-α), LPS, and the CD40 ligand (CD40L) have been found to induce DC-maturation [56]. The degeneration of aged mature mDCs is shown in Figs. 6c and d.

It has been demonstrated that CD83 is expressed only in mature DCs [55]. CD83 is a 45-kD, type-1 membrane glycoprotein belonging to the Ig superfamily. CD83 is released from activated cells, and the soluble form of CD83 has a strong immunosuppressive effect. The immunoregulatory function of CD83 implicates its use for therapy of cancer and autoimmune diseases [57].

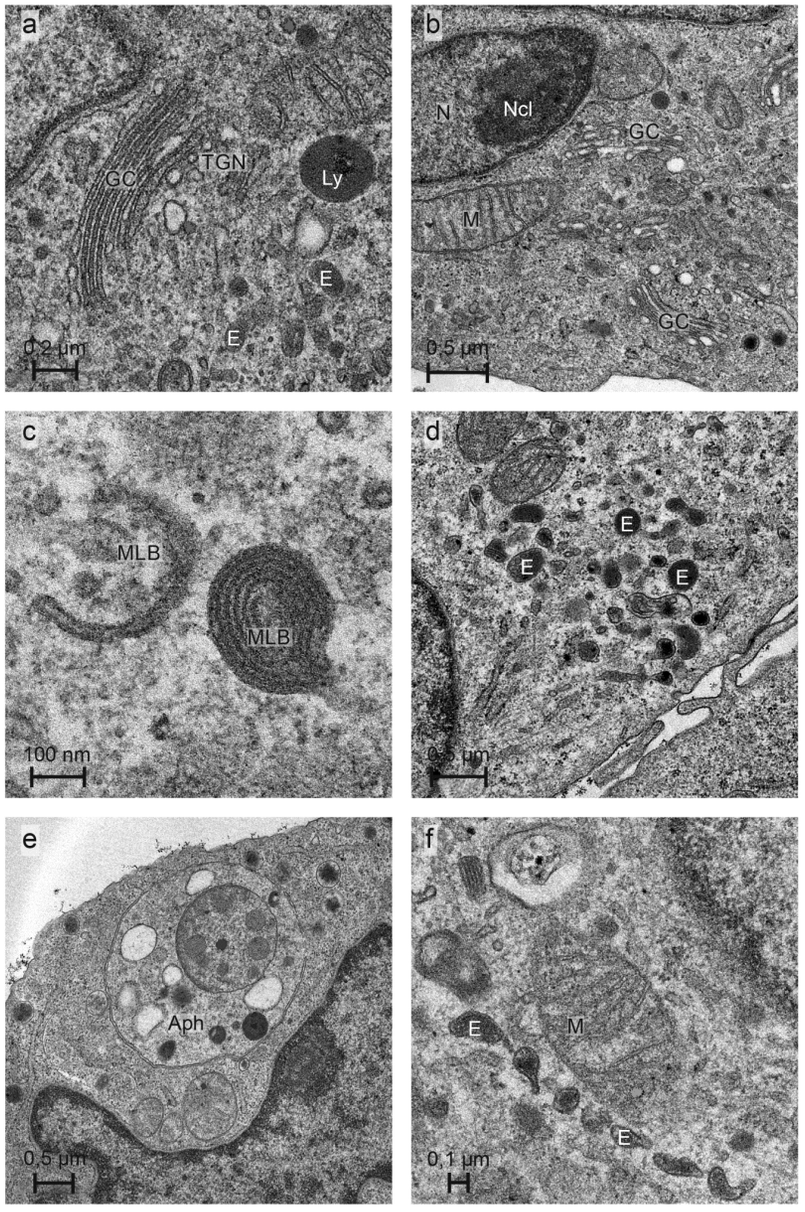

Figure 4. Particular ultrastructural characteristics of immature mDCs visualized by TEM: Well-expressed Golgi complexes (GC) and trans-Golgi networks (TGN) as well as endosomes (E), lysosomes (Ly), mitochondria (M), and an active nucleus (N) with a distinct nucleolus (Ncl) are visible in Figs. 4a, b, d, and e. Multilamellar bodies (MLB) shown in Fig. 4c are part of the MIIC compartment. An autophagosomes (APh) with degraded material is shown in Fig. 4 e. In Fig 4f, a pearl-like structure of aligned endosomes (E) is visible.

4. How sexual hormones influence the development and maturation of mDCs

In vitro, mDCs can be derived from $CD34^+$ HSCs from bone marrow but also from umbilical cord blood. Triggered by the cytokines GM-CSF and TNFα, HSCs differentiate into inter-

http://dx.doi.org/10.5772/62310

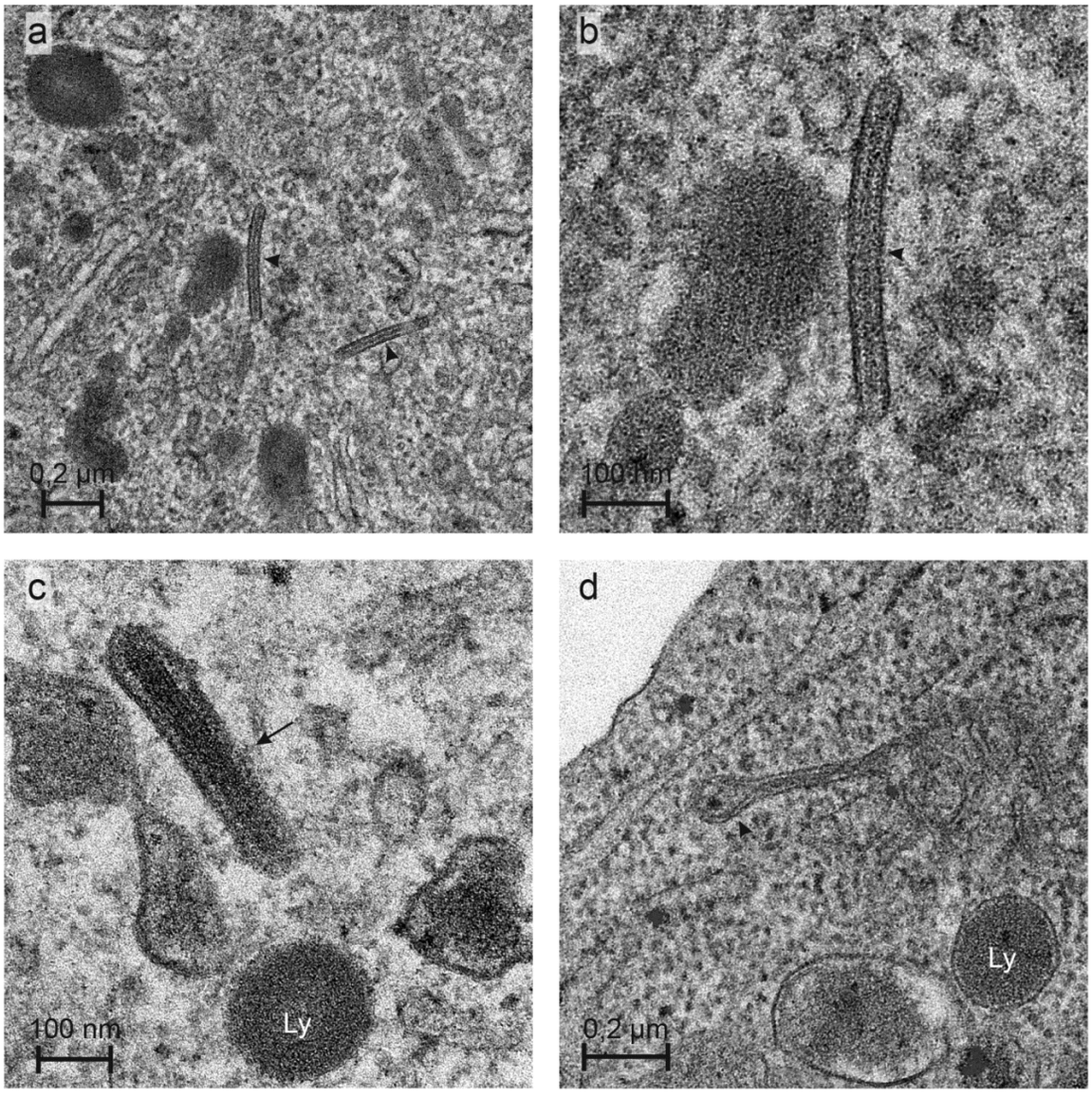

Figure 5. Formation of Birbeck granules and related structures visualized by TEM: Classical Birbeck granules are shown in Figs. 5a and b (arrowheads). They are rod-shaped (Fig. 5a and b) or drumstick-like (Fig. 5d; arrowhead).organelles with a central linear density and a striated appearance. Occasionally, organelles resembling endothelial Weibel-Palade bodies with central microtubular structures (arrow) occur (Fig. 5c). In addition, lysosomes (Ly) are visible.

mediate $CD14^+/CD1a^-$ precursors, which develop consecutively into mature DCs but also to LC-like cells. Bone marrow-derived $CD34^+/CD10^+/Lin^-$ cells mature directly into DCs under the influence of a cytokine cocktail containing IL-1, IL-7, TNFα, GM-CSF, SCF, and Flt3-ligand [30]. ER ligands are potent modulators of hemopoiesis and immune function in health and disease influencing key cytokines such as GM-CSF and Flt3 ligand that promote the maturation of mDCs. However, myeloid progenitors differentiate variably under the influence of 17β estradiol with each of the two cytokines: While GM-CSF promotes the development of LC-like mDCs, Flt3 ligand decreases the number of plasmacytoid, lymphoid, and myeloid DCs in a dose-dependent manner. DC differentiation is mainly regulated by binding of estradiol to

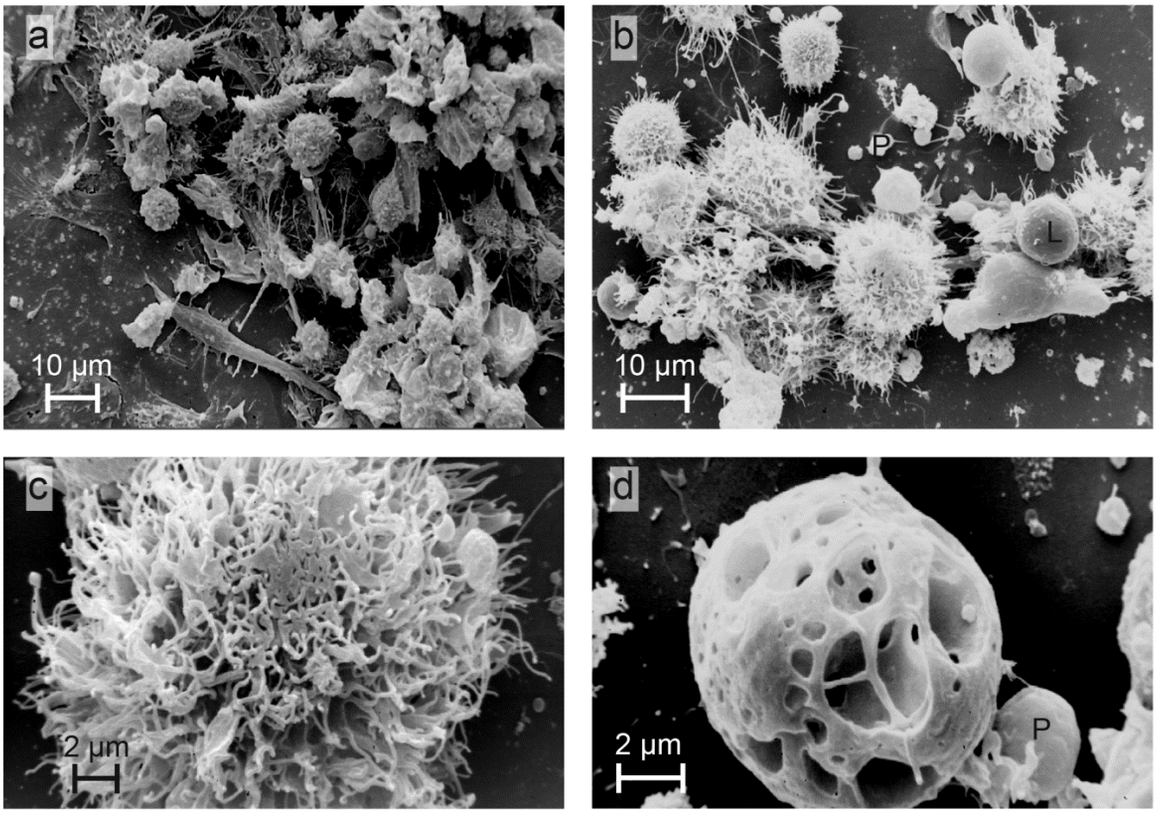

Figure 6. Ultrastructural characteristics of mature and apoptotic/necrotic myeloid DCs investigated by SEM. Figs. 6a and b show clusters of mature DCs with numerous microvillus-like cell projections. Adhesion of lymphocytes (L) and platelets (P) is visible in Fig. 6b. In Fig. 6a, still some immature DCs with long cell projections are visible. Fig. 6c shows abundant cell projections as a sign of beginning degeneration, distinctly pronounced in Fig. 6d.

ERα. Therefore, endogenous or ER ligands produced by pharmaceutical companies may differentially affect DC development in health and disease concerning the DC-mediated immunity [58]. ERα and β belong to the nuclear receptor superfamily encoded by the ESR1 and ESR2 genes, respectively. Different types of ER receptor isoforms are generated by homeotypic or heterotypic dimerization of both chains [59, 60]. Activation of ERs exhibits an epigenetic modification of DNA by chromatin-modifying co-regulators and other transcription factors that initiate DNA transcription [61]. It has been shown that estrogen preferentially promotes the differentiation of immature $CD11c^{+}$ $CD11b^{int}$ DCs from bone marrow precursors [62] as well as the GM-CSF-mediated differentiation of a $CD11b^{+}$ subset from myeloid progenitors via the interferon regulatory factor (IRF4). This transcription factor is induced by GM-CSF [63].

In contrast to ER activation, therapeutic selective ER modulators such as tamoxifen and raloxifene have been shown to impair DC differentiation and activation. As competing with estrogen, both drugs possess antagonistic effects on ER function. They were not able to provide DC differentiation and have, therefore, no effect as ER agonists. Tamoxifen has beneficial effects in respect to the treatment of breast cancer, while it increases the risk for endometrial cancer, whereas raloxifene can be successfully used against osteoporosis since it exerts similar

effects than estrogen. However, tamoxifen and raloxifene medication can lead to a partial immune suppression at the level of antigen presentation and T-cell activation by downregulating the expression of MHC-class II and costimulatory molecules. Unfortunately, this downregulation can interfere with cellular immune therapy against cancer such as vaccination with DCs. [64].

In pregnancy, an immune-modulatory function of progesterone has been discussed [65]. It could be demonstrated that pregnancy-associated elevated levels of progesterone induced the production of IL-10 by mature DCs derived from human blood monocytes, leading to a Th2 immune response. In this respect, the regulation of the Th1- and Th2- related cytokines is important for a successful pregnancy [66]. Impaired DC function has also been reported in the mouse immune system. In this respect, progesterone-treated DCs were characterized by a decreased expression of Ia molecules (MHC-class II), CD80, and CD86 as well as by an increased production of IL-10, and a decreased secretion of IL-12. In addition, an impaired stimulatory capacity for $CD4^+$ helper cells was demonstrated [67].

In vitro experiments with metroxyprogesterone acetate, an anti-contraceptive drug, could impressively demonstrate that TLR3 agonist stimulation decreased the expression of CD40 and CD80 and impaired the initiation of T-cell proliferation [68].

In general, most of functions of the innate and adaptive immune system decline with aging. Therefore, vaccination response against pathogens is also frequently impaired. Postmenopausal women produce higher levels of proinflammatory cytokines such as MCP1, TNFα, and IL-6, which has been implicated in the development of several diseases such as osteoporosis (by activation of osteoclasts) but also in diabetes, atherosclerosis, and cardiovascular diseases. Estrogen (E_2) and progesterone are the master cytokines of the immune system in the female reproductive tract (FRT). Although there are still gaps in our knowledge of the immune system of the FRT, above all concerning the mucosal parts of FRT, there is good evidence for successful treatment of postmenopausal women using an appropriate hormone therapy [69, 70].

4.1. Investigations performed in our laboratory

We visualized the maturation of mDCs cultivated using the differentiation protocol as described above under the influence of 10^{-5}M β-estradiol or alternatively to 10^{-5}M progesterone. After 1 week of cultivation, clusters of immature DCs were transferred to new chambered coverslips containing the same conditioned medium containing the respective hormones and cultivated for another week. Using flow cytometry and cell sorting (Fig. 7a and b), immature (Fig. 7c) and mature mDCs (Fig. 7d) were collected and prepared for SEM. In addition, the percentage of mDCs positive for CD1a, CD14, CD83, CD1a/CD83, and CD14/CD83 was determined.

4.1.1. Immunological characterization with fluoro-labelled antibodies

Immunological characterization with fluoro-labelled antibodies was performed by staining of cells using a fluorescein-isothiocyanate (FITC)-conjugated monoclonal antibody against CD1a (BD Pharmingen™, Vienna, Austria), clone HI149, mouse IgG1, a phycoerythrin (PE)-

conjugated monoclonal anti-HLA DR antibody (BD Biosciences, Vienna, Austria), clone L243, mouse IgG_{2a}, and a FITC-conjugated monoclonal antibody against E-cadherin from BD Biosciences, clone 36/E cadherin, mouse IgG_{2a}. Fluorescence microscopy was performed using an inverted Nikon Eclipse TE-300 Microscope (Nikon Coop., Tokyo, Japan) with conventional filter packs for blue and green light excitation. Micrographs were taken with a Nikon Coolpix 5000 digital microscope camera.

4.1.2. For TEM investigations

For TEM investigations cells were attached to poly L-lysine coated coverslips, washed twice with Ca^{++}- Mg^{++}-free PBS, and fixed in 2.5% glutaraldehyde in 0.1 M cacodylate buffer at pH 7.2 for 60 minutes at 4°C. After washing with cacodylate buffer, cells were postfixed with 1% aqueous OsO_4 for 90 minutes at 4°C. Cells were dehydrated stepwise with ethanol and embedded in Epon. After polymerization, 70 nm ultrathin sections parallel to the growing plane were performed using a diamond knife. Acquisition of digital images was performed using a bottom-mounted CCD camera (Gatan Inc., Munich, Germany) in a Tecnai 20™ transmission electron microscope (FEI company, Eindhoven, The Netherlands).

4.1.3. For SEM investigations

For SEM investigations, cells were treated according to the TEM preparation protocol till fixation and then subjected to a critical point drying procedure and sputtered with gold. Micrographs were taken using a Nikon F3 reflex camera (Nikon Coop.) mounted on a Stereoscan S90 scanning electron microscope (Cambridge Instrument Company, Cambridge, UK).

4.1.4. Flow cytometry and cell sorting

Flow cytometry and cell sorting was performed using a FACSort machine (Becton Dickinson) which utilizes a "catcher tube", a mechanical sorting device, located in the upper portion of the flow cell. By moving in and out of the sample stream, it allows to collect a population of gated cells. In our investigations, sorted $CD1a^{bright}/CD83^{dim}$ immature mDCs (Fig. 7c) and sorted $CD1a^{dim}/CD83^{brigh}$ mature mDCs (Fig. 7d) were shown in SEM. Fig. 7a shows the gating process of mature DCs by forward and side scatter and Fig. 7b, the gating of $CD1a^{dim}/CD83^{brigh}$ mDCs at the fluorescence dot blot (FL1: labeling with a FITC-conjugated anti-CD1a monoclonal antibody; FL2: labeling with a PE-conjugated monoclonal antibody against CD83) using the Attractor software (Becton Dickinson). In addition, the software allows neglecting cell debris and, therefore, cell quantification in terms of absolute counts using reference beads. For demonstration of mature mDCs, a monoclonal PE-conjugated antibody against CD83 (Clone HB15e (RUO) from mouse, IgG1 κ chain) has been used.

4.1.5. Results from our own studies

It could be demonstrated that already at day 7 of cultivation above all the percentage of CD1a and CD14 positive DCs decreased under the influence of progesterone, while it increased

http://dx.doi.org/10.5772/62310

under the influence of β-estradiol (Table 1a). At day 14 of cultivation, a similar situation occurred but CD83 in combination with CD1a and CD14 was markedly reduced due to progesterone treatment but distinctly increased by β-estradiol (Table 1b). In addition, the maturation process concerning the formation of abundant cell projections was demonstrated by SEM analysis, and was still present at day 7 (Table 1a), but more pronounced on day 14 (Table 1b).

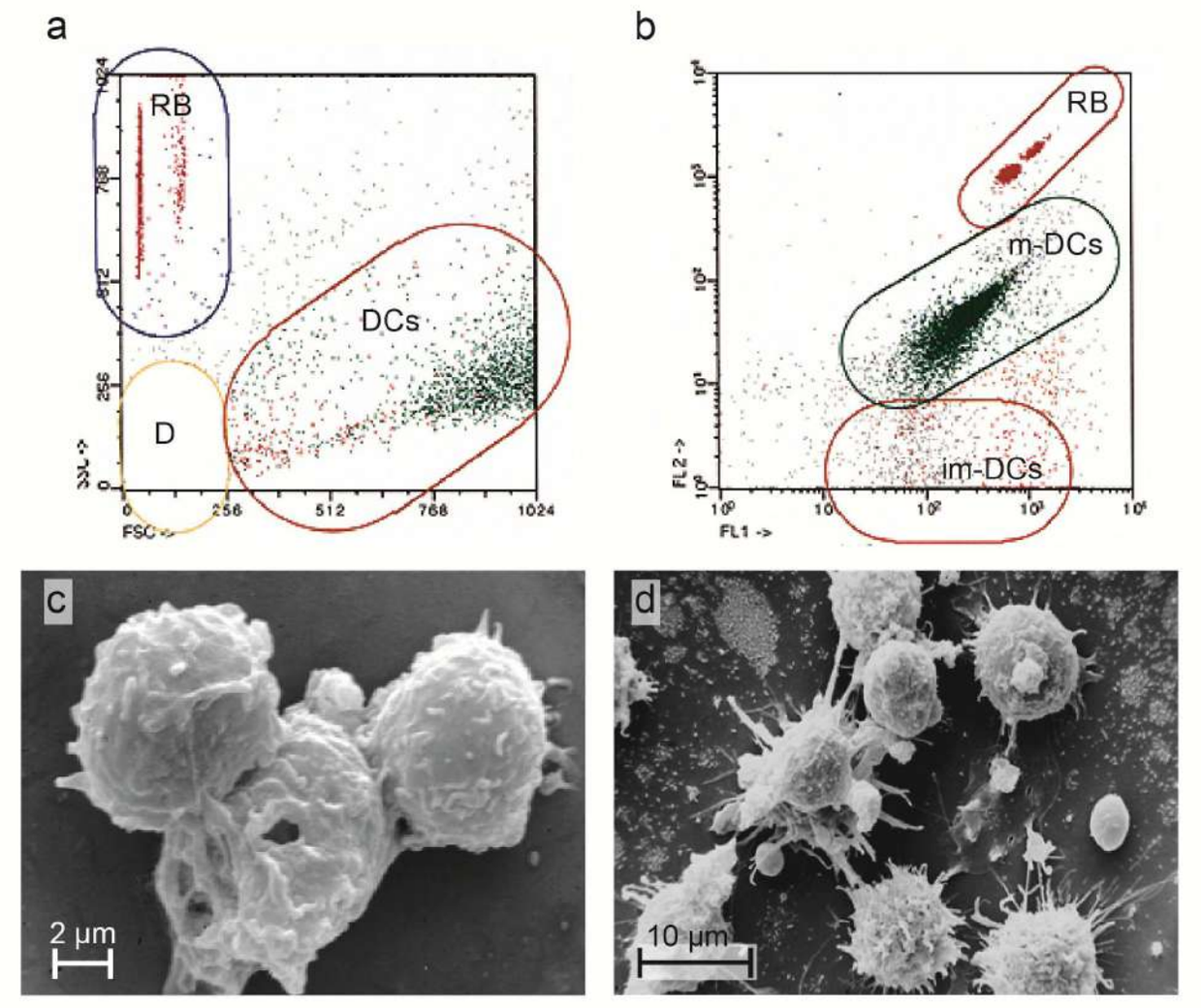

Figure 7. Visualization of immature mDCs by SEM after flow cytometric cell sorting by gating of $CD1a^{bright}/CD83^{dim}$ mDCs (Fig. 7c) and of mature mDCs by gating of $CD1a^{dim}/CD83^{brigh}$ mDCs (Fig. 7d). Fig. 7a shows the gating process of mature DCs using a forward and side scatter dot plot, Fig. 7b the gating of $CD1a^{dim}/CD83^{brigh}$ mDCs at the fluorescence dot plot (FL1, determination of cell labeling with an FITC-conjugated anti-CD1a monoclonal antibody; FL2, cell labeling with a PE-conjugated monoclonal antibody against CD83 using the Attractor software, which allows neglecting cell debris and therefore also cell quantification in terms of absolute counts by using reference beads).

Hormone	Flow cytometry and SEM on day 7					
DC markers	$CD1a^+$	$CD14^+$	$CD83^+$	$CD1a^+/CD83^+$	$CD14^+/CD83^+$	SEM: mature DCs
Control (only medium)	16	23	18	6	4	16
Progesterone	7	5	17	4	3	14
β-estradiol	17	39	11	5	6	26

(a)

Hormone	Flow cytometry and SEM on day 14					
DC markers	$CD1a^+$	$CD14^+$	$CD83^+$	$CD1a^+/CD83^+$	$CD14^+/CD83^+$	SEM: mature DCs
Control (only medium)	57	30	64	45	24	29
Progesterone	26	57	56	24	10	15
β-estradiol	51	25	74	45	23	31

(b)

Table 1. a. Percentage of DC marker expression measured by flow cytometry and visualization of mature mDCs by SEM on day 7 of cultivation under the influence of steroid hormones. b. Percentage of DC marker expression measured by flow cytometry and visualization of mature mDCs by SEM on day 14 of cultivation under the influence of steroid hormones.

5. Generation of DC anti-tumor vaccines

Since two decades, mDCs, in their immature as well as mature state, have been widely used for experimental as well as for clinical purposes. The Nobel Prize Laureate in physiology or medicine Ralph Steinman was a pioneer in DC research. Sorry to say that Steinman never got to know the decision of the Nobel Prize committee since he died on October 3, 2011 [71]. He postulated that DCs could provide an immune attack on cancer, broad enough to encompass multiple targets, including mutant proteins expressed by the cancer. In addition, DCs could be able to activate and expand different arms of cell-mediated immunity such as NK cells, γδ- and αβ-T cells that can recognize different alterations in cancer cells [72]. Still in 1989 an institute for tumor therapy using DC vaccines was founded in Duderstadt near Göttingen (Germany) based on early investigations [73, 74] of the working group of Peters with the focus on gynecological-oncological diseases. Early therapeutic approaches included the following steps: (1) the freezing and storage of tumor material after operation; (2) blood drawing from the tumor patient immediately after operation; (3) isolation of mononuclear cells by gradient centrifugation; cultivation of cells in conditioned medium containing IL4 and GM-CSF in order to obtain immature mDCs; (4) confrontation of mDCs with thawed, irradiated, and homogenized tumor material; and (5) administration of mDCs by creating an intradermal blister. However, early clinical trials have frequently shown that after short recurrence of the disease a relapse occurred which was difficult to treat. The main question in this context is why the immune system fails to attack the tumor. The answer consists in the downregulation of antigen-presentation and T-cell activation of DCs in the tumor environment. The administration of

http://dx.doi.org/10.5772/62310

primed DCs fails also because of the immunosuppressive action of tumor cells [75]. The reason for these pitfalls has been outlined in a recent review by Tran Janco et al. [76]. In tumors, tumor-infiltrating DCs (TIDCs) are functional but several receptors and cytokines of tumor cells compromise them leading to an environment that favors tumor progression. The expression of CD11c allows distinguishing three DC subsets: $CD11c^{bright}$, $CD11c^{intermediate}$, and $CD11c^{dim}$; $CD11c^{intermediate}$ expressing DCs are the predominant group of TIDCs. They fail to express enough quantities of costimulatory molecule, resulting in a hampered T-cell activation. In addition, they produce high levels of the immune-inhibitory molecule, programmed death 1 ligand (PD-L1). PD1 (CD279), a cell surface receptor belonging to the immunoglobulin molecule superfamily, and its ligands PD-L1 and PD-L2, impair the effector phase of immune cells. TIDCs also comprise a high number of pDCs, which promote the expansion of regulatory T cells (Tregs) characterized by high expression of the forkhead box P3 (FOXP3), a master regulator in the development of these cells. The consequence is an immune-tolerance preventing the elimination of the tumor. A further problem, concerning tumor expansion, is the secretion of the cytokine vascular endothelial growth factor (VEGF) and the chemokines CCL2, CXCL1, and CXCL5, leading to a hypervascularization of the tumor and intravasation of metastatic tumor cells. Tumor-induced transcription factors such as STAT3 induce S100A9 protein, preventing full maturation of DCs and consecutively block their responsiveness to local danger signals [77]. In this respect, the high concentration of IL-10 in the tumor cell microenvironment can also lead to STAT3 activation [76].

How could an anti-cancer therapy prevent the immune-compromising function of TIDCs? To influence the function of TIDCs, the PD1 and ligands can be inhibited by antagonist antibodies to PD1 and PD-L1 [78]. Strategies to promote DC maturation or to introduce the delivery of oligonucleotide-coated nanoparticles by DCs in order to influence immune functions at the epigenetic level by modulating the activity of miRNAs have been elaborated [79].

As mentioned above, *ex vivo* expansion of DCs originating from different sources has been used in clinical and pre-clinical trials [80]. The most commonly used approach is the differentiation of DCs from peripheral blood mononuclear cells (PBMCs) obtained via leukapheresis. After cultivation in conditioned medium containing GM-CSF and IL-4 for several days, they differentiate into immature $CD14^-/CD83^-$ DCs. Targeting these cells with maturation stimuli leads to further differentiation into mature $CD14^-/CD83^+$ DCs, that express high quantities of MHC-Class I and II as well as costimulatory molecules. A faster method includes the isolation of $CD14^+$ cells by immunomagnetic isolation and cultivation for 2 days in GM-CSF and IL-4 conditioned medium. Subsequently, the addition of proinflammatory molecules such as TNF-α, IL-1β, IL-6, and PGE_2 for further 24 hours induces maturation. Generation of DCs from $CD34^+$ HSCs requires mobilization of these cells into the peripheral blood of the patient prior to leukapheresis. Cultivation and expansion of these cells involve the cytokines GM-CSF, Flt3L, and TNF-α and results in mDCs with the typical LC-like morphology as described above. These cells are highly potent to initiate T-cell response. The most important step before vaccination is the complete maturation of DCs. In this respect, proinflammatory cytokines and PGE_2 are able to enhance the expression of costimulatory molecules, CD40L and CD70. In addition, TLR agonists can optimize DC function [80]. Loading of anti-tumor peptides to immature or mature

DCs result in an effective antigen presentation. It can be performed with homogenized and irradiated tumor material but also with known tumor-associated antigens. Loading of DCs with tumor antigens can be also carried out using recombinant bacterial or viral vectors or by RNA transfection of DCs. [81, 82]. Finally, DC transfection with mRNAs related to tumor-associated antigens can bypass the use of bacterial or viral vectors [69].

Nevertheless, an efficient DC vaccination requires strategies to overcome the immune modulating tumor environment as outlined above.

6. Conclusion

DCs are powerful mediators of innate and adaptive cellular immune response. There are different DC subtypes in respect to their localization and their functions in immune regulation or antigen presentation. The function of mDCs is highly controlled by steroid hormones. In this respect, β-estradiol supports differentiation and maturation of DCs, whereas progesterone has inhibitory effects. In the FRT, progesterone has an immune-suppressive effect during pregnancy. The estrogen deficiency after menopause also decreases the overall immune responsiveness. Also tumors of the female reproductive system are dependent on steroid hormones with implications for tumor prevention and tumor therapy. Finally, DCs can be propagated *ex vivo,* primed with tumor material, and used for vaccination against tumors. Nevertheless, the immunosuppressive tumor environment has been taken into consideration for an effective therapy.

7. Abbreviations

BDCAs, blood DC-specific antigens; BSA, bovine serum albumin; CD, cluster of differentiation; cDC1s, classical $CD1^+$ DCs; Clec9A, group V C-type lectin-like cell surface receptor mediating endocytosis but not phagocytosis; CXCL10, chemokine CXCL10; DCs, dendritic cells; E2-2, basic helix-loop-helix transcription factor (E protein); EEA1, early endosome antigen 1; ERα, estrogen receptor α; ERC, endosomal recycling compartment; EM, electron microscopy; ER, endoplasmic reticulum; ER60, chaperon thioreductase ER60; flt-3L, fms-like transcript 3 Ligand; FRT, female reproductive tract; G-CSF, granulocyte colony-stimulating factor; GM-CSF, granulocyte macrophage colony-stimulating factor; HLA, human leukocyte antigens; ID2, transcriptional regulator belonging to the inhibitor of DNA binding (ID) family; IDO, indoleamine 2,3-dioxygenase; IFN-α, interferon alpha; IFN-β, Interferon beta; IFN-γ, interferon gamma; Ig, immunoglobulin; IL-10, Interleukin 10; IRFs, interferon regulatory transcription factors; LC, epidermal Langerhans cells; LPS, lipopolysaccharide; MACS, magnetic cell separator; maf, maf transcription factor family; MALT, mucosa-associated lymphoid tissue; M-CSF, macrophage colony-stimulating factor; MIIC, MHC-class II compartment; mDCs, myeloid dendritic cells; MHC, major histocompatibility complex; NF-κB, nuclear factor kappa-light-chain-enhancer of activated B cells; PAMPs, pathogen-associated

molecular patterns; PBS, phosphate-buffered saline; pDCs, plasmacytoid dendritic cells; $PGE_{2,}$ prostaglandin $E_{2;}$ PU.1, hematopoietic transcription factor PU.1; SCF, stem cell factor; SEM, scanning electron microscopy; STATs, signal transducers and activators of transcription; TAPs, transporter proteins associated with antigen processing; TCR, T-cell receptor; TEM, transmission electron microscopy; Th0, Th1, Th2, and Th17, T-helper cells 0, 1, 2 or 17; TLRs, toll-like receptors; TGF-β1, transforming growth factor β1; Treg, regulatory T-cells

Acknowledgements

The authors gratefully acknowledge Mrs. Federenko Ivanna, Mrs. Beatrix Mallinger, and Mrs. Regina Wegscheider for their skillful and excellent technical assistance, and thank Mr. Ulrich Kaindl and Mr. Thomas Nardelli for their valuable help with the artwork.

Author details

Josef Neumüller[1,2], Sylvia Emanuela Neumüller-Guber[3], Johannes Huber[4], Adolf Ellinger[1] and Thomas Wagner[5*]

*Address all correspondence to: thomas.wagner@medunigraz.at

1 Medical University of Vienna, Center for Anatomy and Cell Biology, Department of Cell Biology and Ultrastructure Research, Vienna, Austria

2 Blood Donation Center of the Austrian Red Cross for Vienna, Lower Austria and Burgenland, Vienna, Austria

3 Medical University of Innsbruck, Sektion for Virologie, Department for Hygiene, Microbiology, Social Medicine, Innsbruck, Austria

4 Medical University of Vienna, Department of Gynecologic Endocrinology and Reproductive Medicine, Vienna, Austria

5 Medical University of Graz, Department of Blood Group Serology and Transfusion Medicine, Graz, Austria

References

[1] Steinman RM, Idoyaga J. Features of the dendritic cell lineage. Immunological Reviews. 2010;234(1):5-17. DOI: 10.1111/j.0105-2896.2009.00888.x

[2] Romani N, Clausen BE, Stoitzner P. Langerhans cells and more: Langerin-expressing dendritic cell subsets in the skin. Immunological Reviews. 2010; 234(1):120-141.DOI: 10.1111/j.0105-2896.2009.00886.x

[3] Mc Dermott R, Ziylan U, Spehner D, et al. Birbeck granules are subdomains of endosomal recycling compartment in human epidermal Langerhans cells, which form where Langerin accumulates. Molecular Biology of the Cell. 2002; 13(1):317-335. DOI: 10.1091/mbc.01-06-0300

[4] Christie D, Zhu J. Transcriptional regulatory networks for CD4 T cell differentiation. Current Topics in Microbiology and Immunology. 2014; 381:125-172. DOI: 10.1007/82_2014_372

[5] Brode S, Macary PA. Cross-presentation: Dendritic cells and macrophages bite off more than they can chew! Immunology. 2004; 112(3):345-351. DOI: 10.1111/j.1365-2567.2004.01920.x

[6] Grabbe S, Kampgen E, Schuler G. Dendritic cells: Multi-lineal and multi-functional. Immunology Today. 2000; 21(9):431-433. URL: http://www.ncbi.nlm.nih.gov/pubmed/11012244

[7] Kared H, Camous X, Larbi A. T cells and their cytokines in persistent stimulation of the immune system. Current Opinion in Immunology. 2014; 29:79-85. DOI: 10.1016/j.coi.2014.05.003

[8] Trombetta ES, Ebersold M, Garrett W, Pypaert M, Mellman I. Activation of lysosomal function during dendritic cell maturation. Science. 2003; 299(5611):1400-1403. DOI: 10.1126/science.1080106

[9] Seliger B, Maeurer MJ, Ferrone S. Antigen-processing machinery breakdown and tumor growth. Immunology Today. 2000; 21(9):455-464. URL: http://www.ncbi.nlm.nih.gov/pubmed/10953098

[10] Bykovskaia SN, Shurin GV, Graner S, et al. Differentiation of immunostimulatory stem-cell- and monocyte-derived dendritic cells involves maturation of intracellular compartments responsible for antigen presentation and secretion. Stem Cells 2002; 20(5):380-393. DOI: 10.1634/stemcells.20-5-380

[11] Kaneko T, Okiji T, Kan L, Suda H, Takagi M. An immunoelectron-microscopic study of class II major histocompatibility complex molecule-expressing macrophages and dendritic cells in experimental rat periapical lesions. Archives of Oral Biology. 2001; 46(8):713-720. URL: http://www.ncbi.nlm.nih.gov/pubmed/11389863

[12] Paillot R, Laval F, Audonnet JC, Andreoni C, Juillard V. Functional and phenotypic characterization of distinct porcine dendritic cells derived from peripheral blood monocytes. Immunology. 2001; 102(4):396-404. URL: http://www.ncbi.nlm.nih.gov/pubmed/11328373

[13] Geuze HJ. The role of endosomes and lysosomes in MHC class II functioning. Immunology Today. 1998; 19(6):282-287. URL: http://www.ncbi.nlm.nih.gov/pubmed/9639994

[14] Smyth CM, Logan G, Boadle R, Rowe PB, Smythe JA, Alexander IE. Differential subcellular localization of CD86 in human PBMC-derived macrophages and DCs, and ultrastructural characterization by immuno-electron microscopy. International Immunology. 2005; 17(2):123-132. DOI: 10.1093/intimm/dxh193

[15] Platt CD, Ma JK, Chalouni C, Ebersold M, Bou-Reslan H, Carano RA, Mellman I, Delamarre L. Mature dendritic cells use endocytic receptors to capture and present antigens. Proceedings of the National Academy of Sciences of the United States of America. 2010; 107(9):4287-4292. DOI: 10.1073/pnas.0910609107

[16] ten Broeke T, van Niel G, Wauben MH, Wubbolts R, Stoorvogel W. Endosomally stored MHC class II does not contribute to antigen presentation by dendritic cells at inflammatory conditions. Traffic. 2011; 12(8):1025-1036. DOI: 10.1111/j.1600-0854.2011.01212.x

[17] Ackerman AL, Giodini A, Cresswell P. A role for the endoplasmic reticulum protein retrotranslocation machinery during crosspresentation by dendritic cells. Immunity. 2006; 25(4):607-617. DOI: 10.1016/j.immuni.2006.08.017

[18] Joffre OP, Segura E, Savina A, Amigorena S. Cross-presentation by dendritic cells. Nature Reviews Immunology. 2012; 12(8):557-569. DOI: 10.1038/nri3254

[19] Segura E, Amigorena S. Cross-presentation by human dendritic cell subsets. Immunology Letters. 2014; 158(1-2):73-78. DOI: 10.1016/j.imlet.2013.12.001

[20] Basu S, Binder RJ, Ramalingam T, Srivastava PK. CD91 is a common receptor for heat shock proteins gp96, hsp90, hsp70, and calreticulin. Immunity. 2001; 14(3):303-313. URL: http://www.ncbi.nlm.nih.gov/pubmed/11290339

[21] Berwin B, Hart JP, Rice S, Gass C, Pizzo SV, Post SR, Nicchitta CV. Scavenger receptor-A mediates gp96/GRP94 and calreticulin internalization by antigen-presenting cells. EMBO Journal. 2003; 22(22):6127-6136. DOI: 10.1093/emboj/cdg572

[22] Binder RJ, Han DK, Srivastava PK. CD91: A receptor for heat shock protein gp96. Nature Immunology. 2000; 1(2):151-155. DOI: 10.1038/77835

[23] Delneste Y, Magistrelli G, Gauchat J, et al. Involvement of LOX-1 in dendritic cell-mediated antigen cross-presentation. Immunity. 2002; 17(3):353-362. URL: http://www.ncbi.nlm.nih.gov/pubmed/12354387

[24] Guermonprez P, Valladeau J, Zitvogel L, Thery C, Amigorena S. Antigen presentation and T cell stimulation by dendritic cells. Annual Review of Immunology. 2002; 20:621-667. DOI: 10.1146/annurev.immunol.20.100301.064828

[25] Carbone FR, Kurts C, Bennett SR, Miller JF, Heath WR. Cross-presentation: A general mechanism for CTL immunity and tolerance. Immunology Today 1998; 19(8): 368-373. URL: http://www.ncbi.nlm.nih.gov/pubmed/9709505

[26] Liu K, Nussenzweig MC. Origin and development of dendritic cells. Immunological Reviews. 2010; 234(1):45-54. DOI: 10.1111/j.0105-2896.2009.00879.x

[27] Makala LH, Nagasawa H. Dendritic cells: A specialized complex system of antigen presenting cells. Journal of Veterinary Medical Science/Japanese Society of Veterinary Science. 2002; 64(3):181-193. URL: http://www.ncbi.nlm.nih.gov/pubmed/11999435

[28] Mackensen A, Herbst B, Kohler G, et al. Delineation of the dendritic cell lineage by generating large numbers of Birbeck granule-positive Langerhans cells from human peripheral blood progenitor cells in vitro. Blood. 1995; 86(7):2699-2707. URL: http://www.ncbi.nlm.nih.gov/pubmed/7545468

[29] Manz MG, Traver D, Miyamoto T, Weissman IL, Akashi K. Dendritic cell potentials of early lymphoid and myeloid progenitors. Blood. 2001; 97(11):3333-3341. URL: http://www.ncbi.nlm.nih.gov/pubmed/11369621

[30] Ardavin C, Martinez del Hoyo G, Martin P, et al. Origin and differentiation of dendritic cells. Trends in Immunology. 2001; 22(12):691-700. URL: http://www.ncbi.nlm.nih.gov/pubmed/11739000

[31] Zhou L, Chong MM, Littman DR. Plasticity of CD4+ T cell lineage differentiation. Immunity. 2009; 30(5):646-655. DOI: 10.1016/j.immuni.2009.05.001

[32] Korn T, Bettelli E, Oukka M, Kuchroo VK. IL-17 and Th17 Cells. Annual Review of Immunology. 2009; 27:485-517. DOI: 10.1146/annurev.immunol.021908.132710

[33] Josefowicz SZ, Lu LF, Rudensky AY. Regulatory T cells: Mechanisms of differentiation and function. Annual Review of Immunology. 2012; 30:531-564. DOI: 10.1146/annurev.immunol.25.022106.141623

[34] O'Shea JJ, Plenge R. JAK and STAT signaling molecules in immunoregulation and immune-mediated disease. Immunity. 2012; 36(4):542-550. DOI: 10.1016/j.immuni.2012.03.014

[35] Haniffa M, Bigley V, Collin M. Human mononuclear phagocyte system reunited. Seminars in Cell & Developmental Biology. 2015; 41:59-69. DOI: 10.1016/j.semcdb.2015.05.004

[36] Chistiakov DA, Sobenin IA, Orekhov AN, Bobryshev YV. Myeloid dendritic cells: Development, functions, and role in atherosclerotic inflammation. Immunobiology. 2015; 220(6):833-844. DOI: 10.1016/j.imbio.2014.12.010

[37] Scharf L, Li NS, Hawk AJ, et al. The 2.5 A structure of CD1c in complex with a mycobacterial lipid reveals an open groove ideally suited for diverse antigen presentation. Immunity. 2010; 33(6):853-862. DOI: 10.1016/j.immuni.2010.11.026

[38] Schüller SS, Sadeghi K, Wisgrill L, et al. Preterm neonates display altered plasmacytoid dendritic cell function and morphology. Journal of Leukocyte Biology. 2013; 93(5):781-788. DOI: 10.1189/jlb.1011525

[39] van der Aa E, van Montfoort N, Woltman AM. BDCA3(+)CLEC9A(+) human dendritic cell function and development. Seminars in Cell & Developmental Biology. 2015; 41:39-48. DOI: 10.1016/j.semcdb.2014.05.016

[40] Arnold-Schrauf C, Berod L, Sparwasser T. Dendritic cell specific targeting of MyD88 signalling pathways in vivo. European Journal of Immunology. 2015; 45(1):32-39. DOI: 10.1002/eji.201444747

[41] Maverakis E, Kim K, Shimoda M, et al. Glycans in the immune system and The Altered Glycan Theory of Autoimmunity: A critical review. Journal of Autoimmunity. 2015; 57:1-13. DOI: 10.1016/j.jaut.2014.12.002

[42] Trda L, Boutrot F, Claverie J, Brule D, Dorey S, Poinssot B. Perception of pathogenic or beneficial bacteria and their evasion of host immunity: Pattern recognition receptors in the frontline. Frontiers in Plant Science. 2015; 6:219. DOI: 10.3389/fpls.2015.00219

[43] Land WG. The role of damage-associated molecular patterns in human diseases: Part I – Promoting inflammation and immunity. Sultan Qaboos University Medical Journal. 2015; 15(1):e9-e21. URL: http://www.ncbi.nlm.nih.gov/pubmed/25685392

[44] Land WG. The role of damage-associated molecular patterns (DAMPs) in human diseases: Part II: DAMPs as diagnostics, prognostics and therapeutics in clinical medicine. Sultan Qaboos University Medical Journal. 2015; 15(2):e157-170. URL http://www.ncbi.nlm.nih.gov/pubmed/26052447

[45] Lotze MT, Deisseroth A, Rubartelli A. Damage associated molecular pattern molecules. Clinical Immunology. 2007; 124(1):1-4. DOI: 10.1016/j.clim.2007.02.006

[46] Venereau E, Ceriotti C, Bianchi ME. DAMPs from cell death to new life. Frontiers in Immunology. 2015; 6:422. DOI: 10.3389/fimmu.2015.00422

[47] Strunk D, Rappersberger K, Egger C, Strobl H, Kromer E, Elbe A, Maurer D, Stingl G. Generation of human dendritic cells/Langerhans cells from circulating CD34+ hematopoietic progenitor cells. Blood. 1996; 87(4):1292-1302. URL: http://www.ncbi.nlm.nih.gov/pubmed/8608217

[48] Chang SY, Song JH, Guleng B, et al. Circulatory antigen processing by mucosal dendritic cells controls CD8(+) T cell activation. Immunity. 2013; 38(1):153-165. DOI: 10.1016/j.immuni.2012.09.018

[49] Niess JH, Brand S, Gu X, et al. CX3CR1-mediated dendritic cell access to the intestinal lumen and bacterial clearance. Science. 2005; 307(5707):254-258. DOI: 10.1126/science.1102901

[50] Rescigno M, Rotta G, Valzasina B, Ricciardi-Castagnoli P. Dendritic cells shuttle microbes across gut epithelial monolayers. Immunobiology. 2001; 204(5):572-581. DOI: 10.1078/0171-2985-00094

[51] Neumüller J, Neumüller-Guber SE, Lipovac M, Mosgoeller W, Vetterlein M, Pavelka M, Huber J. Immunological and ultrastructural characterization of endothelial cell cultures differentiated from human cord blood derived endothelial progenitor cells. Histochemistry and Cell Biology. 2006; 126(6):649-664. DOI: 10.1007/s00418-006-0201-6

[52] Srisen K, Rohrl C, Meisslitzer-Ruppitsch C, Ranftler C, Ellinger A, Pavelka M, Neumüller J. Human endothelial progenitor cells internalize high-density lipoprotein. PloS One. 2013; 8(12):e83189. DOI: 10.1371/journal.pone.0083189

[53] Strobl H, Knapp W. TGF-beta1 regulation of dendritic cells. Microbes and Infection/Institut Pasteur. 1999; 1(15):1283-1290. URL: http://www.ncbi.nlm.nih.gov/pubmed/10611756

[54] Strobl H, Riedl E, Scheinecker C, Bello-Fernandez C, Pickl WF, Rappersberger K, Majdic O, Knapp W. TGF-beta 1 promotes in vitro development of dendritic cells from CD34+ hemopoietic progenitors. Journal of Immunology. 1996; 157(4):1499-1507. URL: http://www.ncbi.nlm.nih.gov/pubmed/8759731

[55] Romani N, Reider D, Heuer M, Ebner S, Kampgen E, Eibl B, Niederwieser D, Schuler G. Generation of mature dendritic cells from human blood. An improved method with special regard to clinical applicability. Journal of Immunological Methods. 1996; 196(2):137-151. URL: http://www.ncbi.nlm.nih.gov/pubmed/8841452

[56] Reis e Sousa C. Dendritic cells in a mature age. Nature Reviews Immunology. 2006; 6(6):476-483. DOI: 10.1038/nri1845

[57] Fujimoto Y, Tedder TF. CD83: A regulatory molecule of the immune system with great potential for therapeutic application. Journal of Medical and Dental Sciences. 2006; 53(2):85-91. URL: http://www.ncbi.nlm.nih.gov/pubmed/16913569

[58] Carreras E, Turner S, Paharkova-Vatchkova V, Mao A, Dascher C, Kovats S. Estradiol acts directly on bone marrow myeloid progenitors to differentially regulate GM-CSF or Flt3 ligand-mediated dendritic cell differentiation. Journal of Immunology. 2008; 180(2):727-738. URL: http://www.ncbi.nlm.nih.gov/pubmed/18178810

[59] Heldring N, Pike A, Andersson S, et al. Estrogen receptors: How do they signal and what are their targets. Physiological Reviews. 2007; 87(3):905-931. DOI: 10.1152/physrev.00026.2006

[60] Kovats S. Estrogen receptors regulate innate immune cells and signaling pathways. Cellular Immunology. 2015; 294(2):63-69. DOI: 10.1016/j.cellimm.2015.01.018

[61] Mann M, Cortez V, Vadlamudi RK. Epigenetics of estrogen receptor signaling: role in hormonal cancer progression and therapy. Cancers. 2011; 3(3):1691-1707. DOI: 10.3390/cancers3021691

[62] Paharkova-Vatchkova V, Maldonado R, Kovats S. Estrogen preferentially promotes the differentiation of CD11c+ CD11b(intermediate) dendritic cells from bone marrow precursors. Journal of Immunology. 2004; 172(3):1426-1436. URL: http://www.ncbi.nlm.nih.gov/pubmed/14734718

[63] Carreras E, Turner S, Frank MB, et al. Estrogen receptor signaling promotes dendritic cell differentiation by increasing expression of the transcription factor IRF4. Blood. 2010; 115(2):238-246. DOI: 10.1182/blood-2009-08-236935

[64] Nalbandian G, Paharkova-Vatchkova V, Mao A, Nale S, Kovats S. The selective estrogen receptor modulators, tamoxifen and raloxifene, impair dendritic cell differentiation and activation. Journal of Immunology. 2005; 175(4):2666-2675. URL: http://www.ncbi.nlm.nih.gov/pubmed/16081843

[65] Huck B, Steck T, Habersack M, Dietl J, Kammerer U. Pregnancy associated hormones modulate the cytokine production but not the phenotype of PBMC-derived human dendritic cells. European Journal of Obstetrics, Gynecology, and Reproductive Biology. 2005; 122(1):85-94. DOI: 10.1016/j.ejogrb.2005.02.017

[66] Piccinni MP, Scaletti C, Maggi E, Romagnani S. Role of hormone-controlled Th1- and Th2-type cytokines in successful pregnancy. Journal of Neuroimmunology. 2000; 109(1):30-33. URL: http://www.ncbi.nlm.nih.gov/pubmed/10969178

[67] Xu Y, He H, Li C, Shi Y, Wang Q, Li W, Song W. Immunosuppressive effect of progesterone on dendritic cells in mice. Journal of Reproductive Immunology. 2011; 91(1-2):17-23. DOI: 10.1016/j.jri.2011.06.101

[68] Quispe Calla NE, Ghonime MG, Cherpes TL, Vicetti Miguel RD. Medroxyprogesterone acetate impairs human dendritic cell activation and function. Human Reproduction. 2015; 30(5):1169-1177. DOI: 10.1093/humrep/dev035

[69] Ghosh M, Rodriguez-Garcia M, Wira CR. The immune system in menopause: Pros and cons of hormone therapy. Journal of Steroid Biochemistry and Molecular Biology. 2014; 142:171-175. DOI: 10.1016/j.jsbmb.2013.09.003

[70] Gameiro C, Romao F. Changes in the immune system during menopause and aging. Frontiers in Bioscience. 2010; 2:1299-1303. URL: http://www.ncbi.nlm.nih.gov/pubmed/20515802

[71] Ljunggren HG. Dendritic cells, dendritic cell-based vaccines and Ralph Steinman. Journal of Internal Medicine. 2012; 271(2):174-176. DOI: 10.1111/j.1365-2796.2011.02495.x

[72] Steinman RM, Banchereau J. Taking dendritic cells into medicine. Nature. 2007; 449(7161):419-426. DOI: 10.1038/nature06175

[73] Gieseler R, Heise D, Soruri A, Schwartz P, Peters JH. In-vitro differentiation of mature dendritic cells from human blood monocytes. Developmental Immunology. 1998; 6(1-2):25-39. URL: http://www.ncbi.nlm.nih.gov/pubmed/9716903

[74] Lenzner S, Scholtes U, Peters JH. Focussing human B cell specificity by immunoselection via antigen-presenting cells in vitro. Immunobiology. 1998; 198(5):539-551. DOI: 10.1016/S0171-2985(98)80077-6

[75] Soruri A, Zwirner J. Dendritic cells: Limited potential in immunotherapy. International Journal of Biochemistry & Cell Biology. 2005; 37(2):241-245. DOI: 10.1016/j.biocel.2004.07.003

[76] Tran Janco JM, Lamichhane P, Karyampudi L, Knutson KL. Tumor-infiltrating dendritic cells in cancer pathogenesis. Journal of Immunology. 2015; 194(7):2985-2991. DOI: 10.4049/jimmunol.1403134

[77] Cheng P, Corzo CA, Luetteke N, et al. Inhibition of dendritic cell differentiation and accumulation of myeloid-derived suppressor cells in cancer is regulated by S100A9 protein. Journal of Experimental Medicine. 2008; 205(10):2235-2249. DOI: 10.1084/jem.20080132

[78] Sznol M, Chen L. Antagonist antibodies to PD-1 and B7-H1 (PD-L1) in the treatment of advanced human cancer. Clinical Cancer Research: An Official Journal of the American Association for Cancer Research. 2013; 19(5):1021-1034. DOI: 10.1158/1078-0432.CCR-12-2063

[79] Cubillos-Ruiz JR, Baird JR, Tesone AJ, et al. Reprogramming tumor-associated dendritic cells in vivo using miRNA mimetics triggers protective immunity against ovarian cancer. Cancer Research. 2012; 72(7):1683-1693. DOI: 10.1158/0008-5472.CAN-11-3160

[80] Sabado RL, Bhardwaj N. Directing dendritic cell immunotherapy towards successful cancer treatment. Immunotherapy. 2010; 2(1):37-56. DOI: 10.2217/imt.09.43

[81] Brockstedt DG, Dubensky TW. Promises and challenges for the development of Listeria monocytogenes-based immunotherapies. Expert Review of Vaccines. 2008; 7(7): 1069-1084. DOI: 10.1586/14760584.7.7.1069

[82] Jenne L, Schuler G, Steinkasserer A. Viral vectors for dendritic cell-based immunotherapy. Trends in Immunology. 2001; 22(2):102-107. URL: http://www.ncbi.nlm.nih.gov/pubmed/11286712

Chapter 1

Electron Diffraction

Mohsen Asadi Asadabad and Mohammad Jafari Eskandari

Additional information is available at the end of the chapter

http://dx.doi.org/10.5772/61781

Abstract

Electron microscopes are usually supplied with equipment for obtaining diffraction patterns and micrographs from the same area of a specimen and the best results are attained if the complete use is to be made of these combined facilities. Electron diffraction patterns are used to obtain quantitative data including phase identification, orientation relationship and crystal defects in materials, etc. At first, a general introduction including a geometrical and quantitative approach to electron diffraction from a crystalline specimen, the reciprocal lattice and electron diffraction in the electron microscope are presented. The scattering process by an individual atom as well as a crystal, the Bragg law, Laue conditions and structure factor are also discussed. Types of diffraction patterns such as ring pattern, spot pattern and Kikuchi pattern, and general and unique indexing diffraction patterns are explained. The procedure for indexing simple, complicated and imperfect patterns as well as Kikuchi lines and a combination of Kikuchi lines and spots is outlined. The known and unknown materials are identified by indexing patterns. Practical comparisons between various methods of analysing diffraction patterns are also described. The basic diffraction patterns and the fine structure in the patterns including specimen tilting experiments, orientation relationship determination, phase identification, twinning, second phases, crystallographic information, dislocation, preferred orientation and texture, extra spots and streaks are described in detail. Finally, electron diffraction patterns of new materials are investigated.

Keywords: Electron diffraction pattern, Spot and ring pattern, Kikuchi line, Phase identification

1. General introduction

In quantum mechanics, electrons may be considered as particles or waves. Electrons are used in transmission electron microscopy (TEM) because the wavelength of electrons is shorter than the visible light. For this reason, high magnifications can be achieved in TEM. In TEM, tungsten filament is usually used to produce a monochromatic beam of electrons by thermionic or field

emission processes. Electrons are accelerated by applied voltage and focused by the objective lens. These particles with negative charge travel the spiral path when passing through the electromagnetic lenses. Then, this beam of electrons is transmitted through very thin specimen (thickness about 100–300 nm) and magnified by the electromagnetic lens, forming the electron diffraction pattern. Electrons are accelerated to close to the speed of light at high voltages. So, relativistic effects should be considered in equations of electron beam wavelength in electron microscopy at high accelerated voltage. The modified relativistic wavelength is

$$\lambda = \frac{h}{\left(2m_e Ve\left(1 + eV / 2m_e c^2\right)\right)^{1/2}} \tag{1}$$

where h is Planck's constant, m_e is the rest mass of electrons, e is charge of electrons, V is accelerated voltage of electrons and c is the velocity of light. In fact, electron diffraction directly demonstrates the reciprocal lattice of the crystalline lattice of the selected area from a sample [1].

1.1. Elastic scattering of electrons by individual atom

When a beam of electrons transmits through a thin specimen, different interactions can occur such as ionization, secondary emission and excitation with loss of energy and can be scattered by nuclei and electron cloud without loss of energy. The elastic scattering process by an isolated atom is illustrated in Figure 1.Some of the electrons are backscattered and the rest are scattered by nucleus and electron cloud (Rutherford scattering). The atomic scattering amplitude for electrons f_θ (atomic diffraction factor: a measure of the diffracting capability of an isolated atom) is given by

$$f_\theta = \frac{m_e e^2}{2h^2}\left(\frac{\lambda}{sin\theta}\right)^2 \left(Z - f_x\right) \tag{2}$$

where θ is the scattering angle, Z is the atomic number of isolated atom (Rutherford scattering) and f_x is the atomic scattering factor for X-rays. The elastically scattered electrons' main contribution is in the form of diffraction patterns. Most of the particles are scattered within ±5° of the direct incident beam [2].

1.2. Scattering by an ideal crystal structure

For understanding the essence of electron diffraction by a three-dimensional crystal structure of a material, the principles of diffraction of a monochromatic light by Young's double slit experiment should be investigated. First of all, diffraction by two slits is investigated, then, diffraction is generalized to an infinite number of slits and, finally, diffraction from a regular arrangement of atoms is investigated. In Figure 2, the plane waves collide with a barrier with

http://dx.doi.org/10.5772/61781

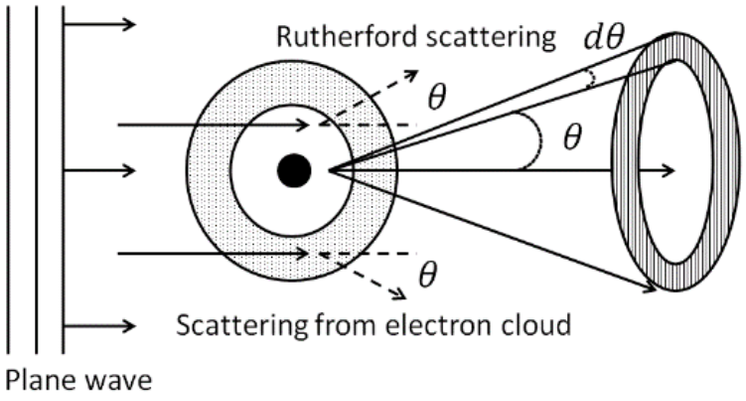

Figure 1. Electrons are as plane wave and black circle is an isolated atom. Electrons are scattered from electron cloud and nucleus of a single atom at the angle θ.

two slits in which the length and width of slits are l and a, respectively, with respect to $l \gg a$. Also, bright and dark fringes are formed on the screen which is placed at a distance S, with respect to $S \gg a$. If the waves are in-phase when passing through the slits, there is relative phase difference between two secondary sources. Two beams of electrons have constructive interference if their relative phase difference is an integer multiple of λ ($\delta = n\lambda$), then the bright fringes are formed on the screen. Similarly, two beams of electrons have unconstructive interference if their relative phase difference is not an integer multiple of λ ($\delta = n\lambda/2$). Therefore, dark fringes are formed on the screen, in which intensity is very low or zero. Alternating bright and dark lines are formed on the screen. The intensity of the bright fringes at the center is very high and away from the center as θ increases, their intensity and width are decreased. In a real three-dimensional crystal lattice, diffraction of electron beams occurs by regular spacing between atoms, which creates an interference pattern.

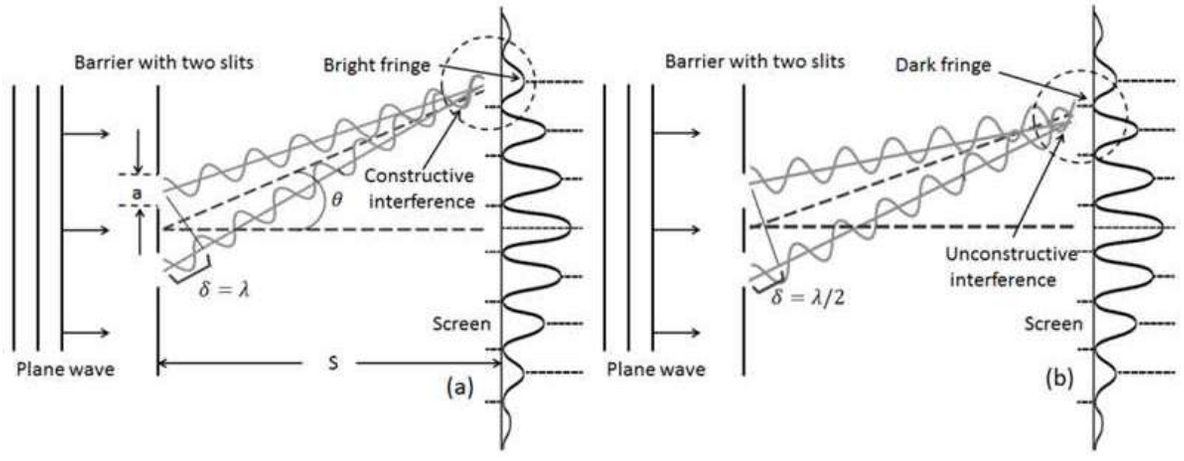

Figure 2. Diffracted beam of electrons by barrier with two slits (Young's slits). (a) Lines bright (constructive interference), (b) Lines dark (unconstructive interference).

In general, electron diffraction is according to kinematical theory and some assumptions must also be considered [2, 3].

1.3. The Bragg law

For studying the scattered and transmitted beams, a cross-section of a thin specimen with a perfect crystal lattice is considered. Incident coherent electron and in-phase beams are radiated from the top surface of the thin specimen. This electron beam is collided with two atoms, each of which belongs to a plane (two adjacent planes) with different *hkl* (Miller indices) with interplanar spacing of crystal lattice being equal to d. Then, the electron beam is diffracted by elastic scattering. These waves are coherent and in-phase after passing through the sample if the path difference of the electron beam is an integer number of wavelength (constructive interference), that is, geometric relationships $AC + AD = n\lambda$ and $AC = AD = dsin\theta$ are satisfied, as can be seen in Figure 3. So, the following relationship is established:

$$2d_{(hkl)}sin\theta = n\lambda \tag{3}$$

where d is the interplanar spacing, θ is the angle between incident and diffracted beams, λ is the electron wavelength and n is the integer number of order diffraction. This relationship is known as the Bragg law. Basically, first-order diffraction is $n=1$ and Miller indices are used for higher orders $n \geq 2$.

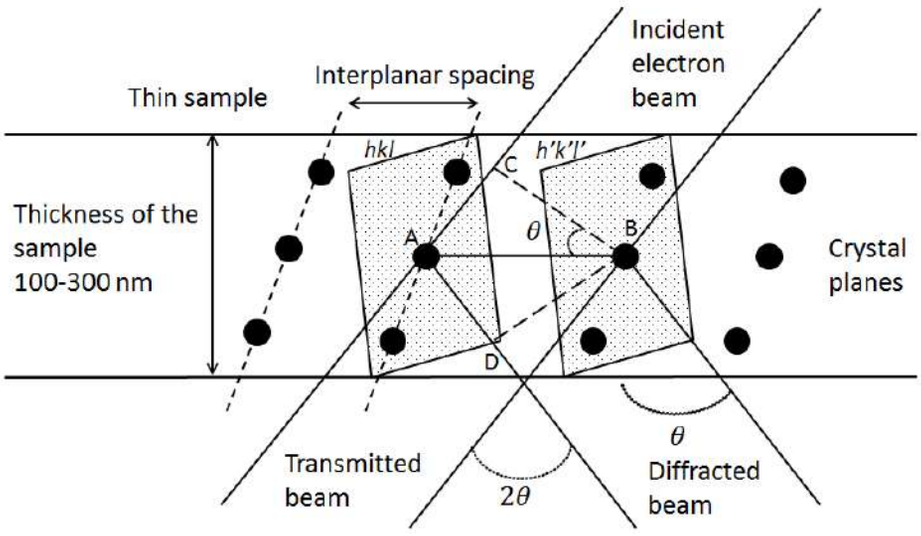

Figure 3. Incident, transmitted and diffracted electron beams in a thin specimen for the Bragg law.

In the Bragg law, electrons are collided with the crystal planes. Some of them are diffracted and the rest are transmitted through the specimen, which does not participate in the formation of the diffraction pattern [1–3].

1.4. The Laue conditions

Diffraction can be considered as a total scattering of individual atoms. So, diffraction is mathematically expressed in terms of total scattering of atoms. The distance from atom A to atom B is described by vector r in three-dimensional space. Also, incident and diffracted beams are described by unit vectors $\boldsymbol{p_0}$ and p, respectively. With the use of these vector notations, we can write paths difference in vector notation as $AC = r.p_0$ and $AD = r.p$. According to the vector relationship in Figure 4, the path difference of wave should be an integer multiple of wavelength and we may write as

$$CAD = \boldsymbol{r}.\boldsymbol{P} = n\lambda \tag{4}$$

The vector $\boldsymbol{r}$, defined in spherical coordinates, is a converted form of vector components x, y and z in Cartesian coordinates, and $\boldsymbol{a}$, $\boldsymbol{b}$ and $\boldsymbol{c}$ are unit vectors defined in the direction of coordinates axes which can be considered as distances between atoms. So, we may write Equation (4) as

$$\begin{aligned} \boldsymbol{P}.\boldsymbol{a} &= h\lambda \\ \boldsymbol{P}.\boldsymbol{b} &= k\lambda \\ \boldsymbol{P}.\boldsymbol{c} &= l\lambda \end{aligned} \tag{5}$$

These algebraic relations are known as Laue conditions. These relations must be satisfied when strong diffraction occurs [2, 3].

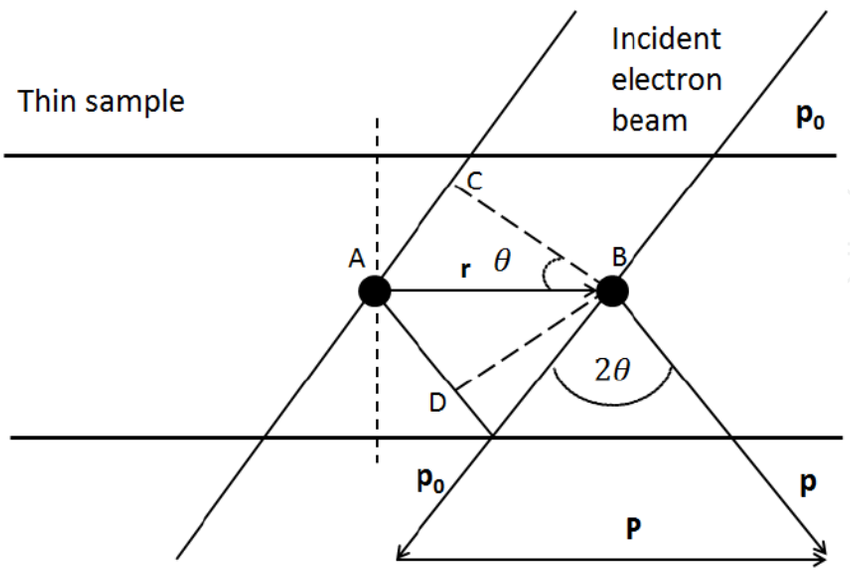

Figure 4. Incident and diffracted waves of atoms in the thin specimen are $\boldsymbol{p_0}$ and p, respectively, the angle between them is 2θ and the distance from atom A to atom B is described by vector r.

1.5. The structure factor

Diffraction intensity is different for each of the crystalline planes because the distribution of atoms per unit area is not the same for individual planes. Using the kinematical theory of electron diffraction, a set of crystal planes can be determined for which the diffraction intensity is zero. The structure factor can be defined as a mathematical function stating the amplitude and phase of electron beam diffracted from crystallographic planes. In the structure factor, the location of atoms in the reflection plane and atomic specifications is considered to describe the diffraction process. Also, the structure factor is the sum of the scattered amplitudes of single atoms f_n and the sum of the phase differences, that is,

$$F_{hkl} = \sum_n f_n exp\left\{2\pi i\left(hx_n + ky_n + lz_n\right)\right\} \tag{6}$$

where x_n, y_n, z_n are positions of the atom in the Cartesian coordinates. The intensity of the diffracted wave is

$$I \propto \left|F\right|^2 \propto f^2\left[1 + cos\left(\pi\left(h+k+l\right)\right)\right]^2 + f^2\left[sin\left(2\pi\left(h+k+l\right)\right)\right]^2 \tag{7}$$

In the above relationship, the intensity is sometimes zero, which belongs to any diffraction not existing in these planes and is called a forbidden reflection. By use of the Bragg law and structure factor, diffracted planes in the crystal can be determined. For intermetallic compounds, the diffraction intensity is different because atomic scattering factors of individual metals forming the intermetallic compound are not the same. For example, intermetallic compounds with an AB structure have diffracted intensity according to the following relations:

$$\begin{aligned} I &\propto \left(f_A + f_B\right)^2 \text{ when } h+k+l \text{ is even} \\ I &\propto \left(f_A - f_B\right)^2 \text{ when } h+k+l \text{ is odd} \end{aligned} \tag{8}$$

Diffraction rules for some of the conventional crystalline structures are presented in Table 1 [2].

Crystal structure	Reflection absent if
simple cubic	all present
f.c.c	*h*, *k*, *l*, mixed odd and even
b.c.c	*h*, *k*, *l* odd
c.p.h	$h+2k=3n$ and *l* is odd
b.c.t	$h+k+l$ odd
Zinc blende	*h*, *k*, *l*, mixed odd and even
Sodium chloride	*h*, *k*, *l*, mixed odd and even
diamond	*h*, *k*, *l*, all even and $h+k+l$ not divisible by four, or *h*, *k*, *l* mixed odd and even

Table 1. Diffraction rules for conventional crystalline structures

1.6. The reciprocal lattice

The reciprocal lattice is an array of points in which each point corresponds to a special plane in the crystal lattice. In fact, each of the planes in real crystal lattice is represented by a point in the reciprocal lattice located at distance $1/d_{hkl}$ from the center O. The distance of a point in the reciprocal lattice to the center is illustrated by the vector $g_{(hkl)}$, which is called the diffraction vector. Diffraction pattern and reciprocal lattice are related to each other and this relation is used for the interpretation of different diffraction patterns. The reciprocal lattice has two special properties:

a. The diffraction vector $g_{(hkl)}$ of reciprocal lattice is perpendicular to the plane of the crystal lattice

b. $g_{(hkl)}=1/d_{hkl}$

The Ewald sphere displays the relation between the reciprocal lattice and the diffraction pattern with a radius of $1/\lambda$. The formation of the Ewald sphere in the reciprocal lattice and the diffraction pattern are depicted in Figure 5. Also, the algebraic relations between incident, transmitted and diffracted beams are shown in this figure. The incident beam of electrons is collided with the thin specimen and then, a certain percentage of the incident beam is transmitted and the rest is diffracted. Using Figure 5, the geometrical relations for distances and angle may be determined from the relation

$$tg2\theta = R/L \tag{9}$$

where θ is the angle between transmitted and diffracted beams, R is the distance between collision points of transmitted and diffracted beams with the screen and L is the distance between the specimen and the screen (the effective camera length). Using the Bragg law and with the assumption of a small θ, relation (9) can be written as follows

$$Rd_{hkl} = L\lambda \tag{10}$$

where $L\lambda$ is a camera constant. The effective camera length and wavelength of the electron are constant and depend on the characterization of transmission electron microscopy [2, 3].

2. Types of electron diffraction patterns

Electron diffraction patterns give crystallographic information about a material and determine different types of materials which can be amorphous, single crystalline or polycrystalline. There are three types of electron diffraction patterns and the formation of each pattern depends on the different conditions of the specimen such as thickness, crystal structure and so on.

1. The polycrystalline materials exhibit ring pattern

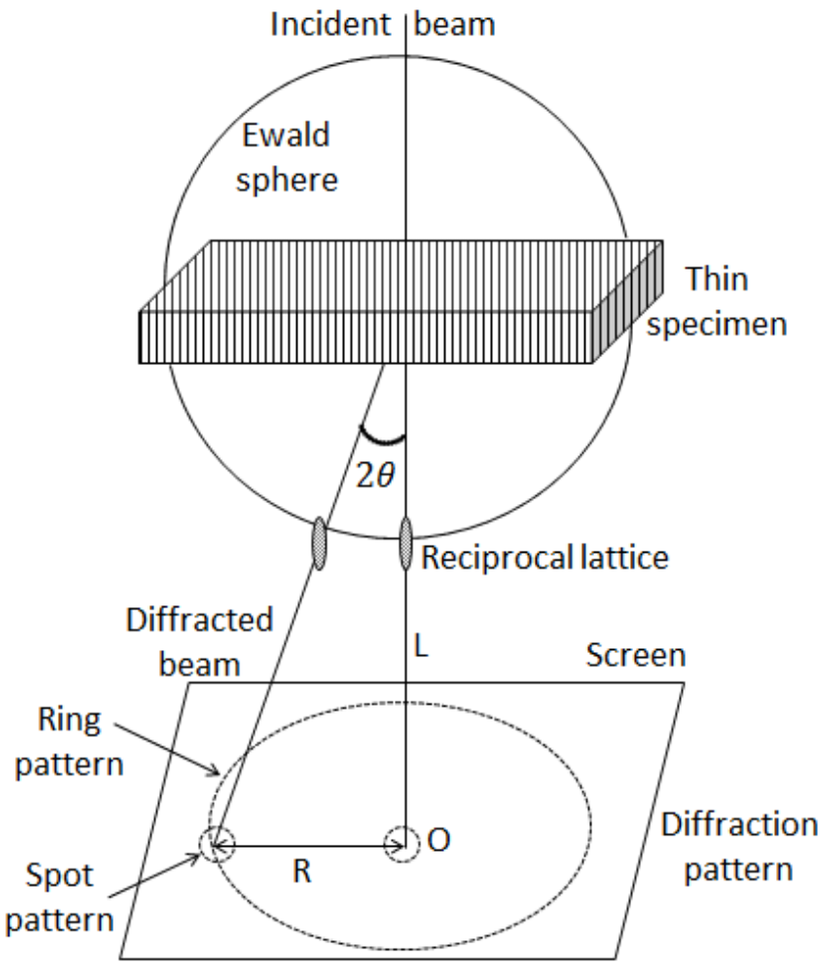

Figure 5. The Ewald sphere is drown in reciprocal lattice. The formation of a diffraction pattern is shown geometrically. The relations between incident, transmitted and diffracted beams, the Ewald sphere and different diffraction patterns are illustrated.

2. The single crystalline materials show (a) spot pattern or (b) Kikuchi line pattern or (c) a combination of spot and Kikuchi line patterns

The spot and Kikuchi line patterns are obtained from a special area of specimen which is called the 'selected area' [5–8]. Selected area electron diffraction (SAED) is a technique in TEM to obtain diffraction patterns that result from the electron beam scattered by the sample lattice.

2.1. Ring pattern

These patterns are created by ultrafine grains of polycrystalline materials. Basically, phases in various polycrystalline materials are determined by interpretation of their ring patterns. For this purpose, we must use a reference specimen for identification of phases as well as specifying interplanar spacing and Miller indices of crystalline planes. Polycrystalline specimens such as pure gold (Au, f.c.c crystal structure with lattice parameter a=4.07 $\mathring{A}$) or pure aluminum (Al, f.c.c crystal structure with lattice parameter a=4.04 $\mathring{A}$) as reference specimens are used to index diffraction patterns of various materials and specify the camera length. To obtain a reference

specimen with a ring diffraction pattern, at first, a copper grid with amorphous carbon coating is provided. Then, by use of a sputter coating device, a thin layer of pure gold with a thickness of about 20 nm is coated on the grid. Finally, the diffraction pattern of the specimen is taken which is in a ring shape and continuous, as can be seen in Figure 6. The planes of the gold specimen are specified by Miller indices. The pure gold sample is known as standard sample and is used for identification of crystalline planes and measurement of interplanar spacing of unknown materials with ring patterns and determination of phases in alloys.

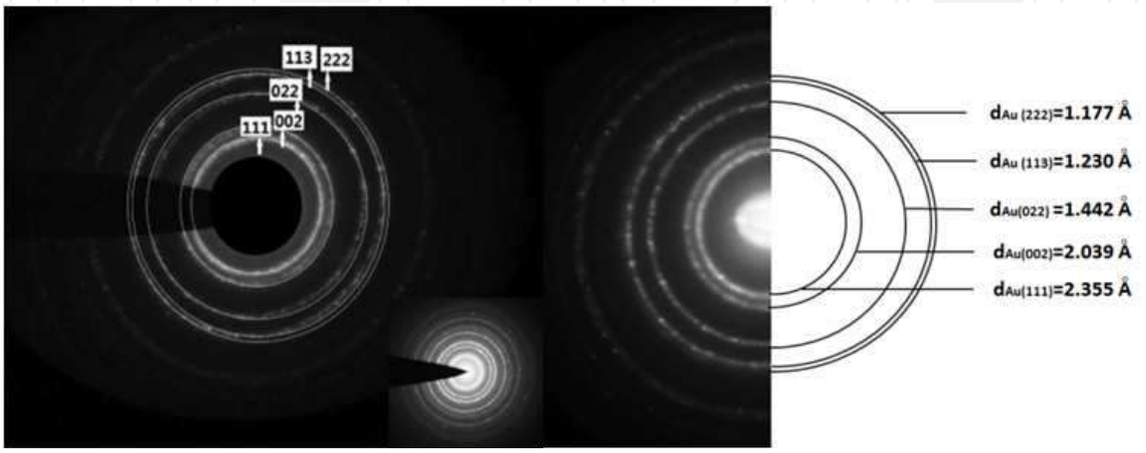

Figure 6. The ring diffraction pattern from a polycrystalline pure gold film with an f.c.c crystal structure. Crystal planes and interplanar spacing are shown by Miller indices. Camera lengths are 180 and 88 mm, respectively [4].

Analysis of ring patterns in polycrystalline materials (ultrafine grain) leads to identification of phases in materials. Diffraction patterns of nanoparticles produced by different methods form a ring pattern. In fact, the ring patterns are created when the nanoparticle is formed. Using the radius of each ring, we can specify the distance between the planes or interplanar spacing. Also, XRD analysis is used to determine the Miller indices for a set of planes. So, XRD analysis confirms the results of diffraction pattern from TEM for certain materials. A ring diffraction pattern from a polycrystalline gold specimen is shown in Figure 6. The interplanar spacing and lattice parameter can be calculated by measuring the radius of each diffraction ring (using Equation (10) and Table 2). Also, indexing ring patterns can be performed by XRD analysis [4–10].

2.1.1. Indexing ring patterns

In this chapter, an EM208S (Philips) transmission electron microscope operating at an accelerating voltage of 100 kV with a wavelength $\lambda = 3.7 \times 10^{-3}$ nm and camera length $L = 180,\ 88$ mm are used. One thing to note is that, accuracy and focus of TEM are very important to obtain an accurate diffraction pattern. Indexing methods used for ring diffraction patterns are as follows:

a. For known materials

1. Using the gold standard diffraction pattern, we define a scale on the picture of patterns to measure the radius diffraction pattern of specimens.

2. The first solution, with known lattice parameters, interplanar spacing is obtained from Equation (10) and Miller indices can be obtained using Table 2. The second solution, the ratio of outer ring to the first ring is equal to the reverse ratio of their interplanar spacing with possible Miller indices.

$$\frac{R_{outer}}{R_{first}} = \frac{d_{first}}{d_{outer}}$$

These possible Miller indices for planes are correct if the result of proportional relation above is almost the same.

b. For unknown material

1. Measure the radius of diffraction pattern like in the previous section.

2. Knowing the camera constant, interplanar spacing is obtained from Equation (10).

3. Compare interplanar spacing of unknown material with the ASTM index* to identify phases in diffraction patterns, Miller indices are determined for crystalline planes of phases in alloys [2, 6, 8].

*ASTM index to the powder diffraction file.

Crystal structure	Proportional relation for interplanar spacing	Possible values of algebraic relations Miller indices	Standard
Simple cubic	$\frac{1}{d^2} = \frac{h^2+k^2+l^2}{a^2} = \frac{N}{a^2}$	N an integer except 7 or 15	Proportional relation of squares of radius $\propto N$
f.c.c	$\frac{1}{d^2} = \frac{h^2+k^2+l^2}{a^2} = \frac{N}{a^2}$	N =3, 4, 8, 11, 12, 16, 19, 20	Proportional relation $\propto N$
b.c.c	$\frac{1}{d^2} = \frac{h^2+k^2+l^2}{a^2} = \frac{N}{a^2}$	N =2, 4, 6, 8, 10, 12, 14, 16, 18, 20	Proportional relation $\propto N$
Diamond structure	$\frac{1}{d^2} = \frac{h^2+k^2+l^2}{a^2} = \frac{N}{a^2}$	N =2, 8, 11, 16, 19	Proportional relation $\propto N$
Tetragonal	$\frac{1}{d^2} = \frac{h^2+k^2}{a^2} + \frac{l^2}{c^2}$	h^2+k^2=1, 2, 4, 5, 8, 9, 10, 13, 16, 17, 18, 20	Proportional relation often is 2
Hexagonal	$\frac{1}{d^2} = \frac{4}{3}\frac{h^2+hk+k^2}{a^2} + \frac{l^2}{c^2}$	h^2+hk+l^2=1, 3, 4, 7, 9, 12, 13, 16, 19	Proportional relation often is 3

Table 2. Proportional relations for interplanar spacing, Miller indices and lattice constant for different crystal structures [2]

2.2. Spot patterns

There are two basic parameters in spot diffraction patterns which are used to interpret and index such types of patterns. These parameters include

1. R is the distance between the diffracted and transmit (center spot) beams in the diffraction pattern screen. Also, this distance can be considered as a normal vector to the plane reflection.

2. The angles such as θ between two vectors drawn from the center to two adjacent points. In fact, each of these spots represents a set of planes, as can be seen in Figure 7.

The zone axis vector is parallel to the incident beam and is almost parallel with a set of reflected planes that is shown by $z=[uvw]$ with components u, v and w along the axis. The spots are in symmetry about the center of the pattern and, using the rules of vectors and the basic parallelogram, we can index spot patterns.

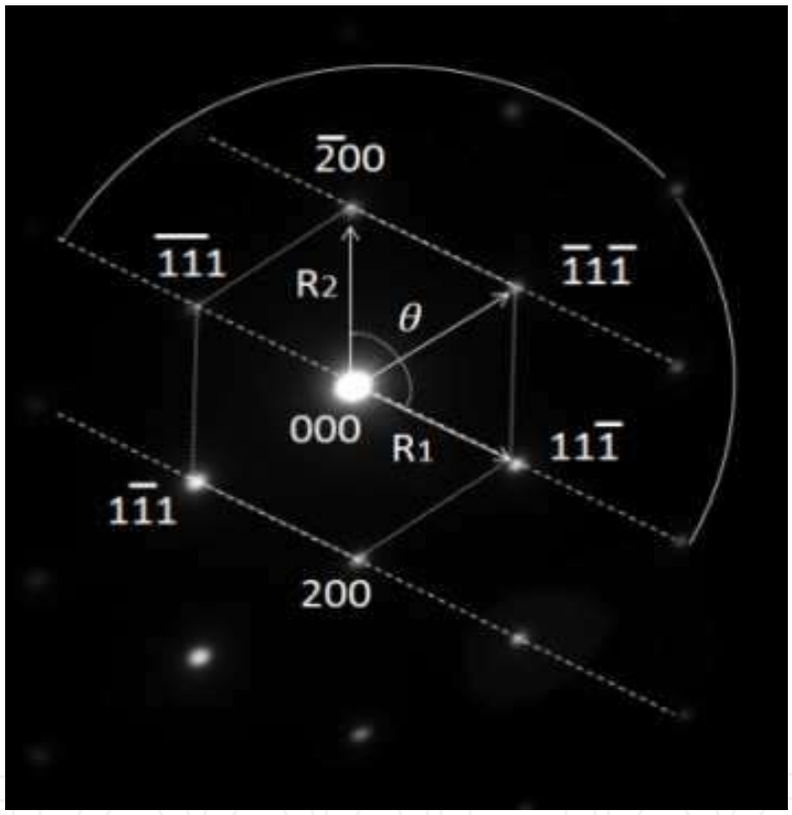

Figure 7. The spot diffraction pattern from a single crystal along zone axis $z=[011]$ of Al 1050 alloy with 10 passes of straight rolling.

2.2.1. Indexing spot patterns

For indexing spot patterns, indices of the spots and zone axis of single crystal materials should be determined. Here, we use the same indexing methods utilized for ring patterns as described in the previous section. In the experimental method, we measure distances of different spots from the center spot as well as angles on the micrograph of patterns and compare with patterns in the International Standard [17]. So, indices of spot and zone axis in pattern can be determined. The zone axis $z=[uvw]$ may be specified by the relations

$$\begin{aligned} u &= k_1 l_2 - k_2 l_1 \\ v &= l_1 h_2 - l_2 h_1 \\ w &= h_1 k_2 - h_2 k_1 \end{aligned} \tag{11}$$

where $h_1 k_1 l_1$ and $h_2 k_2 l_2$ are coordinates of each spot in the diffraction pattern [2, 5, 6, 8–12].

2.3. Kikuchi patterns

Kikuchi line pattern may happen when the thickness of the specimen is more than normal and almost perfect. These patterns occur by electrons scattered inelastically in small angles with a small loss of energy. Then, this beam of electrons is scattered elastically and creates Kikuchi lines in the patterns. Kikuchi lines in the pattern are pairs of parallel dark and bright lines. The distance between pairs of dark and bright lines is obtained by the following relation:

$$Dd_{hkl} = L\lambda \tag{12}$$

where D is the distance between pairs of Kikuchi lines. Also, the angle between Kikuchi lines in the pattern is in accordance with the angle between the diffraction planes because these lines are parallel with reflecting planes. The pairs of dark and bright lines, sets of reflecting planes and distance of paired lines are shown in Figure 8. The dashed lines are traces of the intersection of reflecting planes. By tilting the specimen, the Kikuchi line pattern changes by the displacement of paired lines. By increasing the sample thickness, the intensity of the spot pattern decreases and the intensity of Kikuchi line pattern increases. Most of the time, spot and Kikuchi line patterns exist simultaneously in micrographs, such as Figure 8. Basically, Kikuchi line patterns present more detailed information than the spot pattern. The appearance of explicit Kikuchi line patterns is a sign of crystal perfection.

2.3.1. Indexing Kikuchi line patterns

To study the crystal defects and to find out the orientation relationships, a tilting experiment should be used. The position of the Kikuchi line and spot patterns can be seen in Figure 9 in Al 7075 alloy in which a thermomechanical processing has been performed. To index the paired Kikuchi lines in the pattern, the distance between the pair of the Kikuchi lines may be measured. So, interplanar spacing can be determined using Equation (12). Consequently, a set of planes can be specified using the interplanar spacing and the type of material crystal structure.

3. Structural characterization of electron diffraction patterns

3.1. Orientation relationship

Relations between phases are determined by orientation relationships. Orientation relationships are indicated by a pair of parallel directions and a pair of parallel planes in two-phase

http://dx.doi.org/10.5772/61781

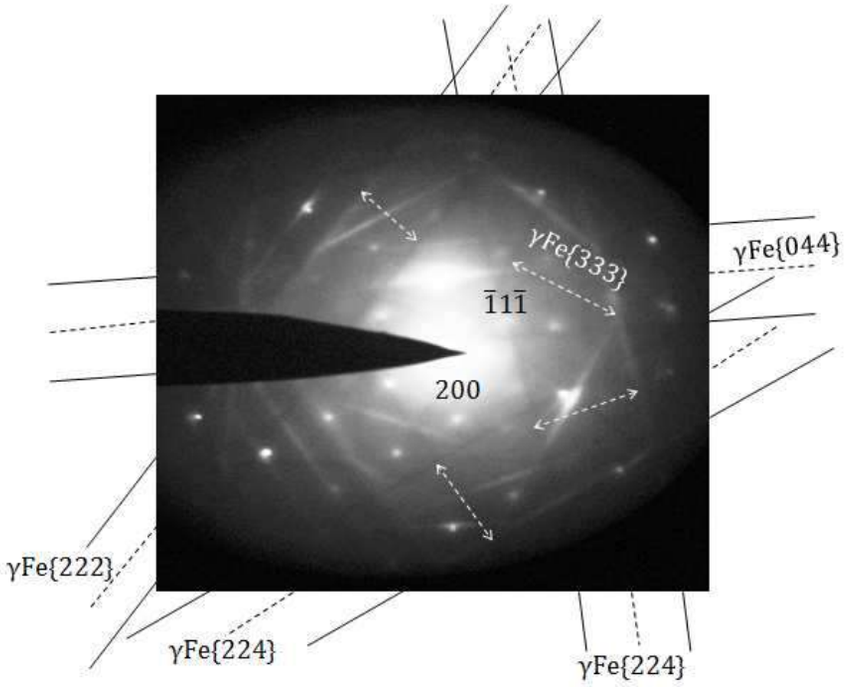

Figure 8. The spots, Kikuchi lines and the distance between paired Kikuchi lines in the pattern of γFe are determined.

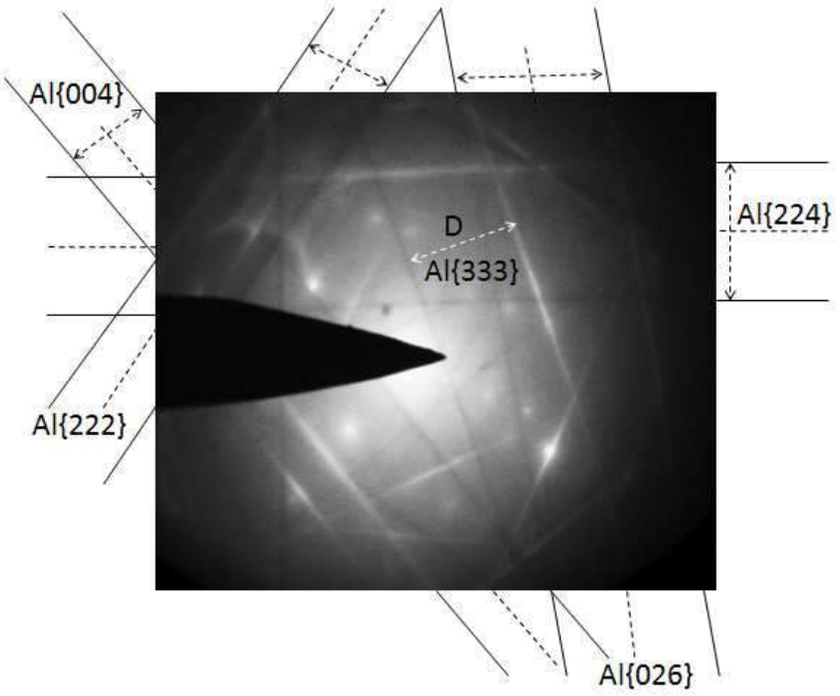

Figure 9. Spot and Kikuchi lines in the pattern of thermomechanically processed Al 7075 alloy. The distance between paired Kikuchi lines is presented as dark and bright lines.

materials. With the use of the spot pattern and Kikuchi line pattern methods, orientation relationships can be determined. Orientation relationships in two-phase alloys depend on

different factors such as types of crystal structural matrix, crystal structural precipitates, shape and size of precipitates. The spot diffraction pattern of quenched and tempered steel 0.1C-2.5V-2W-4.5Cr with chemical composition is illustrated in Figure 10a, which includes matrix spots (αFe) and precipitate spots (carbide$M_{23}C_6$). In the spot pattern of two-phase alloys, there exists two kinds of spots, as shown in Figure 10b. The precipitates and matrix are shown by small spots and big spots, respectively. Matrix has a b.c.c crystal structure and precipitates have a f.c.c crystal structure. So, the orientation relationship may be represented as

$$\left[\bar{1}11\right]_{\text{matrix}} // \left[\bar{1}11\right]_{\text{precipitate}}$$
$$\{011\}_{\text{matrix}} // \{022\}_{\text{precipitate}}$$

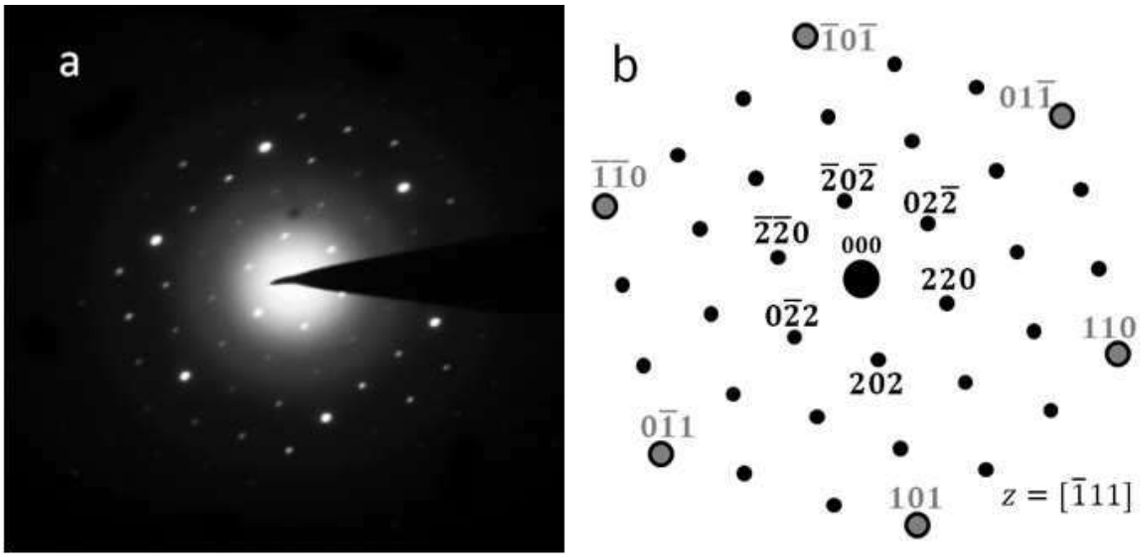

Figure 10. Spot diffraction pattern of quenched and tempered steel with 0.1C-2.5V-2W-4.5Cr composition that includes matrix spots (αFe) and precipitate spots ($carbide\ \ M_{23}C_6$). Small spots and big spots illustrate planes of matrix and planes of precipitate, respectively.

3.2. Phase identification

3.2.1. Phase identification in spot pattern

Interpretation and analysis of diffraction pattern is a method to identify the phases. These patterns can be composed of rings or spots. Generally, identification of phases using diffraction pattern is difficult, and other methods such as XRD should be used to verify the results. To identify the phases in a spot pattern, a spot diffraction pattern of Ti-6Al-4V alloy processed by forging is considered. This alloy contains α and β phases with c.p.h and b.c.c crystal structures, respectively. This pattern contains three different phases as shown in Figure 11. In this pattern, the bright and big spots are related to the α phase and the dim and small spots are related to the β phase.

http://dx.doi.org/10.5772/61781

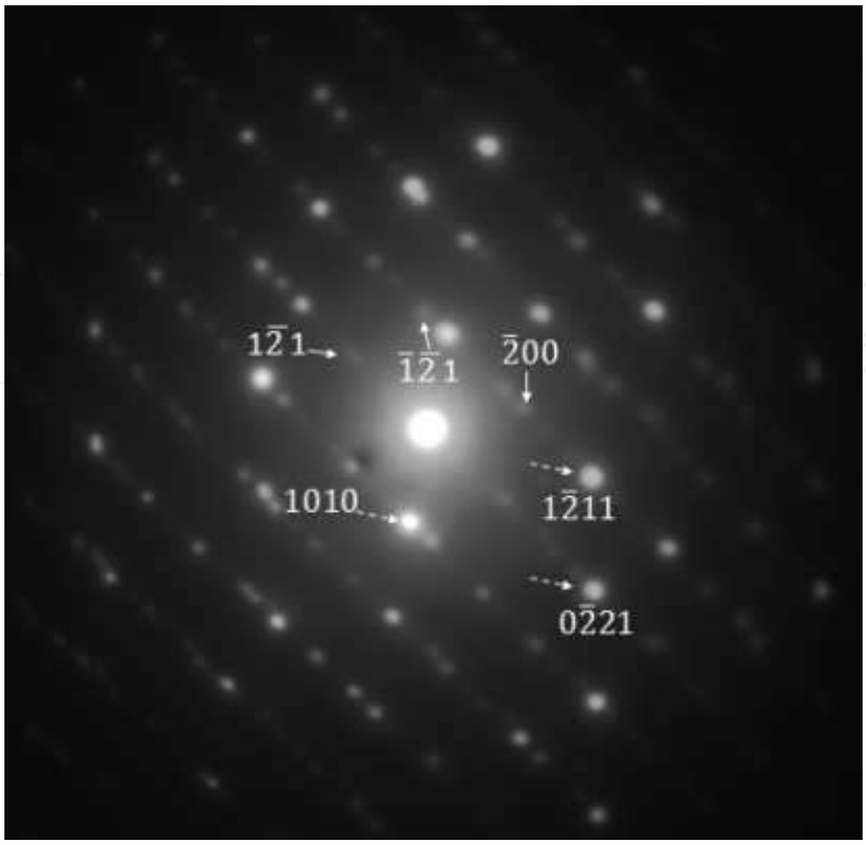

Figure 11. Spot diffraction pattern of forged $Ti-6Al-4V$ alloy. Two phases are observed in the pattern, namely, α and β with $Z=[\bar{1}2\bar{1}6]$ and $Z=[012]$, respectively.

3.2.2. Phase identification in the ring pattern

Carbon nanotubes (CNTs) added to a metal matrix can exhibit significant properties. The main challenge in CNTs-reinforced composites is the uniform dispersion of CNTs in the matrix. Several methods such as ball milling have been developed for distribution of the CNTs in metal matrices. For example, a milled sample of 20 wt% multi-wall carbon nanotubes (MWCNT) + Al powder was investigated using the EDP method. In addition, their corresponding EDP is shown in Figure 12a. To separate ring patterns of CNTs and aluminum, a ring pattern of Al was attached to the EDP of Al-CNTs composite, as illustrated in Figure 12b. This technique helps to better identify the two phases [7].

3.3. Twinning

Twinning is one of the crystalline defects that appear mainly as two parallel planes. Additional spots are created around the main spots of diffracted planes in the pattern by twinning because orientation of twinning is different from the crystal lattice. The direction of the reflected planes inside the twinning is not the same as the whole crystal structure and extra spots become visible in the diffraction pattern.

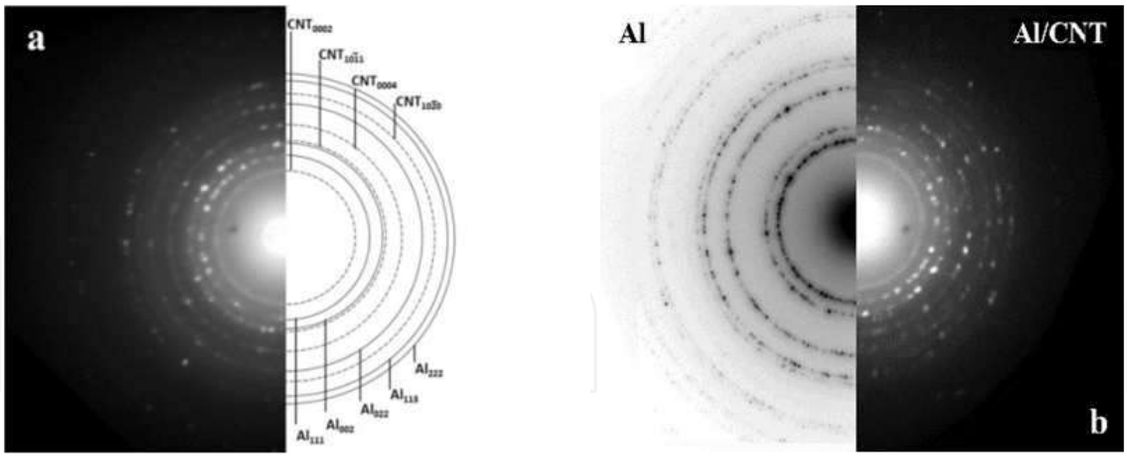

Figure 12. The SAED patterns of CNT-reinforced Al powders, (a) planes of Al and CNT are determined and indexed (b) Al/CNT and Al patterns are in a single pattern to identify phases.

For indexing a twining spot pattern in a cubic crystal structure

1. The main spots of the material are identified and indexed in accordance with the previous section.

2. Twinning spots are determined and indexed by 180° rotation around the {111} and {112} planes for f.c.c and b.c.c crystal lattices, respectively.

Basically, f.c.c crystal structure twins on {111} planes and b.c.c crystal structure on {112}. Twin spots in γFe pattern with a f.c.c crystal lattice are indexed according to Figure 13. The spot diffraction pattern of matrix and twin are mirror reflections across the $(1\bar{1}1)$ plane.

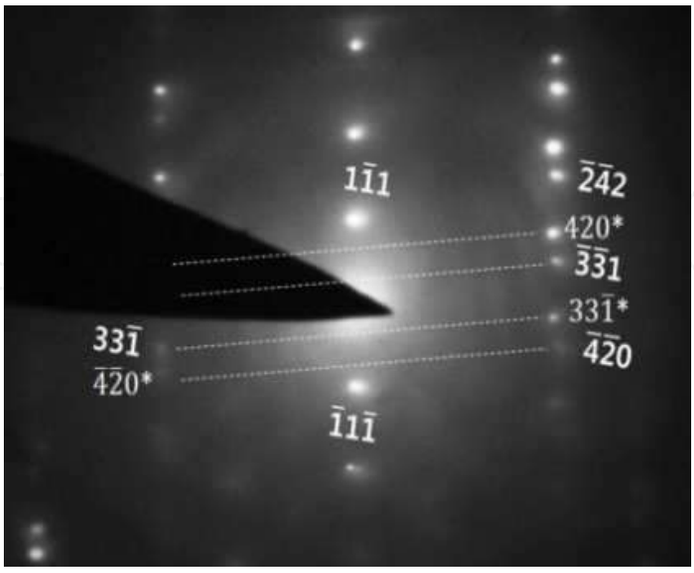

Figure 13. Twinning spots pattern from γFe with f.c.c crystal lattice which index matrix and twin spots with zone axis $z=[\bar{1}23]$, twinned on $(1\bar{1}1)$, hkl* planes related to twin planes and hkl planes related to main reflected planes.

3.4. Dislocation

The equal channel angular pressing (ECAP) and cryo-cross-rolling process have been performed on Al 5083 alloy and Al 1050 alloy with two passes and ten passes, respectively. These processes create a high dislocation density in Al matrix, which affects the shapes of spots in the diffraction pattern. Also, the diffraction patterns of these alloys illustrate streaks on spots due to high accumulation of dislocations and many partial rings due to preferred orientation. Spots in the pattern deform from a usual shape (circular shape) to stretched and irregular spots (disk-type halo). Dislocations change the crystal orientation locally and diffraction spots are extended along the diffraction ring as seen in Figure 14a,b.

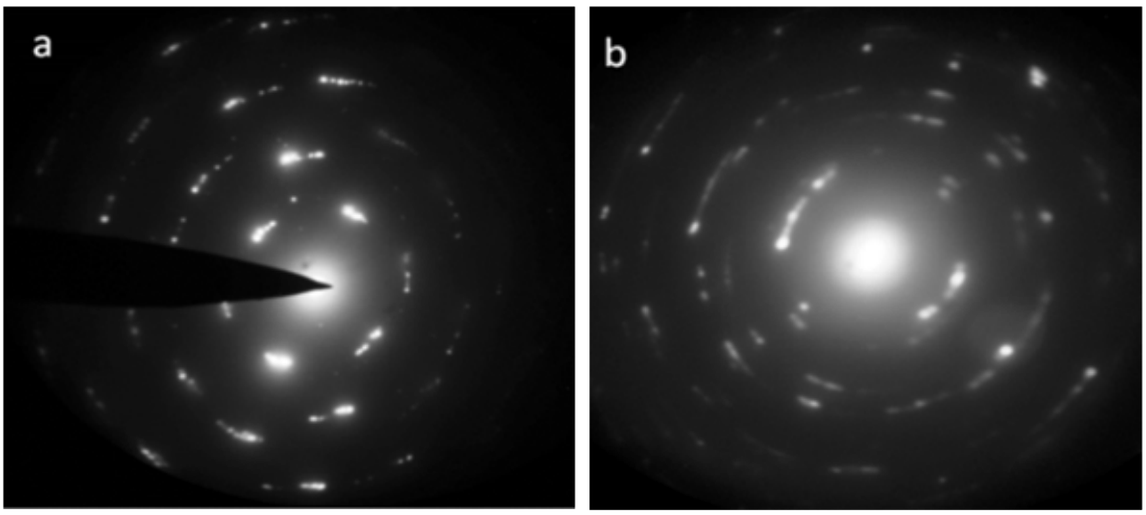

Figure 14. (a) Diffraction pattern of Al 5083 alloy with two passes of equal channel angular pressing and (b) diffraction pattern of Al 1050 alloy with ten passes of cryo-cross-rolling process illustrate streaks on spots due to high density of dislocations.

3.5. Preferred orientation and texture

In certain specimens, preferred orientation of planes occur by some mechanical processes such as various types of rolling and ECAP. If the crystal structure in the specimen is oriented in a favored and preferred direction, the SAED pattern will be formed from many partial rings, as shown in Figure 15. Diffraction pattern obtained from the texture can be considered as an intermediate case between the diffraction from a single crystal and a polycrystalline material. The texture created in alloys may be investigated by interpretation of their diffraction patterns. The preferred orientation {110} [001] is created in Al 2024 alloy by ECAP process.

3.6. Streaks

Presence of fine structure such as streaks and extra spots in many patterns is an indication of the presence of crystal defects which include dislocations, different types of precipitates, twins and staking faults. So, the type of streaks arising in patterns depends on several factors such as various structural defects in the lattice, specimen conditions and diffraction conditions. The

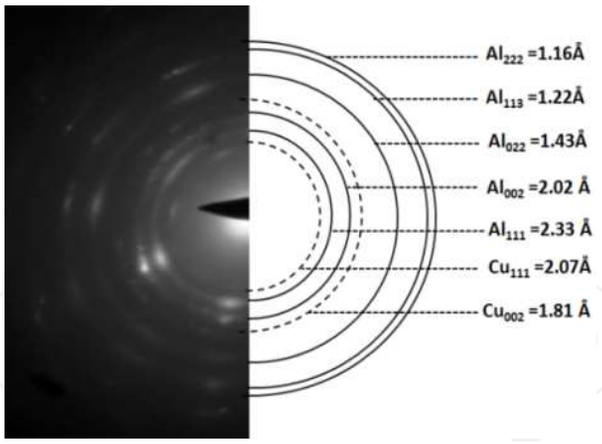

Figure 15. The diffraction pattern for Al 2024 alloy with 4 passes of ECAP, showing the preferred orientation of specimen.

main factors in streaks are precipitates, stacking faults, twins and dislocations. Different shapes of precipitate determine the shapes of reciprocal lattice. So, the final shape of spot patterns depends on the types of precipitates. Streaks on spot pattern are created by stacking faults of quasi-sphere and rod particles of carbide M_7C_3, as shown in Figure 16a. The corresponding spot diffraction pattern illustrates long streaks (diffuse scattering). In fact, streaks in the diffraction pattern can be created by stacking faults in any crystal structure. Depending on the diffraction conditions, streaks or enlarged spots and extra spots or pseudo-satellites will be created, as shown in Figure 16b.

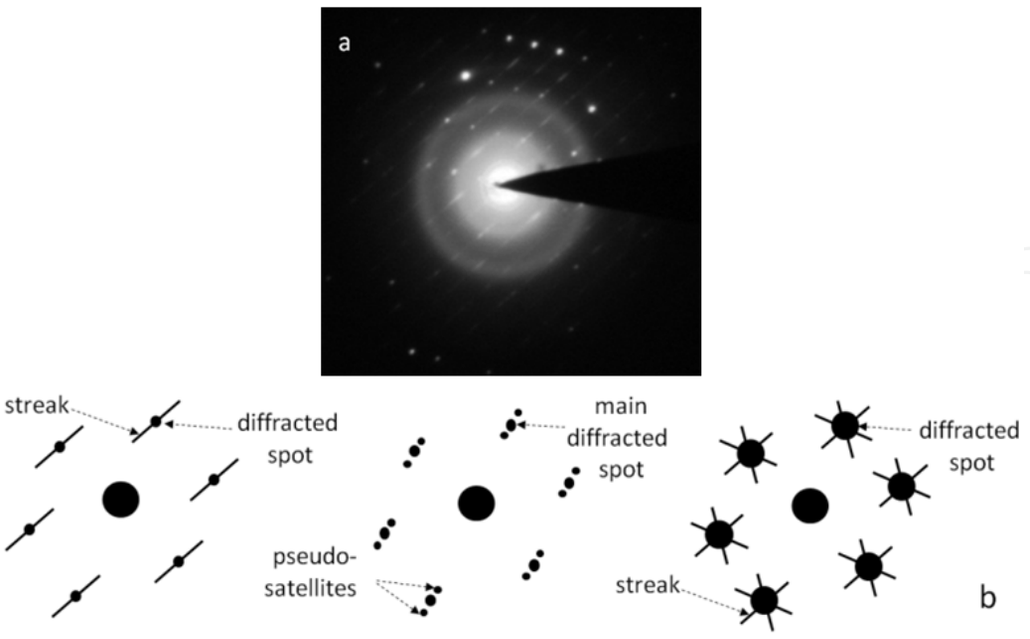

Figure 16. (a) Streaks on spots due to stacking faults of carbide M_7C_3 quasi-sphere and rod particles are created, (b) different types of streaks in the spot diffraction pattern in various conditions of diffraction.

http://dx.doi.org/10.5772/61781

4. Electron diffraction pattern of new materials

4.1. Highly crystalline Multi-Wall carbon Nanotubes (MWNTs)

It should be noted that the structure of CNTs depends substantially on the synthesis methods. A ring pattern of the sample demonstrates a crystal structure corresponding to a graphite ring pattern. As a result, the interplanar spacing of MWCNTs is almost similar to the interplanar spacing of graphite. Thus, the interplanar spacing of nanotubes is indexed using the graphite crystal structure as shown in Figure 17a. With this interpretation, crystal structure of MWCNTs is hexagonal and its lattice parameters are a=2.41 $\mathring{A}$ and c=6.61$\mathring{A}$. In MWCNTs, many amorphous carbons exist as impurities which are created during the production process. Also, the CNTs are complicated and in the shape of a coil. For this reason, the shape of their EDP is a coaxial ring as well as the halo shown in Figure 17b. The EDP of MWCNTs have many rings, each one corresponds to a set of atomic planes. Highly crystalline MWCNTs are a type of MWCNTs with identical chiralities of zigzag type that do not have any impurity and are constructed from monochirality graphite shells. These kinds of CNTs are synthesized by a low-temperature chemical vapor deposition process in plasma. The EDP of highly crystalline MWCNT made of two simple hexagonal patterns overlapping each other is seen in Figure 17b. It is noteworthy that the EDP is taken from an area on the wall of the nanotube. Their spot pattern shows that all of the layers have almost the same chirality.

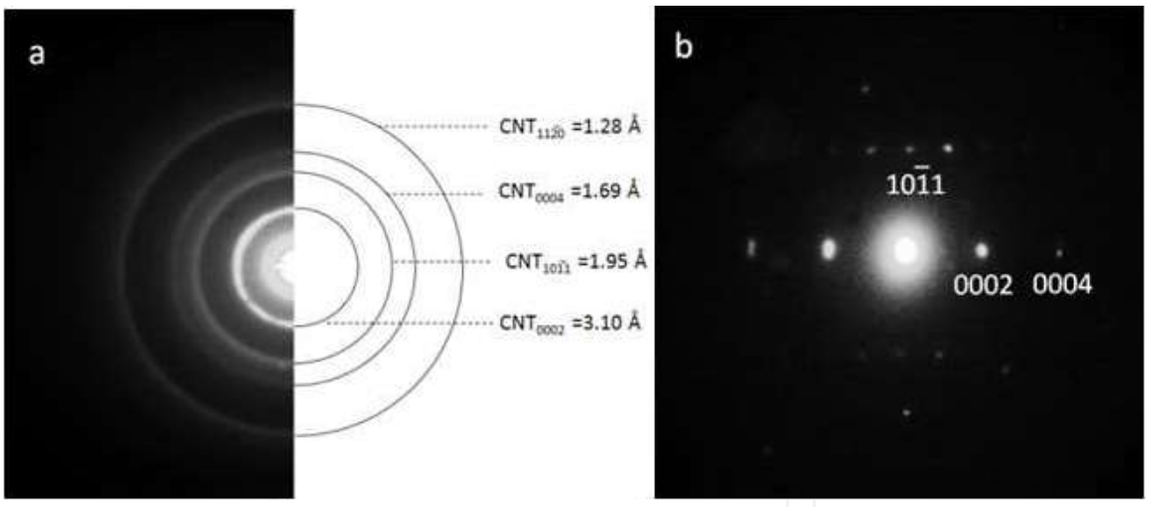

Figure 17. (a) The ring diffraction pattern of coiled MWCNT, (b) the spot diffraction pattern of highly crystalline MWCNT.

4.2. Palladium doping into MWCNTs

Various methods are available for doping nanoparticles into CNTs which give specific features to them and changes the optical, transport, magnetic, electronic and chemical properties of CNTs. In this investigation, a couple of Pd nanoparticles doped into MWCNTs by chemical methods are selected. The EDP of the selected area on the sample is shown in Figure 18. The

ring and spot patterns belong to CNTs and palladium nanoparticles, respectively. Atomic planes can be determined by measuring distances and angles between spots. According to the results of measurements, palladium has a f.c.c crystal structure and the lattice parameter and zone axis of the sample are 3.90 $\mathring{A}$ and z=[$\bar{1}$22], respectively.

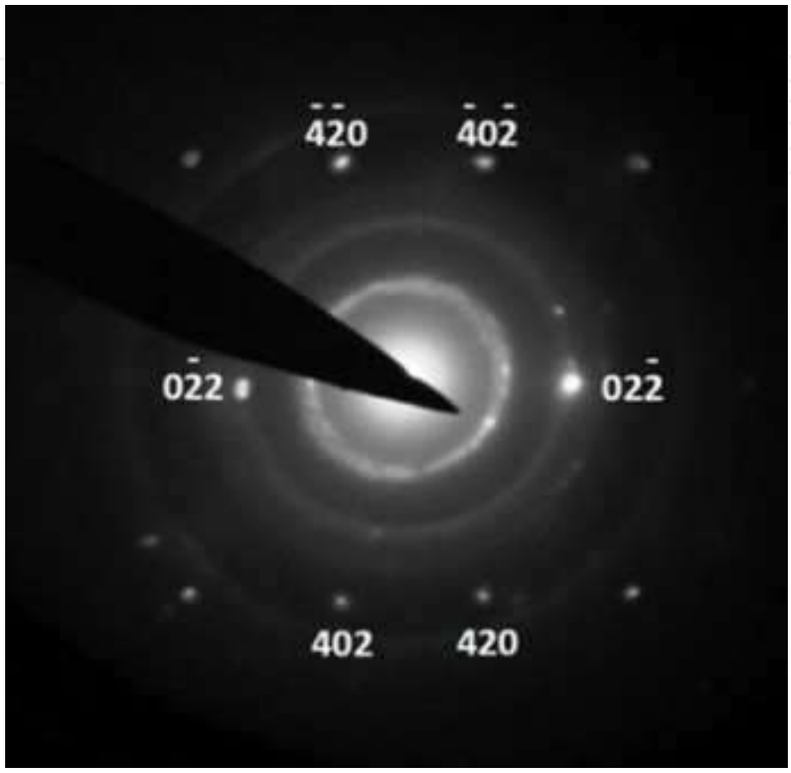

Figure 18. The ring pattern of MWCNTs superimposed on the spot patterns of palladium.

4.3. Vanadium Oxide Nanotubes (VONTs)

In order to study the organic nanotubes, VONTs were selected. It is noteworthy that using EDP method and its interpretation results, structure of various nanotubes will be predictable. Figure 19 shows a ring diffraction pattern of VONTs. Interplanar spacing and lattice parameter can be determined by analysing the ring diffraction pattern. The ring pattern with the Miller indices according to the interplanar spacing of VONTs crystal structure is given. Based on the results of the measurements, VONT has a f.c.c crystal structure and its lattice parameter was 3.92 $\mathring{A}$. In addition, the results of EDP technique have been approved by XRD analysis.

4.4. Amorphous coating

When the grain size of the specimen is extremely fine or completely amorphous, the feature of concentric rings in the pattern disappears and a halo is left around the bright center spot, which shows that the electrons are scattered randomly by the amorphous structure of specimen. The amorphous and glassy materials are identified by this method. Diffraction

http://dx.doi.org/10.5772/61781

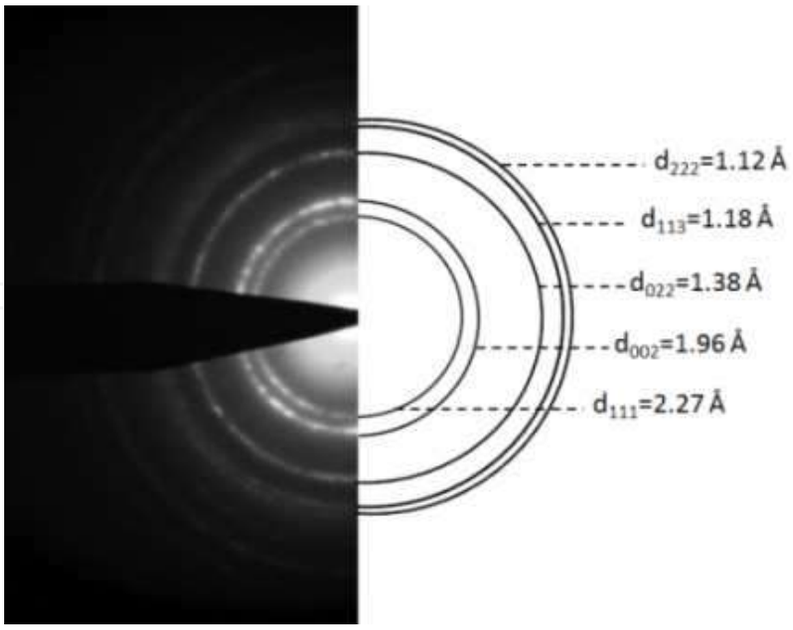

Figure 19. The ring diffraction pattern of VONT, interplanar spacing and planes are determined.

pattern for amorphous coating of silica-zinc oxide multilayered nano-porous membrane on α-alumina substrate prepared by sol-gel method is shown in Figure 20.

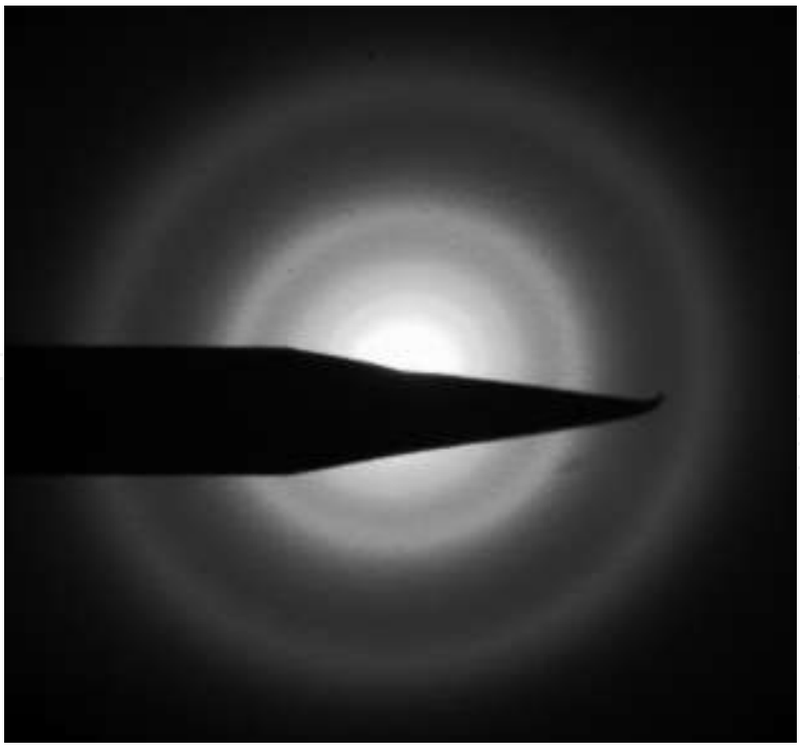

Figure 20. The diffraction pattern of amorphous coating $SiO_2-10\%$ ZnO prepared with sol-gel method on α-alumina substrate.

5. Appendix 1

Accelerating voltages (kV)	λ (Å)
50	0.0536
100	0.0370
200	0.0251
500	0.0142
1000	0.0087

Table 3. Electron wavelength λ for applied accelerating voltages in electron microscopy

Author details

Mohsen Asadi Asadabad* and Mohammad Jafari Eskandari

*Address all correspondence to: asadimohsen@gmail.com

Materials Research School, NSTRI, Isfahan, Iran

References

[1] Cowley J M. Diffraction Physics, third revised edition, Elsevier; 1995. DOI:10.1016/B978-0-444-82218-5.50024-9.

[2] Edindton J W. Electron Diffraction in the Electron Microscope. London, Macmillan; 1975.

[3] K. W. Andrews. Interpretation of Electron Diffraction Patterns. London, ADAM HILGER LTD, 1971.

[4] Asadi Asadabad M, Jafari Eskandari M. Transmission electron microscopy as best technique for characterization in nanotechnology. Synthesis and Reactivity in Inorganic, Journal of Metal-Organic, and Nano-Metal Chemistry. 2015; 45, 323–326. DOI: 10.1080/15533174.2013.831901.

[5] Weirich T E, Lábár J L, Zou X. Electron crystallography. Novel Approaches for Structure Determination of Nanosized Materials. Springer; 2004.

[6] Beeston B E P, Horne R W, and Markham R. Electron Diffraction and Optical Methods in Electron Diffraction Techniques. Elsevier, North Holland. 1972.

[7] Asadi Asadabad M, Jafari Eskandari M, Tafrishi R, Emamalizadeh M. Transmission electron microscopy characterization of diffraction nanotubes, Submitted.

[8] Hammond C. The Basic of Crystallography and Diffraction. Oxford, Oxford Science Publications; 1997.

[9] M. Jafari Eskandari, R. Tafrishi, M. Asadi Asadabad. Study of the nanostructure evolution in aluminum 1050 sheet by cryo-cross-rolling process, Submitted.

[10] Hirsch P B, Howie A, Nicholson R B, Pashley D W, and Whelan M. Electron Microscopy of Thin Crystals, London, Butterworth; 1965.

[11] Hren J J, Goldstein J I, and Joy D C. Introduction to Analytical Electron Microscopy. Plenum; 1979.

[12] Ball C J. An Introduction to the Theory of Diffraction. Pergamon, Oxford; 1971.

[13] Rymer T B, Electron Diffraction, Methuen, London; 1970.

[14] Vainshtien B K, Structure Analysis by Electron Diffraction. Pergamon Press, Oxford; 1964.

[15] Asadi Asadabad M, Jafari Eskandari M, Tafrishi R, Bagherzadeh M. The effect of cross-rolling process on nanostructure of Al 1050 alloy. Journal of Nanoanalysis. 2014; 1: 93–98.

[16] Microbeam analysis, analytical electron microscopy, selected-area electron diffraction analysis using a transmission electron microscope, International Standard, ISO 25498, First edition, 2010.

[17] David B, Williams C. Barry Carter. Transmission electron microscopy. A Textbook for Materials Science. Springer Science Business Media; LLC 1996, 2009.

[18] Mogilevsky P, et al., Evolution of texture in rhabdophane-derived monazite coatings. Journal of the American Ceramic Society. 2003; 86: 1767–1772. DOI: 10.1111/j. 1151-2916.2003.tb03552.

[19] Fillingham P J, Leamy H J, and Tanner L E. Electron Microscopy and Structure of Materials, University of California Press; 1972.

[20] Hollox G E, Rowcliffe D J, and Edington J W, Electron Microscopy and Structure of Materials. University of California Press; 1972.

[21] Thomas G, Modern Diffraction and Imaging Techniques in Materials Science. North-Holland; 1970.

IntechOpen

Chapter 10

TEM as an Important Tool to Study Aquatic Microorganisms and their Relationships with Ecological Processes

Thiago P. Silva, Juliana P. Gamalier and Rossana C.N. Melo

Additional information is available at the end of the chapter

http://dx.doi.org/10.5772/61804

Abstract

Microorganisms are critically important for ecological processes in aquatic environments. Bacteria and viruses are key components of the microbial loop and are central for biogeochemical cycles in aquatic ecosystems. Our group has been using transmission electron microscopy (TEM) to study aquatic microorganisms in both natural tropical ecosystems and cultures. In this review, we highlight structural aspects of freshwater bacteria, based on TEM findings that have provided insights into the functional capabilities of these cells in aquatic tropical ecosystems. First, we focus on TEM applied to the study of the ultrastructural diversity and morphological alterations of bacteria in response to environmental stress. Second, we address the relationship between viruses and bacteria in freshwater ecosystems. Third, we demonstrate by TEM that outer membrane vesicles (OMVs), structures associated with cell secretion and cell communication, are released by aquatic bacteria into natural ecosystems and cultures. Thus, TEM has proven to be a powerful technique to study aquatic microorganisms, contributing to the understanding of ecological processes, including regulation of bacterial populations, during different environmental conditions.

Keywords: Transmission electron microscopy, freshwater bacteria, ultrastructure, aquatic ecosystems, cell viability, cell death

1. Introduction

Aquatic microorganisms such as bacteria and viruses are critically important for ecological processes, for example, carbon cycling and energy flow in aquatic environments [1]. Bacteria are key components of the microbial loop in aquatic ecosystems, an alternative route of dissolved organic matter and nutrient transfer to metazoan trophic levels and consequently

influence the flow of carbon and energy within an ecosystem [2, 3]. Viruses are remarkably abundant in aquatic ecosystems and within bacteria play an important role in the aquatic microbial loop. Viruses can infect bacteria and act in their mortality, thus exerting a significant control over aquatic bacterial and phytoplankton communities. Therefore, viruses can impact the pathways of matter and energy transfer in aquatic ecosystems [4, 5].

The understanding of the functional capabilities of microorganisms in microbial food webs and human health issues is largely dependent on methods applied to the direct visualization of them during physiological and environmental stress conditions. For example, individual imaging of bacteria is valuable to recognize bacterial viability and their physiological functions at single-cell level [6]. Our group has been using transmission electron microscopy (TEM) to study aquatic microorganisms, especially bacteria, from tropical ecosystems. The structural organization of these organisms has been investigated in water samples directly collected from natural environmental sites or kept in cultures. In this review, we highlight the ultrastructural aspects of freshwater bacteria, based on TEM findings, which have provided insights into the functional capabilities of these cells in aquatic tropical ecosystems.

2. Ultrastructure of freshwater bacteria: diversity and morphological alterations in response to environmental stress

While observation of aquatic bacteria by light microscopy is an approach extensively used in studies of planktonic bacteria, the ultrastructure of these organisms is not completely understood [7-9]. In the past, bacteria were considered as prokaryotic microorganisms with a very simple ultrastructure. However, improvement of electron microscopy techniques and more refined analyses have revealed well-defined structures and higher levels of cell organization in bacteria [9].

In aquatic ecosystems, short-time physicochemical variations are frequent and affect environmental properties. Thus, bacterial communities need to be able to respond efficiently to fluctuating conditions of the aquatic environment [5, 10, 11]. On the other hand, bacterial cells can exhibit morphological and ultrastructural changes in response to environmental stress.

2.1. Ultrastructural diversity of bacteria from aquatic ecosystems

The morphological diversity of bacteria goes far beyond a simple description of the bacterial shape, as frequently reported by ecological studies [12-16]. Bacteria from aquatic ecosystems have a complex cell ultrastructure with a cell envelope enclosing a cytoplasm with a variety of cell structures and compartments that can serve as organelles [17-19]. Freshwater bacteria, in addition of showing typical structures in the cytoplasm, such as nucleoid, granules, and lipid bodies, can exhibit intracellular membrane systems represented by mesosomes and thylakoid membranes. External structures such as cell envelope with distinct compositions, S-layer, external capsule, and extracellular vesicles, are also found in freshwater bacteria. The main bacterial structures depicted by TEM are listed in Table 1.

http://dx.doi.org/10.5772/61804

Structure	Morphological Description	Functions	Figures
Cell envelope	A complex multilayered structure which envelopes bacteria. Basically, there are two types of bacterial cell envelopes: (1) Gram-positive, composed of plasma membrane and cell wall and (2) Gram-negative, composed of plasma membrane, periplasm and outer membrane. Capsular structures and S-layers may also constitute the cellular envelope.	This structure serves to protect bacteria from their unpredictable and often hostile environment.	1A, 1Ai, 1B, 1Bi, 2A, 2Ai
Plasma membrane	A bilayer membrane seen under TEM as a classical trilaminar structure limiting the cell contents.	Plasma membrane acts as a permeability barrier for most molecules and serves as sites for transport of molecules into the cell. In addition, it is functionally associated with energy conservation as the location in which a proton motive force is generated.	1A, 1Ai, 1B, 1Bi, 2A, 2Ai
Cell Wall	Structural layer adjacent to the plasma membrane that appears as an electron-dense layer composed by peptidoglycans (gram-positive envelope) or a complex formed by periplasm and outer membrane (gram-negative envelope).	Cell wall provides structural integrity to the cell and prevents osmotic lysis.	1A, 1Ai, 1B, 1Bi, 2A, 2Ai
Periplasm (periplasmic space)	The periplasm is a concentrated gel-like matrix in the space between the inner plasma membrane and the bacterial outer membrane in gram-negative bacteria. This space is called periplasmic space. Gram-positive bacteria present this structure as a conspicuous space between the plasma membrane and the cell wall. Periplasm is filled with water and proteins and is therefore somewhat reminiscent of the cytoplasm	Periplasmic proteins have various functions in cellular processes including cell transport, cell degradation and cell motility.	1A, 1Ai, 1B, 1Bi, 2A, 2Ai
S-Layer	Cell surface protein layer that is composed of a two-dimensional array of proteins with a crystalline appearance.	Uncertain functions. It has been suggested that this layer acts as a partial permeability barrier for large substrates and provides resistance, adhesion and stabilization to the cell.	2A, 2Ai

Structure	Morphological Description	Functions	Figures
Capsule	Electron-lucent extracellular layer attached to the cellular envelope. This layer is formed by an exopolymeric matrix of polysaccharides.	Bacterial capsule has important functions related to cell recognition, defense and virulence.	2B, 2Bi
Outer Membrane	Outer bilayer membrane with a typical trilaminar appearance, delimiting gram-negative bacteria, and, for this reason, is a distinguishing feature of these bacteria. It is adjacent to the periplasmic space. The outer membrane composition differs from that of the inner plasma membrane, being composed of glycolipids, mainly lipopolysaccharides, which are located at its outer leaflet.	This membrane acts as a permeability barrier despite containing many passive transport channels. In addition, contributes for the increase of bacterial virulence.	3A
Outer Membrane vesicles (OMVs)	Spherical or rod-shaped vesicles, which are released from the outer membrane. OMVs are delimited by a bilayer membrane with typical trilaminar aspect and variable electron-density. OMVs can vary in size from 20 to 300 nm in diameter.	OMVs may contain proteins and other molecules that are related with cellular communication, defense, biofilm formation and DNA transfer.	3A, 3B, 3Bi
Mesosomes	Folded invaginations of the plasma membrane, which appear as tubular, vesicular or lamellar sacs.	Uncertain functions. It seems associated with cell division.	1A
Thylakoid membranes	System of lamellar membranes located in a large area of the cell cytoplasm.	These membranes serve as sites for the photosynthetic apparatus, enzymatic systems and electron transfer chains.	3A
Granules	Appear as spherical electron-dense structures in the bacterial cytoplasm.	These structures store a variety of organic and inorganic compounds.	1B, 2B, 2Bi
Nucleoid	Non-delimited electron-lucent areas in the cytoplasm. It is composed of DNA with a small amount of RNA and proteins.	Regulator center of cellular activities and cell replication.	1A, 1B, 2B, 2Bi
Gas Vesicles	Cylindrical tubes closed by conical end caps with perimeter size varying from 45 to 200 nm. They are mostly restricted to planktonic microorganisms (cyanobacteria and some bacterial species).	Gas vesicles promote cell buoyance in aquatic environments and enable vertical migration of cyanobacteria.	-

http://dx.doi.org/10.5772/61804

Structure	Morphological Description	Functions	Figures
Lipid Bodies	Electron-dense or electron-lucent spherical organelles surrounded by a half-unit membrane.	Lipid bodies store lipophilic compounds that are used as metabolic energy. However, they might be related with other more complex yet unclear functions in prokaryotes and may have associated proteins.	-
Flagella	Tubular filamentous structures attached to the cell surface. It is better observed by TEM when samples are negatively stained.	The flagellar filament is rotated by a motor apparatus in the plasma membrane and allows the motility of the cell in aquatic environments.	-

Table 1. Main ultrastructural components of freshwater bacteria

TEM has been helping to understand the ultrastructural diversity among bacteria from aquatic ecosystems, associated with the presence of different internal and external structures. Our studies from tropical aquatic ecosystems have shown that ultrastructural diversity is an important aspect to be considered for better understanding of the role of these microorganisms. For example, variations in the cytoplasmic electron density (Figures 1 and 2) are frequently observed in freshwater bacteria and might reflect different stages of metabolism and/or differential molecular compositions. We also found a substantial variation in the bacterial cell envelope thicknesses (Figure 1) and compositions (Figures 1 and 2A), which are related to the presence of gram-positive and gram-negative bacteria, both commonly found in aquatic ecosystems. Our quantitative TEM analyses revealed a significant proportion of bacteria with a limiting capsule (Figure 2B and 2Bi). Our data showed that 31 % of freshwater bacteria had capsular structures [20]. This frequency is higher than that found in marine bacteria (7–27 %) [21-23]. This structural component is important for multiple functions, such as cell interaction with the environment, absorption and storage of nutrients, barrier against toxic agents from the medium and predation, and protection from viral infection and biofilm formation. Moreover, some bacteria showed particles adhered to the bacterial capsular structure (Figure 2v and 2Bi), which may be indicative of a survival strategy important for acquisition of organic or inorganic nutrients and protection against predators [24]. The well-defined coating formed by particles around bacteria, revealed by TEM observations, may act as an important micro-environment that is not identified by other techniques and open new frontiers in the understanding of bacterial ecology [25].

An interesting ultrastructural observation is the presence of membranous secretory vesicles projecting from the bacterium outer membrane into the extracellular medium in samples from

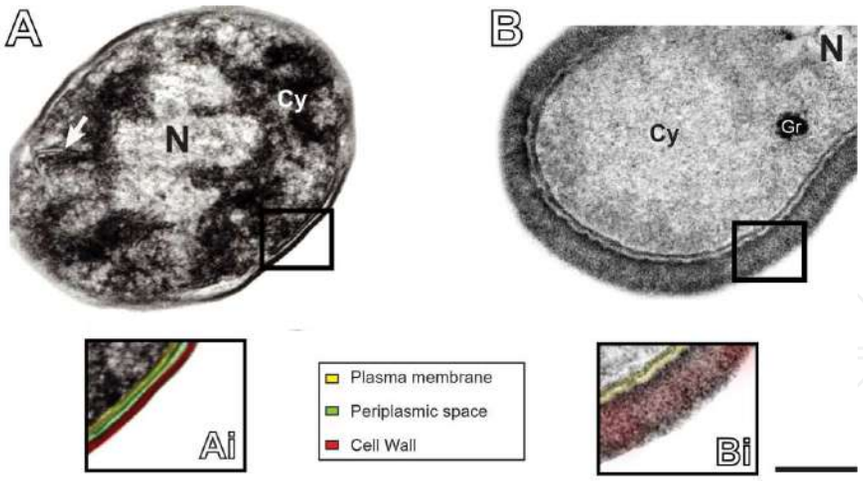

Figure 1. Ultrastructural views of aquatic bacteria collected from an Amazonian ecosystem. (A and B) In the cytoplasm (Cy), observe typical compartments and structures, as nucleoid (N), mesosomes (arrow), and granule (Gr). In (Ai) and (Bi), note the cell envelopes with different thicknesses and composed of plasma membrane (highlighted in yellow) and cell wall (red), with (Ai) and without (Bi) periplasmic space (green). Bacteria also show the cytoplasm with distinct electron-density. Reprinted from ref. [20] with permission. Scale bar: 160nm (A), 60nm (B), 120nm (Ai), and 30nm (Bi).

both natural environments and cultures (Figures 3A and 3B). This particular aspect is discussed in more detail in Section 3.0.

TEM also revealed that bacteria from aquatic ecosystems may exhibit a consistent system of endomembranes, — mesosomes and/or thylakoid membranes in the bacterial cytoplasm. Mesosomes (Figure 1A, arrow), considered as artifacts in the past, have, more recently, been receiving increasing attention because of their association with some cell functions, such as chromosome segregation during cell division. Intriguingly, mesosomes have been documented in bacteria in response to stress conditions [26]. The presence of thylakoids is a distinct morphological feature, found in cyanobacteria and a small group of bacteria [27] (Figure 3B). These endomembranes have a crucial function related to metabolic processes, particularly photosynthesis. Because thylakoids are unambiguously identified in high resolution by TEM, this technique is a reliable tool to distinguish between heterotrophic and autotrophic aquatic prokaryotes in environmental samples. Routine evaluation of these types of organisms currently relies on the use of light microscopy and appropriate fluorochromes, which do not enable detailed visualization of the thylakoids.

Our TEM data reinforce the fact that bacteria constitute structurally complex organisms and denote the functional complexity of these microorganisms, likely related to their metabolic and adaptive diversity [2, 24].

2.2. Ultrastructural alterations and death of bacteria in response to environmental stress

The physiological state of bacteria is an important parameter in aquatic ecosystems to understand variations on microbial communities and their potential impact on the food web and fluctuations in geochemical cycles in which these microorganisms are involved. Bacterial communities from aquatic ecosystems cannot be restrictively categorized as active or inactive,

http://dx.doi.org/10.5772/61804

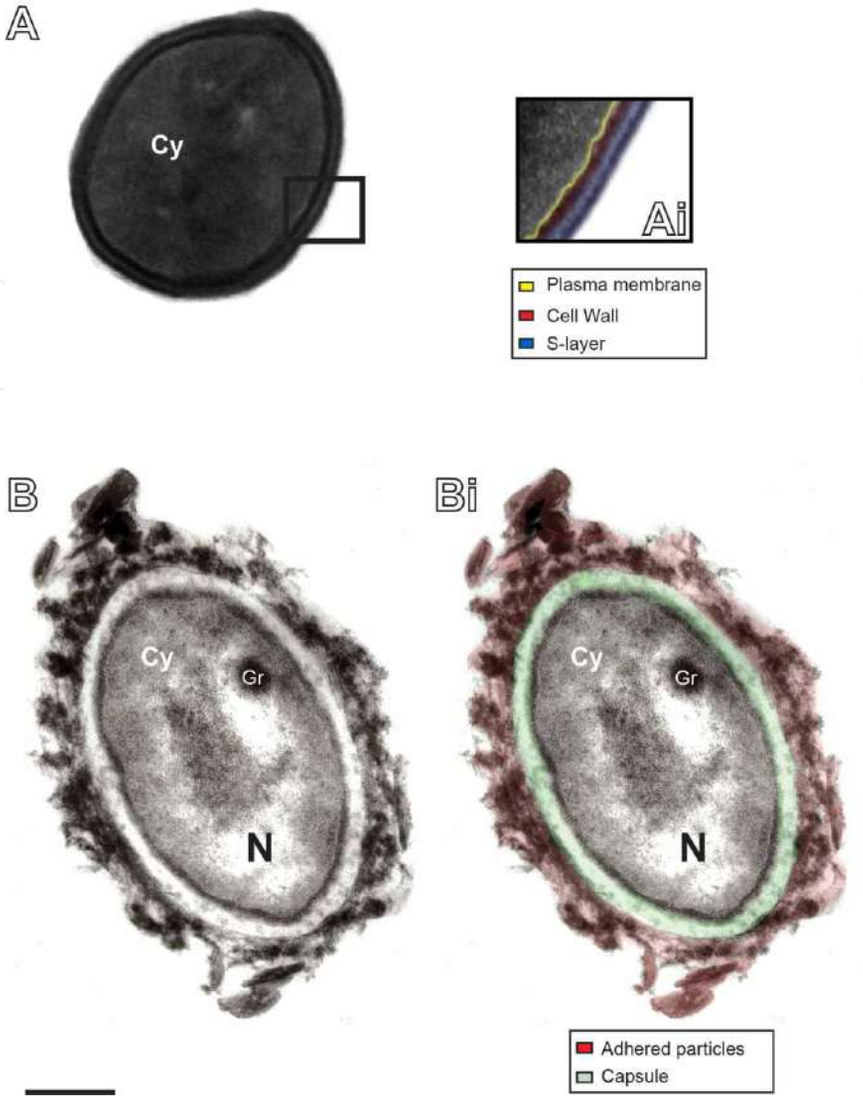

Figure 2. Ultrastructural components of freshwater bacteria. (A and Ai) A cultured bacterium shows the cell envelope composed by plasma membrane (highlighted in yellow), cell wall (red, and S-layer (purple). (B and Bi) Substratum particles (highlighted in red in Bi) are seen as an adhered coating localized externally to the capsular structure (highlighted in green in Bi) of a bacterium collected from a natural environment. Typical bacterial structures such as nucleoid (N) and granule (Gr) are observed in the cytoplasm (Cy). Figure 2B was reprinted from ref. [20] with permission. Scale bar: 130 nm.

since these cells present a continuous variation of their physiological state. From an ecological point of view, bacteria can be distinguished within microbial communities as viable/live cells, which play a functional role and participate in the production of biomass or dead cells, which no longer play a role in secondary production [28]. It is well documented a continuum of physiological status of bacterial life and death in aquatic ecosystems and a great variation in bacterial viability depending on factors such as heterogeneity of bacterial populations, environmental stress, nutrient competition and predation [6, 28-30].

Live/dead bacteria can be characterized by: (i) presence/absence of structures, (ii) genetic parameters, (iii) metabolism or functional activity, and (iv) reproduction and growth viability

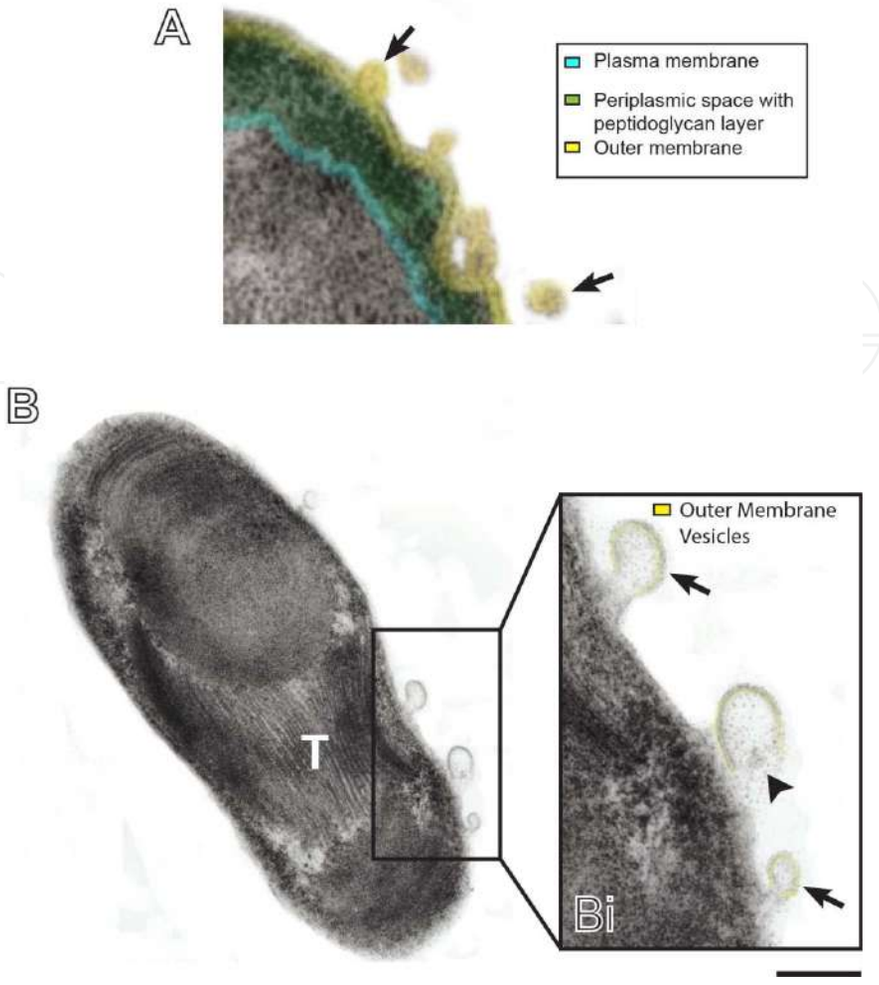

Figure 3. Ultrastructure of gram-negative bacteria from aquatic ecosystems. Observe in (A), a typical gram-negative envelope of a bacterium exhibiting plasma membrane (highlighted in blue), periplasmic space with periplasmic layer (green) and outer membrane (yellow). In (B), an autotrophic aquatic bacterium shows thylakoids membranes (T), organized as a system of membranes in the bacterium cytoplasm. Note in (A) and (Bi) the formation of secretory vesicles from the bacterial outer membrane (arrows) and the release of vesicle contents into the extracellular environment (arrowhead in Bi). The trilaminar aspect of the outer membrane (highlighted in yellow) is clearly observed in high magnification in (Bi). Figure 3B was reprinted from ref. [20] with permission. Scale bar: 80 nm (A, Bi), 200 nm (B).

[31]. Yet, under an ecological perspective, the definition of bacterial life/death in aquatic ecosystems relies mostly on cell viability and growth analyses [32-36].

Although epifluorescence microscopy became the standard method for evaluating environmental bacteria death through indirect quantification of bacterial concentration (35-37), this approach, which is based on the use of routine fluorochromes such as DAPI and Acradine Orange, do not enable accurate assessment of the viability state of bacterial cells and may highlight other particles that are not necessarily bacteria (38). Moreover, this technique does not consider physiological aspects of bacterial cells [37-39]. More recently, other bacterial counting methods, which use more specific fluorescent dyes that consider the physiological aspects of bacterial cells, have been described [40]. However, TEM is the only technique with sufficient resolution to reveal morphological aspects indicative of cell viability and physiology,

enabling the detection of cell alterations that occur even before cell lysis. Therefore, bacteria with intact structures and bacteria presenting damaged cellular structures can be considered live or in process of death, respectively.

By studying impacted freshwater ecosystems in Brazil: Batata Lake (Amazonian region) that received tremendous amounts of bauxite tailings from a mining operation [41], and Funil Reservoir (Rio de Janeiro state) that received industrial, domestic, and erosive process effluents [42], we found several ultrastructural aspects indicative of bacterial cell death. The most frequent bacterial changes in response to environmental stress were: clumped granules (Figure 4A), cytoplasmic condensation (Figure 4B), structural damage of the cell envelope (Figure 4B), loss of cell shape (Figure 4C), and cell elongation (Figure 4D). Bacteria lacking internal structures known as "ghost bacteria" [43] were also observed (Figure 4A). Therefore, ultrastructural analyses were revealing in clarifying the effects of environmental stress on bacterial cell structures and bacterial dynamics in aquatic ecosystems.

2.3. Visualizing virus-infected bacteria in aquatic ecosystems

Viruses are the smallest biological entities known. They are intracellular parasites, which can infect prokaryotic or eukaryotic cells. Viruses are ubiquitous in aquatic ecosystems, and increasing attention has been paid on their role in aquatic food webs since it was discovered that they are the most abundant aquatic components. Because viruses play an important biogeochemical function by releasing dissolved organic matter and nutrients through host cell lysis, they can affect various ecological factors, such as ecosystem respiration, primary production, genetic transfer between microorganisms, and species distribution [5].

TEM studies frequently report the occurrence of viral particles infecting bacteria termed bacteriophages [4, 29, 44]. Viruses are seen by TEM as small electron-dense particles with varied shapes and perimeter size varying from 20–200 nm (Figure 5). Viruses consist of genetic material (DNA or RNA, single- or double-stranded) surrounded by a protein coat (some also have lipids) [45]. They act on the control of bacterial population and are responsible for 40% of bacterial mortality in aquatic ecosystems [4, 46].

Bacteriophages have basically two different life cycles considering the onset of a viral infection until lysis of host cell: (1) Lytic cycle: viruses attach to host bacteria and inject their genetic material (DNA or RNA) into the cell, then they drive the host to produce numerous progeny viruses leading to bacterial cell burst and infection spreading to other cells. (2) Lysogenic cycle: viral genome integrates the genome of host bacteria and reproduces as genetic material without cell lyses. In this case, stress to the host bacteria can trigger a switch to lytic infection (lysogenic ↔ lytic) [5].

Our group has been investigating the relationship of virus—bacteria by TEM and has demonstrated an important correlation among free-living bacteria and virus in an Amazonian ecosystem (Batata Lake) [44]. Although there is a growing body of research on aquatic viral ecology, little is known about viral function in tropical ecosystems, particularly in Amazon environments [44, 47]. TEM revealed the occurrence of viruses with nearly spherical heads and without tails (Figure 5). The structure of the virus capsid with its repetitive morphological

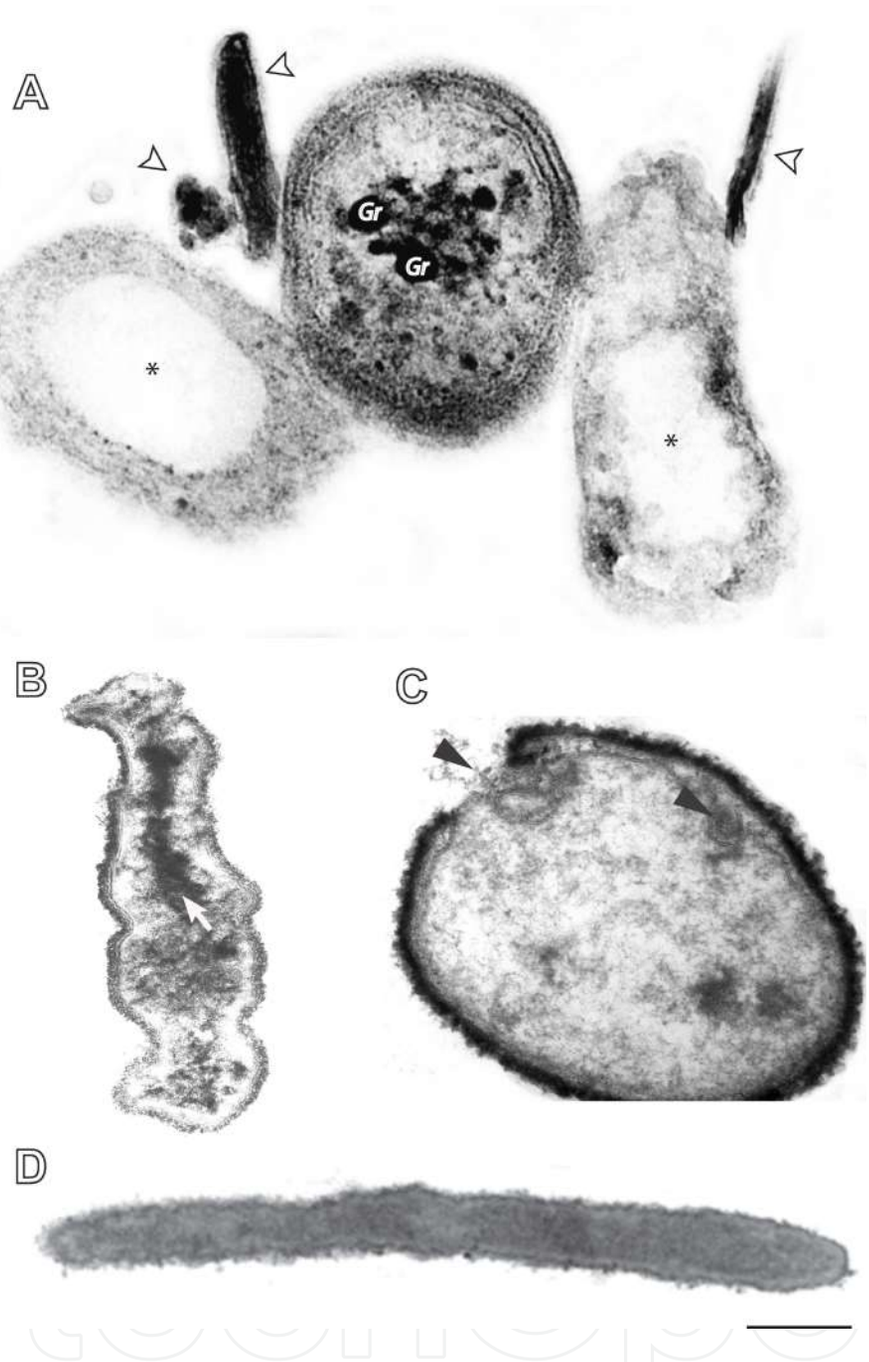

Figure 4. Bacteria from impacted aquatic environments show clear ultrastructural alterations. In (A), a damaged bacterium with clumped granules (Gr) is seen between two "ghost" bacteria, characterized by the presence of an empty cytoplasm (*). Bacteria-associated cellular debris is observed (A, white arrowhead). In (B), note bacterial cytoplasmic condensation (arrow) and loss of cell shape while in (C) a clear structural damage of the cell envelope is observed (arrowheads). Cell elongation is shown in (D). Water samples were collected from Batata Lake (Amazonian region, Brazil), immediately fixed and processed for TEM as ref. [20]. Scale bar: 180 nm (A, B, and C) and 350 nm (D).

units occasionally could be observed in some cells (Figure 5, boxed area). On the other hand, some infected bacteria lacked an intact cell membrane or were partially empty. This morphological aspect indicates that viruses can induce bacterial cell death, which is associated with the lytic cycle of the virus in aquatic environments.

http://dx.doi.org/10.5772/61804

Our data demonstrated that a variable number of phages are present within virus-infected bacteria. TEM quantitative analyses showed that 34.2% of bacteria had viruses in the cytoplasm (Figure 5), with 10.0 ± 3.5 (mean ± SEM) phages per cell-section. Additionally, we have found virus-infected bacteria in cultured samples from Funil Reservoir, indicating that the presence of viruses in tropical ecosystems is a broad event.

Several environmental factors, including solar radiation and temperature, can influence viral abundance. Exposure to UV radiation decreases viral abundance, while low temperatures decrease their capability of infection in aquatic ecosystems [48-50]. It is also described that the increase of organic matter and anthropogenic pollutants increase the abundance of viral particles in water environments [44, 47, 51].

Altogether, our ultrastructural data showed a variable number of viruses within the bacterial cytoplasm, which demonstrates a clear interaction between these organisms. Assessment of viral production and virally caused mortality of bacteria are crucial parameters to understand the detailed role of viruses in food webs.

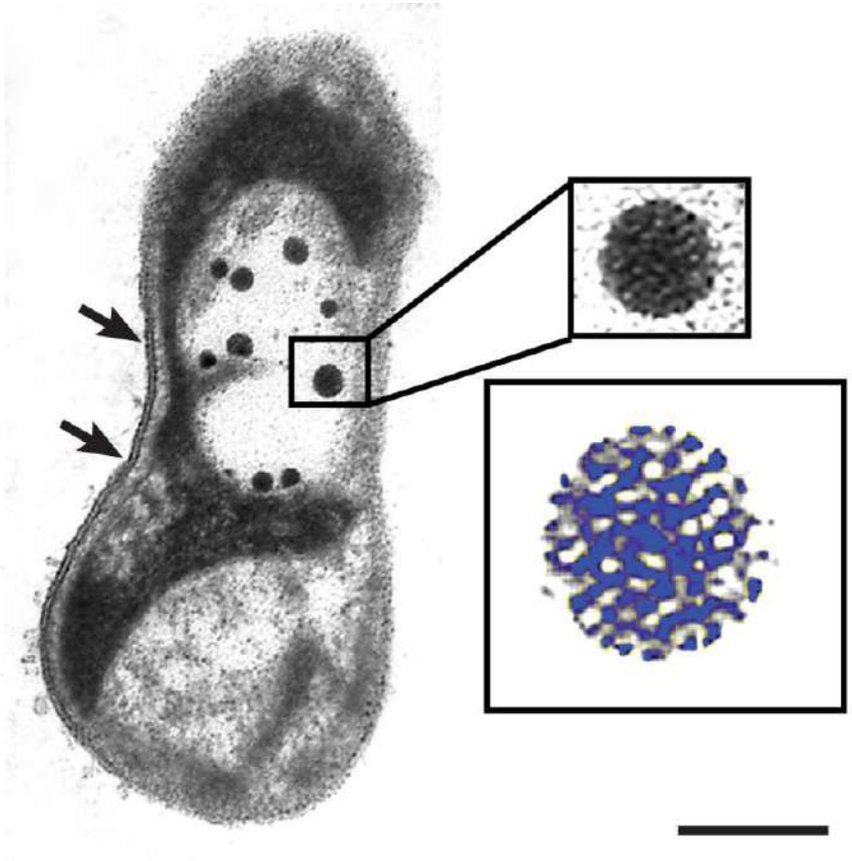

Figure 5. A virus-infected bacterium from an aquatic ecosystem shows several phages. The boxed area shows the virus capsid structure at high magnification. Note that the capsid is composed of repetitive morphological units (highlighted in blue at a higher magnification). The trilaminar structure of the plasma membrane is partially observed (arrows). Scale bar: 266 nm, 80 nm (Box, virus at high magnification), and 40 nm (Box, highlighted in blue). Reprinted from ref. [44] with permission.

3. Production of outer membrane vesicles by freshwater bacteria

In recent years, the extracellular release of membrane-bound vesicles by prokaryotic cells has become the subject of great interest. In prokaryotes, these vesicles are frequently extruded from the outer membrane (OM) of gram-negative bacteria and cyanobacteria, and, for this reason, they are known as outer membrane vesicles (OMVs). By TEM, OMVs appear as spherical or rod-shaped vesicles enveloped by a double membrane with variable electron-density content and diameter size varying from 20 to 300 nm [52-54] (Figure 3).

OMVs have been shown to contribute to diverse bacterial processes, such as pathogenesis [55, 56], cellular defense [53, 57], cell-to-cell communication [58], and DNA transfer [52, 59]. OMVs are able to store and transport a broad range of cargo repertory from bacterial periplasm and cytoplasm, that can explain the variable electron-density observed by TEM. Thus vesicular transport represents a relevant signal trafficking system in prokaryotes (reviewed in [54, 60]). Despite the numerous ways in which vesicles may affect microbial communities, their abundance and potential functions in aquatic ecosystems remain unknown. Recently, these vesicles were recognized as abundant and important to carbon flux in marine ecosystems [61]. Vesicle release occurs during the normal growth of many species, and although growth conditions, stressors, and membrane structure can influence the number of vesicles produced, the regulation of vesicle production is still unclear.

By studying microorganisms from freshwater ecosystems in both natural environmental and cultures through TEM, we have identified a consistent production of OMVs by bacteria [20]. These vesicles were round, delimited by classical membrane with trilaminar appearance, and exhibited morphology similar to those described on the surfaces of other bacterial species [52] (Figure 3). They appeared attached to the outer membrane of the bacteria with typical gram-negative envelope or free in the extracellular environment (Figure 3).

Our data from samples collected from Batata Lake suggest that OMV-mediated secretion is an important cell process of freshwater bacteria (Figure 3). Although the function of OMV remains to be defined, these secretory vesicles, observed for the first time by us in aquatic bacteria from a tropical ecosystem [20], may be important for bacterial survival and inhibition of lysis induced by viral infection that is relevant in this ecosystem [44], as mentioned before. Moreover, OMVs may be relevant in the transport of products involved in the formation of the cell wall, inhibition of toxic components present in the surrounding environment, and formation of biofilms. They may also be associated with delivery of enzymes for nutrients acquisition and autolysins for degradation of other bacteria favoring the competition for niches. All these environmental factors may be more prominent in an impacted ecosystem.

4. Concluding remarks and perspectives

Although our understanding of the biological aspects of bacteria from aquatic ecosystems has advanced significantly, our knowledge of the structural organization of these ecologically

important microorganisms is still incomplete. It is unknown how bacteria differ in their cellular architecture and respond at the structural level to abiotic and biotic stress in aquatic environments. This knowledge is essential for an integrative understanding of the bacterial physiology and ecology. TEM has helped to elucidate the internal organization of aquatic bacteria at the nanometer scale. Earlier views of the ultrastructure of these microorganisms, considered in the past as cells with a very simple structure, are now being expanded to encompass a new understanding of their multifunctional activities and cellular complexity. Our results from environmental and culture-based TEM studies have revealed an ultrastructurally diverse population of bacteria in freshwater ecosystems, characterized by distinct cytoplasmic and external structures. The recognition that these microorganisms have cytoplasmic membranes and are able to release membrane-bound vesicles may be crucial to the understanding of their functional capabilities. Several aspects of the bacteria life remain to be defined. For example, it is not understood how bacteria interact with each other in aquatic ecosystems. Is there a regulated vesicular transport-mediated secretion from/to bacterium? If yes, can this pathway be blocked or stimulated by a cell stressor? These and other aspects, including the bacterial responses to several environmental stresses, mechanisms of bacterial cell death and the bacteria—viruses interaction, need to be investigated in more detail so that the functional significance of bacteria and other microorganisms from aquatic ecosystems can be fully appreciated as critical regulators of ecological processes.

Acknowledgements

The works of the authors were supported by Conselho Nacional de Desenvolvimento Científico e Tecnológico (CNPq, Brazil) and Fundação de Amparo à Pesquisa do Estado de Minas Gerais (FAPEMIG, Brazil).

Author details

Thiago P. Silva, Juliana P. Gamalier and Rossana C.N. Melo*

*Address all correspondence to: rossana.melo@ufjf.edu.br

Laboratory of Cellular Biology, Department of Biology, Federal University of Juiz de Fora (UFJF), Juiz de Fora, MG, Brazil

References

[1] Fenchel T. The microbial loop–25 years later. Journal of Experimental Marine Biology and Ecology. 2008;366(1):99–103.

[2] Azam F. Microbial control of oceanic carbon flux: the plot thickens. Science. 1998;280:694–6.

[3] Pomeroy LR. The ocean's food web, a changing paradigm. Bioscience. 1974;24(9):499–504.

[4] Fuhrman JA, Noble RT. Viruses and protists cause similar bacterial mortality in coastal seawater. Limnology Oceonography. 1995;40(7):1236–42.

[5] Fuhrman JA. Marine viruses and their biogeochemical and ecological effects. Nature. 1999;399:541–8.

[6] Joux F, Lebaron P. Use of fluorescent probes to assess physiological functions of bacteriaat single-cell level. Microbes and Infection. 2000;2(12):1523–35.

[7] Moriarty DJW, Hayward AC. Ultrastructure of bacteria and the proportion of Gram-negative bacteria in marine sediments. Microbial Ecology. 1982;8(1):1–14.

[8] Nell RM, Szymanowski JE, Fein JB. The effects of bacterial surface adsorption and exudates on HgO precipitation. Geomicrobiology Journal. 2015(just-accepted):00-.

[9] Hoppert M, Mayer F. Principles of macromolecular organization and cell function in bacteria and Archaea. Cell Biochemistry and Biophysics. 1999;31:247–85.

[10] Ram ASP, Sime-Ngando T. Functional responses of prokaryotes and viruses to grazer effects and nutrient additions in freshwater microcosms. The ISME Journal. 2008;2(5):498–509.

[11] Rodriguez-Brito B, Li L, Wegley L, Furlan M, Angly F, Breitbart M, et al. Viral and microbial community dynamics in four aquatic environments. The ISME journal. 2010;4(6):739–51.

[12] Balkwill DL. Numbers, diversity, and morphological characteristics of aerobic, chemoheterotrophic bacteria in deep subsurface sediments from a site in South Carolina. Geomicrobiology Journal. 1989;7(1-2):33–52.

[13] Nakahara A, Shimada Y, Wakita J-i, Matsushita M, Matsuyama T. Morphological diversity of the colony produced by bacteria Proteus mirabilis. Journal of the Physical Society of Japan. 1996;65(8):2700–6.

[14] Vandamme P, Pot B, Gillis M, De Vos P, Kersters K, Swings J. Polyphasic taxonomy, a consensus approach to bacterial systematics. Microbiological reviews. 1996;60(2): 407–38.

[15] Jürgens K, Pernthaler J, Schalla S, Amann R. Morphological and compositional changes in a planktonic bacterial community in response to enhanced protozoan grazing. Applied and environmental microbiology. 1999;65(3):1241–50.

[16] Pinho MG, Kjos M, Veening J-W. How to get (a) round: mechanisms controlling growth and division of coccoid bacteria. Nature reviews microbiology. 2013;11(9): 601–14.

[17] Kerfeld CA, Sawaya MR, Tanaka S, Nguyen CV, Phillips M, Beeby M, et al. Protein structures forming the shell of primitive bacterial organelles. Science. 2005;309(5736): 936–8.

[18] Bobik TA, Lehman BP, Yeates TO. Bacterial microcompartments: widespread prokaryotic organelles for isolation and optimization of metabolic pathways. Molecular microbiology. 2015.

[19] Kerfeld CA, Erbilgin O. Bacterial microcompartments and the modular construction of microbial metabolism. Trends in microbiology. 2015;23(1):22–34.

[20] Silva TP, Noyma NP, Duque TL, Gamalier JP, Vidal LO, Lobão LM, et al. Visualizing aquatic bacteria by light and transmission electron microscopy. Antonie van Leeuwenhoek. 2014:1–14.

[21] Heissenberger A, Leppard GG, Herndl GJ. Relationship between the intracellular integrity and the morphology of the capsular envelope in attached and free-living marine bacteria. Applied and Environmental Microbiology. 1996;62(12):4521–8.

[22] Stoderegger KE, Herndl GJ. Visualization of the exopolysaccharide bacterial capsule and its distribution in oceanic environments. Aquatic Microbial Ecology. 2001;26(2): 195–9.

[23] Cowen J. Morphological study of marine bacterial capsules: implications for marine aggregates. Marine Biology. 1992;114(1):85–95.

[24] Grossart HP, Tang KW. www.aquaticmicrobial.net. Communicative & Integrative Biology. 2010;3(6):491–4.

[25] Grossart HP. Ecological consequences of bacterioplankton lifestyles: changes in concepts are needed. Environmental Microbiology Reports. 2010;2(6):706–14.

[26] Hartmann M, Berditsch M, Hawecker J, Ardakani MF, Gerthsen D, Ulrich AS. Damage of the bacterial cell envelope by antimicrobial peptides gramicidin S and PGLa as revealed by transmission and scanning electron microscopy. Antimicrobial agents and chemotherapy. 2010;54(8):3132–42.

[27] Drews G, Dawes EA. Molecular biology of membrane-bound complexes in phototrophic bacteria: Springer science & business media; 2013.

[28] Smith EM, del Giorgio PA. Low fractions of active bacteria in natural aquatic communities? Aquatic microbial ecology. 2003;31(2):203–8.

[29] Sawstrom C, Pearce I, Davidson AT, Rosen P, Laybourn-Parry J. Influence of environmental conditions, bacterial activity and viability on the viral component in 10 Antarctic lakes. FEMS Microbiology Ecology. 2008;63(1):12–22.

[30] Romanova N, Sazhin A. Methodological aspects of the determination of the bacterioplankton number, biomass, and production. Oceanology. 2011;51(3):518–27.

[31] Nebe-von Caron G, Badley RA. Viability assessment of bacteria in mixed populations using flow cytometry. Journal of Microscopy: Oxford. 1995;179:55–66.

[32] Haglund A-L, Lantz P, Törnblom E, Tranvik L. Depth distribution of active bacteria and bacterial activity in lake sediment. FEMS Microbiology Ecology. 2003;46(1):31–8.

[33] Signoretto C, Burlacchini G, Pruzzo C, Canepari P. Persistence of enterococcus faecalis in aquatic environments via surface interactions with copepods. Applied and environmental microbiology. 2005;71(5):2756–61.

[34] Hammes F, Berney M, Egli T. Cultivation-independent assessment of bacterial viability. High resolution microbial single cell analytics: Springer; 2011. p. 123–50.

[35] Foladori P, Bruni L, Tamburini S. Bacteria viability and decay in water and soil of vertical subsurface flow constructed wetlands. Ecological Engineering. 2015;82:49–56.

[36] Vezzulli L, Pezzati E, Stauder M, Stagnaro L, Venier P, Pruzzo C. Aquatic ecology of the oyster pathogens Vibrio splendidus and Vibrio aestuarianus. Environmental microbiology. 2015;17(4):1065–80.

[37] Ross J, Boon P, Sharma R, Beckett R. Variations in the fluorescence intensity of intact DAPI-stained bacteria and their implications for rapid bacterial quantification. Letters in applied microbiology. 1996;22(4):283–7.

[38] Mostajir B, Dolan JR, Rassoulzadegan F. A simple method for the quantification of a class of labile marine pico-and nano-sized detritus: DAPI Yellow Particles (DYP). Aquatic Microbial Ecology. 1995;9(3):259–66.

[39] Yan X, Yu M, Wu L, Huang T, Wang S. Rapid detection and enumeration of total bacteria in drinking water and tea beverages by a laboratory-built high-sensitivity flow cytometer. Analytical Methods. 2015.

[40] Senjarini K, Karsten U, Schumann R. Application of fluorescence markers for the diagnosis of bacterial abundance and viability in aquatic ecosystem. Journal of Microbiology Research. 2013;3(4):143–7.

[41] Esteves F, Enrich-Prast A, Biesboer D. Potential denitrification in submerged natural and impacted sediments of Lake Batata, an Amazonian lake. Hydrobiologia. 2001;444(1-3):111–7.

[42] Rocha MIA. Avaliação de fatores que contribuem para a dominância de cianobactérias no reservatório do Funil e preposição de medidas para melhoria da qualidade da água.: Instituto de Biofísica Carlos Chagas Filho; 2012.

[43] Zweifel UL, Hagstrom A. Total counts of marine bacteria include a large fraction of non-nucleoid-containing bacteria (ghosts). Applied and Environmental Microbiology. 1995;61(6):2180–5.

[44] Barros NO, Farjalla VF, Soares MC, Melo RCN, Roland F. Virus-bacterium coupling driven by both Tubidity and hydrodynamics in an Amazonian floodplain lake. Applied and Environmental Microbiology. 2010;76(21):7194–201.

[45] Bradley DE. Ultrastructure of bacteriophage and bacteriocins. Bacteriological reviews. 1967;31(4):230.

[46] Weinbauer MG. Ecology of prokaryotic viruses. FEMS Microbiology Review. 2004;28(2):127–81.

[47] Almeida RM, Roland F, Cardoso SJ, Farjalla VF, Bozelli RL, Barros NO. Viruses and bacteria in floodplain lakes along a major Amazon tributary respond to distance to the Amazon River. Frontiers in microbiology. 2015;6.

[48] Grabow W. Bacteriophages: update on application as models for viruses in water. Water SA. 2004;27(2):251–68.

[49] Häder D-P, Williamson CE, Wängberg S-Å, Rautio M, Rose KC, Gao K, et al. Effects of UV radiation on aquatic ecosystems and interactions with other environmental factors. Photochemical & Photobiological Sciences. 2015;14(1):108–26.

[50] Häder D-P, Kumar H, Smith R, Worrest R. Effects of solar UV radiation on aquatic ecosystems and interactions with climate change. Photochemical & Photobiological Sciences. 2007;6(3):267–85.

[51] Danovaro R, Corinaldesi C. Sunscreen products increase virus production through prophage induction in marine bacterioplankton. Microbial ecology. 2003;45(2):109–18.

[52] Pérez-Cruz C, Carrión O, Delgado L, Martinez G, López-Iglesias C, Mercade E. New type of outer membrane vesicle produced by the Gram-negative bacterium Shewanella vesiculosa M7T: implications for DNA content. Applied and environmental microbiology. 2013;79(6):1874–81.

[53] Manning AJ, Kuehn MJ. Contribution of bacterial outer membrane vesicles to innate bacterial defense. BMC microbiology. 2011;11(1):258.

[54] Kulp A, Kuehn MJ. Biological functions and biogenesis of secreted bacterial outer membrane vesicles. Annual review of microbiology. 2010;64:163.

[55] Rivera J, Cordero RJ, Nakouzi AS, Frases S, Nicola A, Casadevall A. Bacillus anthracis produces membrane-derived vesicles containing biologically active toxins. Proceedings of the National Academy of Sciences. 2010;107(44):19002–7.

[56] Kolling GL, Matthews KR. Export of virulence genes and Shiga toxin by membrane vesicles of Escherichia coli O157: H7. Applied and environmental microbiology. 1999;65(5):1843–8.

[57] Baumgarten T, Vazquez J, Bastisch C, Veron W, Feuilloley MG, Nietzsche S, et al. Alkanols and chlorophenols cause different physiological adaptive responses on the

level of cell surface properties and membrane vesicle formation in Pseudomonas putida DOT-T1E. Applied microbiology and biotechnology. 2012;93(2):837–45.

[58] Mashburn LM, Whiteley M. Membrane vesicles traffic signals and facilitate group activities in a prokaryote. Nature. 2005;437(7057):422–5.

[59] Rumbo C, Fernandez-Moreira E, Merino M, Poza M, Mendez JA, Soares NC, et al. Horizontal transfer of the OXA-24 carbapenemase gene via outer membrane vesicles: a new mechanism of dissemination of carbapenem resistance genes in Acinetobacter baumannii. Antimicrob Agents Chemother. 2011;55(7):3084–90.

[60] Haurat MF, Elhenawy W, Feldman MF. Prokaryotic membrane vesicles: new insights on biogenesis and biological roles. Biological chemistry. 2015;396(2):95–109.

[61] Biller SJ, Schubotz F, Roggensack SE, Thompson AW, Summons RE, Chisholm SW. Bacterial vesicles in marine ecosystems. Science. 2014;343(6167):183–6.